NTNU – Trondheim
Norwegian University of
Science and Technology

Effect of Sulfide Inclusions in Austenitic Stainless Steel on the Initiation of Pitting in Base Metal and Heat Affected Zone after Welding

Anders Welde Gjønnes

Materials Technology
Submission date: June 2012
Supervisor: Kemal Nisancioglu, IMTE
Co-supervisor: Ole Øystein Knudsen, SINTEF

Norwegian University of Science and Technology
Department of Materials Science and Engineering

Master Thesis, Spring 2012

Effect of Sulfide Inclusions in Austenitic Stainless Steel on the Initiation of Pitting in Base Metal and Heat Affected Zone after Welding

Norwegian University of Science and Technology
Department of Materials Science and Engineering

Anders Welde Gjønnes

June 14, 2012

Supervisors:
Prof. Dr. Ole Øystein Knudsen
Prof. Dr. Kemal Nisancioglu

NTNU – Trondheim
Norwegian University of
Science and Technology

Abstract

The predominant site for the initiation of pitting on austenitic stainless steel has been shown to be sulfide inclusions and notably the manganese types of sulfides. Dissolution of inclusions has been observed and suggested to be the initial step for pit initiation, though several explanations for the mechanisms causing initiation has been proposed. Regarding welded stainless steels, several microstructural changes have been described and suggested to contribute to the decreased corrosion resistance in the weld zone. An area which has not been investigated much is the contribution of inclusions, in particular MnS inclusions, to the reduced corrosion resistance and the initiation of pitting in the weld zone. In the present work a literature review of the investigations focusing on the initiation of pitting by sulfide inclusions in austenitic stainless steels has been provided. A literature review of investigations focusing on the effects of welding on the microstructure, inclusions and the corrosion properties in the weld zone of austenitic stainless steels has also been provided.

Experimental work was performed to obtain results which could be compared to or verify findings and suggestions from the reviewed literature regarding the initiation of pitting by inclusions. Observations of MnS inclusions as the preferential site for pit initiation in austenitic stainless steel was tried recreated. The hypothesis saying that dissolution of MnS inclusions occur prior to the initiation of pitting was also tried verified. It was also performed experiments to obtain results which could give knowledge about the effects of MnS inclusions on the corrosion properties and the initiation of pitting in the weld zone of an austenitic stainless steel. Along with this, the corrosion behaviour and microstructural changes in the weld zone in general and compared with the base metal were studied. A part of the work was also to study the effect of a lacking inert shielding gas during welding.

Samples of a 316L stainless steel were first examined in SEM to study the microstructure and to identify inclusions. Then, some samples were welded, followed by SEM examination. Then all samples were polarized electrochemically in synthetic seawater with the purpose of initiating pitting. After the polarization, all samples were examined in SEM again to correlate pitting attack to inclusions and to compare microstructural changes and the corrosion behaviour in the base metal and the weld zone.

It was verified that the main initiation site for pitting in the base metal was MnS inclusions. It was indicated that dissolution of the MnS inclusions started the pit initiation process, with the contribution of released compounds from the inclusions. An average percent of inclusions showing an inactive behavior regarding the initiation of pitting was 38 %, verifying similar observations reported in earlier investigations. A nitric acid treatment to remove MnS inclusions improved the pitting resistance significantly.

The welding caused the initiation of corrosion at lower potentials when performing electrochemical polarization in synthetic seawater. The corrosion mechanism was probably grain boundary corrosion caused by precipitation of chromium carbides in the grain boundaries. A lacking inert shielding gas during welding did not have any

effect on the potential for the initiation of corrosion when comparing two samples welded with and without shielding gas.

It was indicated that compositional changes had occurred for MnS inclusions in a certain distance from the fusion line. These changes may have caused the inclusions to be more prone to initiate pitting. Further investigation should be performed to clarify the behaviour of such inclusions, and their susceptibility towards the initiation of corrosion.

Grain boundary corrosion in various grades had occurred in the HAZ in certain distances from the fusion line. In a further distance from the fusion line pitting-like corrosion in clusters, possibly induced by chromium depletion after forming chromium oxides combined with a thin oxide film, had occurred. The grain boundary corrosion and the pitting cluster attack are from the experimental results believed to be more important for the failure of the welded stainless steel investigated in this work, than pitting initiated at MnS inclusions changed by the welding process.

Sammendrag

Det har blitt vist at det dominerende initieringspunktet for pitting på austenittisk rustfrie stål er sulfid-inneslutninger, hovedsakelig mangansulfider. Oppløsning av inneslutninger har blitt observert og foreslått som det første steget for pit initiering, selv om flere forklaringer på forårsakende mekanismer for initiering har blitt foreslått. Når det gjelder sveiste rustfrie stål, har ulike endringer i mikrostrukturen som et resultat av sveisingen blitt beskrevet og foreslått til å bidra til redusert korrosjonsmotstand i sveisesonen. Et område det har blitt forsket lite på er bidraget inneslutninger, og da spesielt MnS inneslutninger, har til den reduserte korrosjonsmotstanden og på initiering av pitting i sveisesonen. Et litteraturstudie som tar for seg forskingen som har fokusert på initiering av pitting på grunn av sulfid-inneslutninger i austenittiske rustfrie stål har blitt presentert som en del av denne rapporten. Et litteraturstudie om forskning gjort på effekt av sveising på mikrostruktur, inneslutninger og korrosjonsegenskaper i sveisesonen på austenittiske rustfrie stål har også blitt utført.

Eksperimentelle forsøk ble utført for å oppnå resultater som kunne sammenlignes med eller verifisere funn og forslag fra den gjennomgåtte litteraturen om initiering av pitting på grunn av inneslutninger. Observasjoner av MnS inneslutninger som hovedinitieringspunkt for pitting i austenittiske rustfrie stål ble forsøkt gjenskapt. Hypotesen om at oppløsning av MnS inneslutninger skjer før pitting initieres ble også forsøkt verifisert. Forsøk ble også gjort for å oppnå resultater som kunne gi kunnskap om effekten MnS inneslutninger har på korrosjonsegenskapene og initieringen av pitting i sveisesonen på et austenittisk rustfritt stål. Parallelt med dette ble korrosjonsangrep og endringer i mikrostruktur studert. Som en del av dette arbeidet ble også effekten av manglende inert dekkgass ved sveising studert.

Prøver av et 316L rustfritt stål ble først undersøkt i SEM for å studere mikrostruktur og for å identifisere inneslutninger. Deretter ble noen prøver sveist, etterfulgt av SEM undersøkelse. Deretter ble alle prøver polarisert elektrokjemisk i syntetisk sjøvann med den hensikt å initiere pitting. Etter polarisasjonen ble alle prøver undersøkt i SEM igjen, for å identifisere pitting angrep i forhold til inneslutninger og for å sammenligne endringer i mikrostruktur og korrosjonsangrep i grunnmetallet og sveisesonen.

Det ble verifisert at hovedinitieringspunktet for pitting i grunnmetallet var MnS inneslutninger. Det ble indikert at oppløsning av MnS inneslutningene startet pit-initieringsprosessen, med bidrag fra løste elementer fra inneslutningene. En gjennomsnittlig prosent av inneslutninger som viste en inaktiv oppførsel i forhold til initiering av pitting var 38%. Dette verifiserte samme type observasjoner rapportert i tidligere forskning. En behandling med salpetersyre for å fjerne MnS inneslutninger forbedret pittingresistansen betraktelig.

Sveising førte til initiering av korrosjon ved lavere potensialer, ved elektrokjemisk polarisasjon utført i syntetisk sjøvann. Korrosjonsmekanismen var sannsynligvis korngrensekorrosjon på grunn av utfelte kromkarbider på korngrenser. Manglende inert dekkgass ved sveising hadde ingen effekt på potensialet for initiering av korrosjon når to prøver sveiset med og uten dekkgass ble sammenlignet.

Det ble indikert at endringer i komposisjon hadde skjedd for MnS inneslutninger i den varmepåvirkede sonen i en bestemt avstand fra smeltegrensen. Disse endringene kan ha forårsaket at disse inneslutningene ble mer utsatt for å initiere pitting. Videre undersøkelser bør utføres for å få klarhet i oppførselen til slike inneslutninger ved sveising, og inneslutningenes tendens til å initiere korrosjon.

Korngrensekorrosjon i varierende grad hadde oppstått i den varmepåvirkede sonen i bestemte avstander fra smeltegrensen. I en lengre avstand fra smeltegrensen hadde et område med samlet pitting-liknende korrosjon oppstått, muligens indusert av kromutarming etter dannelse av kromoksider, kombinert med en tynn oksidfilm. Korngrensekorrosjonen og dette pittingangrepet antas å være viktigere for feil i det sveisede rustfrie stålet undersøkt i dette arbeidet, enn pitting initiert på MnS inneslutninger endret som et resultat av sveiseprosessen.

Preface

This work was performed at the Norwegian University of Science and Technology (NTNU) in Trondheim, Norway. The report completes the course TMT 4905 – Materials Technology, Master Thesis. Parts of this thesis are based on the work performed in the course TMT – Materials Technology, Specialization Project. The practical work has been performed at the corrosion laboratory at SINTEF Materials and Chemistry and in the SEM laboratory at the Department of Materials Science and Engineering.

I would like to thank my supervisors Prof. Dr. Ole Øystein Knudsen at SINTEF and Prof. Dr. Kemal Nisancioglu at the Department of Materials Science and Engineering at the Norwegian University of Science and Technology (NTNU).

I would also like to thank Nils Inge Nilsen for practical solutions during the experimental work, Tone Anzjøn for assistance with the sample preparation, and Julian Tolchard for SEM and EDS guidance.

Thanks also to Weld Partner A/S for the welding of samples, and to the Engineering Workshop at the Faculty of Natural Sciences and Technology at NTNU, Realfagsbygget for the machining of samples and additional welding.

In addition, I would like to thank FORCE Technology Norway AS, Trondheim division for the general support and positivism during my work.

Declaration

I declare that this work has been performed independently and in accordance with the rules and regulations at the Norwegian University of Science and Technology (NTNU).

Trondheim, June 14

Anders Welde Gjønnes

Contents

1. Abbreviations

CRA	Corrosion Resistant Alloy
EDS	Energy-dispersive X-ray Spectroscopy
FIB	Focused Ion Beam
GTAW	Gas Tungsten Arc Welding
HAZ	Heat Affected Zone
LBW	Laser-Beam Welding
MIG	Metal Inert Gas
SAM	Scanning Auger Microscope
SCE	Saturated Calomel Electrode
SEM	Scanning Electron Microscope
SHE	Standard Hydrogen Electrode
SIMS	Secondary Ion Mass Spectroscopy
TEM	Transmission Electron Microscopy
TIG	Tungsten Inert Gas

2. Introduction

Stainless steels are susceptible to localized corrosion attack. This may lead to a catastrophic failure of the stainless steel structure, caused by very rapid localized corrosion, referred to as pitting. Pitting of stainless steel involves locally extreme conditions of chloride concentration and pH, which are maintained as a consequence of very high local current density [1]. Much is known about the progress of pitting corrosion on stainless steel after it is initiated. However, the very first step in the initiation process is not yet fully understood.

It has been shown that the predominant site for the initiation of pitting on austenitic stainless steel is sulfide inclusions and notably the manganese types of sulfides. Dissolution of inclusions have been observed and suggested to be the initial step for pit initiation [2, 3], though several explanations for the mechanisms causing initiation has been proposed.

The presence of MnS inclusions, which has been observed to be a preferential site for the initiation of pitting in austenitic stainless steel, originates from the addition of manganese in the steel, with the purpose of segregating sulfur as MnS instead of FeS. FeS is thermodynamically much more unstable than MnS and has a much lower melting point. Thus, the formation of FeS along grain boundaries with subsequent problems arising in the hot-rolling of the steel is prevented [4]. Manganese has also been considered as an austenite former, and has been added to increase the solubility of nitrogen [5].

It is well known that the corrosion resistance of stainless steels is significantly decreased during welding. Several microstructural changes have been described and suggested to contribute to the decreased corrosion resistance in the weld zone. An area which has not been investigated much is the contribution of inclusions, in

particular MnS inclusions, to the reduced corrosion resistance and the initiation of pitting in the weld zone of stainless steels.

The first goal of the present work was to provide a literature review of the investigations focusing on the initiation of pitting by sulfide inclusions in austenitic stainless steel in general and of the investigations focusing on the effects of welding on the microstructure, inclusions and the corrosion properties in the weld zone of austenitic stainless steels.

The literature review covers the topics which have been the focus of the investigations regarding pit initiation by inclusions in austenitic stainless steels over the years. Further it covers investigations which have focused on the microstructural changes occurring in austenitic stainless steel during welding and the reasons for the reduced corrosion resistance in the weld zone.

The second goal of the present work was to perform experiments to obtain results which could be compared to or verify findings and suggestions from the reviewed literature regarding the initiation of pitting by inclusions. Observations of MnS inclusions as the preferential site for pit initiation in austenitic stainless steel was tried recreated. The hypothesis saying that dissolution of MnS inclusions occur prior to the initiation of pitting was also tried verified.

A third goal was to obtain results which could give knowledge about the effects of MnS inclusions on the corrosion properties and the initiation of pitting in the weld zone of an austenitic stainless steel. Along with this, the corrosion behaviour and microstructural changes in the weld zone in general and compared with the base metal was studied. A part of the work was also to study the effect of a lacking inert shielding gas during welding.

Samples of a 316L stainless steel were first examined in SEM to study the microstructure and to identify inclusions. Then, some samples were welded, followed by SEM examination. Then all samples were polarized electrochemically with the purpose of initiating pitting. After the polarization, all samples were examined in SEM again to correlate pitting attack to inclusions and to compare microstructural changes and the corrosion behaviour in base metal and welded samples.

3. Theory

3.1. Effect of Inclusions on the Initiation of Pitting on Austenitic Stainless Steel

Several investigations have shown that sulfide inclusions are the preferred initiation site for pitting on austenitic stainless steel. Most investigations have focused on MnS inclusions, which have shown to be the most detrimental regarding the initiation of pitting. In this section the factors causing pitting attack due to inclusions are reviewed. The mechanisms describing how pitting is initiated at inclusions and how these processes develop to further attack is of special interest. Prediction and control of the initiation of pitting cannot be managed before the underlying mechanisms for the initiation processes are understood. Several mechanisms have been suggested by different researchers to be the cause of initiation of pitting at MnS inclusions on stainless steel.

3.1.1. Pit Initiation at Inclusions

It has been shown by Eklund [6] that pitting starts almost exclusively at non-metallic inclusions in stainless steels and that sulfide inclusions, notably MnS, are the most detrimental. Also Wranglén [7] reported the initiation of pitting due to sulfide inclusions, usually MnS, in stainless steel. These observations has been supported, among others, by Stewart and Williams [8] who has shown by microstructural characterization and electrochemical experiments that pits nucleated predominantly at sulfur-rich inclusions in type 304L stainless steel in dilute neutral chloride solutions. Rossi *et al.* [9] detected ions at MnS inclusions after immersion in a $FeCl_3$ test solution and found enrichment of chloride at the inclusions. This indicated a preferential adsorption of chloride ions onto the MnS inclusion, further indicating a preferential pit initiation site at these inclusions. Schmuki *et al.* [10] demonstrated that pitting corrosion of a high sulfur-containing stainless steel during immersion in $FeCl_3$ always started at MnS inclusions.

Pitting has also been observed on grains close to MnS inclusions short time after immersion of a 304L stainless steel in 1 M NaCl [11].

3.1.2. Pitting Susceptibility in Different Electrolytes

Some different types of electrolytes have been compared by several researchers regarding their influence on pit initiation at inclusions.

Böhni *et al.* [12] indicated that chloride was a necessary ingredient to initiate pitting at inclusions, based on electrochemical experiments indicating that in sulfate solutions (1M Na_2SO_4) only the inclusion material was dissolved without metal dissolution being detected, compared to a chloride solution (1M NaCl) where both dissolution of inclusions and metal, followed by stable pitting, occurred.

Park and Böhni [13] polarized an AISI 304 stainless steel with MnS inclusions in 1 M Na_2SO_4 and 0.1 M NaCl solutions. In 1 M Na_2SO_4 the MnS inclusions dissolved above 300 mV vs. SCE. The dissolution of the MnS inclusion in Na_2SO_4 was seen as an increased current during the dissolution, followed by a decrease in current at an even higher potential. No initiation of pitting was detected. In 0.1 M NaCl, dissolution of MnS inclusions and metastable pitting occurred between 380 and 520 mV vs. SCE. This was observed as a temporary increased current with, at the same time, many current peaks. The experiments showed that pits were initiated only in the presence of chlorides.

Webb and Alkire [14] also showed the importance of chlorides for pit initiation, and in addition the effect of thiosulfate. They performed electrochemical measurements with the use of a microcell on single sulfide inclusions in a 304 stainless steel. Measurements were performed in a chloride-free electrolyte consisting of thiosulfate (0.1 M $Na_2S_2O_3$) and in NaCl with various chloride concentrations and with the addition of thiosulfate. The experiments showed that dissolution of sulfide inclusions occurred in the chloride-free solution (thiosulfate), but no metastable pits formed. In NaCl the dissolution rate of sulfide inclusions increased with increasing chloride concentration, and metastable pitting occurred. When thiosulfate was added to the NaCl solution it caused an accelerated dissolution of inclusions, and present above a critical concentration it caused stable pitting. Also, a second critical value of thiosulfate concentration was found, which above this value pitting did not occur. The thiosulfate and the chloride were suggested to have varying inhibiting effects on each other at different concentrations.

Park *et al.* [15] investigated the influences of temperature and chloride concentration on pit initiation on AISI 304 stainless steels. In the experiments different electrolytes were used; 0.1 M Na_2SO_4, 0.01 – 5 M NaCl and 10 M LiCl. The temperature was varied. It was shown that MnS inclusions dissolved at lower potentials, and showed higher current densities as the temperature increased. Metastable or stable pitting did not occur in the Na_2SO_4 solution. In chloride containing solutions pitting was initiated as metastable pitting at the interface of the MnS inclusion and the metal matrix. The metal dissolution occurred more rapid as the chloride concentration and the temperature was increased. In 10 M LiCl and at 90 ^{o}C in 5 M NaCl numerous additional initiation processes was observed further away from the inclusion-metal matrix interface, suggesting that other heterogeneities in the passive metal surface was activated. The effect of the temperature on metastable pit initiation was not possible to study at elevated temperatures, because stable pitting was obtained too easily.

From the observations regarding electrolytes it can be summarized that chloride is required to initiate pitting attack of the metal surrounding the MnS inclusions, but the inclusions themselves may dissolve in both chloride and chloride-free solutions. The dissolution of inclusions is observed as an increased current in a limited potential range. The presence of thiosulfate in the solution seems to accelerate both dissolution of the inclusion and the rate of pitting. The pitting attack is also worsened by increased temperature and chloride concentration.

3.1.3. The Influence of Steel Composition on the Pitting Susceptibility

Some experiments have paid attention to the bulk composition of the steel and its correlation with pitting susceptibility at inclusions.

Degerbeck and Wold [16] performed electrochemical potentiodynamic polarization of several austenitic stainless steel grades in NaCl to study the effect of a reduced manganese content on the resistance to pitting. They found that the pitting potential was considerably increased with the reduction of the manganese content from 1.8 % to 0.2 %. They also found that an increase in the sulfur content from 0.007 % to 0.03 % resulted in a minor decrease in the pitting potential. They found by investigating sulfide inclusions with SEM (Scanning Electron Microscopy) and EDS (Energy-dispersive X-ray Spectroscopy) that a reduction of the manganese content in the steel affected the composition of the sulfide inclusions; the manganese content decreased and the chromium content increased. By this observation they attributed the positive effect of the reduced manganese content in the steel on the pitting resistance to the change of the sulfide inclusion composition, resulting in an increased content of chromium in the inclusions.

Suter *et al.* [17] polarized four stainless steels with different sulfur content in 1 M NaCl. They found that the steel with a sulfur content of 0.003 % had a pitting potential of about 790 mV vs. SCE. When the sulfur content was increased to 0.017 % and 0.3 %, the pitting potential was decreased respectively to 380 mV and 170 mV vs. SCE.

Lim *et al.* [18] investigated the effects of nitrogen alloying on pitting corrosion of regular type 316L and 20 wt% Mn-substituted type 316L stainless steels. They found that pitting was initiated almost exclusively at non-metallic inclusions, most likely MnS inclusions. They showed that nitrogen alloying had beneficial effects on the pitting potential of the steels. They also found that the current transients due to metastable pitting were suppressed by nitrogen alloying in the 20 wt% Mn-substituted type 316L stainless steel. They believed that nitrogen facilitated the repassivation process of the exposed bare metal in the vacancy from the dissolved MnS inclusion, due to an easier formation of the passive film within the pit during MnS dissolution. Dissolution of inclusions would still occur, but this did not lead to metal dissolution as much as it did without nitrogen alloying.

Ilevbare and Burstein [19] investigated the effect of alloyed Mo on the development of pitting on stainless steels. They found that the presence of molybdenum reduced the occurrence of both nucleations and metastable pits. They discussed why Mo reduced initiation of pitting and suggested that it formed Mo sulfides in advance of Mn sulfides, and that Mo sulfides are more difficult to dissolve than MnS sulfides or are in some cases insoluble. The increased amount of Mo reduced the number of active sulfides on the metal surface, thereby reducing the nucleation sites for pitting.

The effect of Mo was also investigated by Pardo *et al.* [5]. They studied the pitting behavior of 10 different austenitic stainless steels with different concentrations of Mo and Mn. They suggested that when MnS inclusions dissolve, metal cations are released from the metal matrix adjacent to the inclusion. These cations are Fe^{2+}, Ni^{2+}, Cr^{3+} and particularly Mo^{3+}, dependent of the Mo concentration. Molybdenum oxides

will, in the conditions created after the dissolution (low pH and high potentials), be formed. These are highly stable and insoluble and can cover the exposed metal in the pit and thereby repassivate the pit. This will reduce their probability of becoming a stable pit, thus tend to make the pits metastable.

Stewart and Williams [8] demonstrated that the bulk sulfur content of an alloy did not itself control the pitting susceptibility. It was rather the size and distribution of sulfide inclusions which were controlling factors for the initiation of pitting. This was demonstrated by comparing two 304 stainless steels with a sulfur content of 0.08 wt%, in which one of the samples was laser treated, causing surface melting in a depth of 150 – 300 µm. The melting caused sulfur-rich inclusions to dissolve and transform to very small spherical particles. The sulfur content was 0.07 wt% after the laser treatment, showing that most of the sulfur had been retained in the melted zone. Hence, the sulfur content was approximately the same in the two samples, but only one of them contained sulfide inclusions. Pitting experiments revealed that the laser surface treatment reduced the nucleation frequency and lifetime of micropits markedly compared to the untreated sample, which contained sulfide inclusions.

Rossi *et al.* [9] compared two stainless steels with different sulfur contents by characterization with optical microscopy. The stainless steel with the lowest sulfur content (0.003 wt%) showed practically no inclusions on a micrometer scale, while the steel with a sulfur content of 0.29 wt% showed a large number of inclusions of various sizes. The high sulfur content steel was assumed to have a higher probability for localized corrosion attack. Their assumption was based on another study by Suter and Böhni [20] which compared two stainless steels with different sulfur contents in 1 M Na_2SO_4 regarding dissolution of MnS inclusions. They demonstrated that the stainless steel with the highest sulfur content had a much larger amount of current transients caused by the dissolution of MnS inclusions. It was believed that this would have further developed to stable pit growth in a chloride containing environment. After immersion in $FeCl_3$ solutions both steels in the experiments by Rossi *et al.* [9] showed pitting attack. The severeness of the pitting attacks for the two steels was however not compared.

From the investigation regarding the influence of the steel composition it can be summarized that the bulk sulfur content of the stainless steel can indirectly control the susceptibility of pit initiation, by forming a greater amount of sulfide inclusions which acts as initiation sites. It has been demonstrated that the pitting potential is increased by the reduction of the bulk content of manganese and that the alloying of nitrogen and molybdenum have beneficial effects on the pitting potential and the initiation of pitting in general.

3.1.4. Various Types of Inclusions Initiating Pitting

Some work has been performed to compare different types of inclusions regarding the initiation of pitting. Szklarska-Smialowska [2] investigated an 18Cr-9Ni austenitic stainless steel in 0.5M NaCl at a constant potential of 0.5 V vs. SHE. Sulfide inclusions surrounded by particles of mixed Al, Mn and Cr oxide was found. In SEM it was observed that, after the polarization Mn bound with S was removed from the inclusion, whereas Mn and Al bound with oxygen remained almost intact. These

results indicated that pits preferentially nucleated at sulfide inclusions while the oxides did not nucleate pits. From a literature review the author referred to several investigations which also had observed pit initiation at other types of inclusions in the same type of stainless steels in an environment consisting of NaCl and $K_3Fe(CN)_6$. Pits had been seen to nucleate at both oxides, sulfides, silicates and precipitates of carbides and carbonitrides.

Baker and Castle [21] exposed samples of stainless steel in 0.5 M H_2SO_4 + 0.5 M NaCl + 0.08% H_2O_2 at the free corrosion potential for 10 s. They found that pitting had initiated at the oxide inclusion/metal matrix boundary on mixed Ti/Mn/Cr/Al oxide inclusions. A possible explanation for the initiation of pitting at these inclusions was that the inclusions were partly dissolved.

Noh *et al.* [22] referred to investigations showing that MnS is preferred sites for pit initiation especially when physically associated with another type of inclusion, such as an oxide or silicate. Suter and Böhni [20] reported that especially MnS inclusions which contained aluminum oxide particles or existed as mixed oxide/sulfide inclusions behaved mostly active, as opposed to pure MnS inclusions which could be inactive in both chloride and non-chloride solutions.

Muto *et al.* [23] compared CrS and manganese-rich inclusions with respect to electrochemical polarization behavior in chloride solutions. They found that CrS inclusions were resistant to pit initiation compared to manganese-rich inclusions in the passive region of an AISI 304 stainless steel. Dissolution of the manganese-rich inclusions and subsequent stable pitting was initiated in the passive potential region of the steel. Dissolution did also occur for the CrS inclusions, but in the transpassive region, i.e. at a much higher potential. Stable pitting occurred at the CrS inclusions in the same manner as for the manganese-rich inclusions in this high potential region.

In another work, Muto *et al.* [24] compared the polarization behavior of sulfide inclusions and oxides in chloride solutions of various concentrations in a Type 304 stainless steel. While the sulfide inclusions dissolved and initiated pitting in the passive region of the steel (at potentials of 0.4 – 0.7 V in 0.1M NaCl), the oxides did not dissolve below 1.25 V, and showed resistance to pitting in solutions with chloride-ion concentrations up to 6M. However, pitting was initiated in 8M LiCl solution on oxide inclusions. The potentials were measured against Ag/AgCl (3.33M KCl). In these experiments, the oxide inclusions indicated an inert characteristic as pit initiation sites compared to the sulfide inclusions.

Webb *et al.* [25] polarized three different surfaces of 304 stainless steel in 1M NaCl; the first containing a MnS inclusion with a shallow geometry, the second containing a deep MnS inclusion and the third contained no visible MnS inclusions from SEM imaging. Both the shallow and the deep MnS inclusion had associated SiO particles. The results showed that in the absence of a MnS inclusion the current remained at the passive current density of the stainless steel. For the shallow inclusion, many current spikes were observed, indicating metastable pitting. For the deep inclusion metastable pitting occurred, followed by stable pitting. From SEM investigation it was seen that the associated SiO particles in all experiments were inactive.

It can be summarized that sulfide inclusions are seen to dissolve, while oxides did not dissolve, in NaCl. In various environments other types of inclusions like oxides are also seen to initiate pitting. In NaCl solutions, however, MnS is seen to be the most detrimental regarding the initiation of pitting. MnS physically associated with e.g.

oxides have been observed to be particularly active compared to pure MnS inclusions.

3.1.5. Electrochemical Properties of Inclusions

In order to understand the role of inclusions in the initiation of pitting on stainless steels the electrochemical properties of the inclusions themselves has to be studied. Some work has been performed to study the electrochemical behavior of MnS inclusions and its relation to the dissolution of the inclusions.

The melting point of pure MnS has been measured to be 1655 ± 5°C [26]. Electrochemical dissolution of MnS inclusions has however been observed and suggested. Eklund [3] showed by thermodynamic calculations and a potential – pH diagram for the system MnS-H_2O-Cl^- that the MnS sulfides are not stable at potentials higher than -100 mV vs. SHE in a pH range between 4.8 and 13.8 in chloride environment, and tend to dissolve above this level, i.e. in the passive potential region of the steel. The potential – pH diagram is presented in Figure 1. He correlated the dissolution of inclusions to the potential increase by the fact that the inclusions are electronic conductors, because they contain variable amounts of dissolved iron and chromium. Thus, the inclusions can be polarized to a potential level where they are not stable.

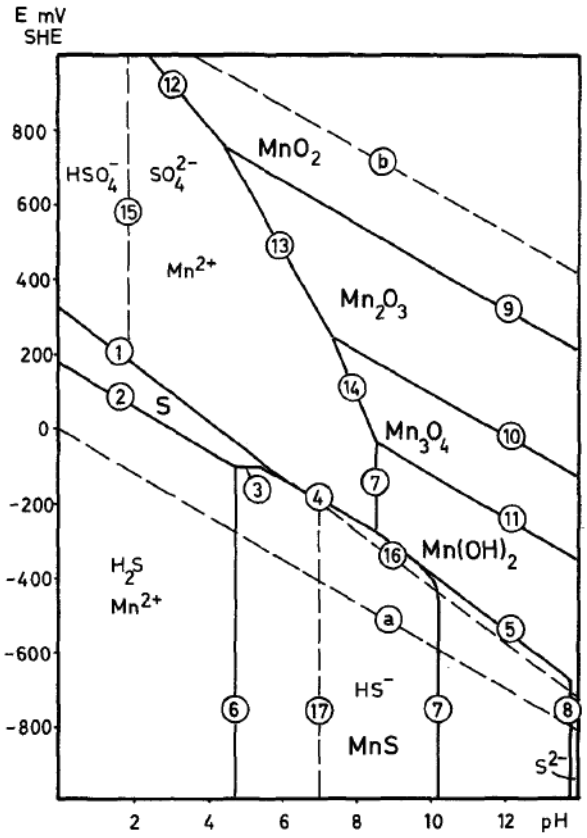

Figure 1 Potential – pH diagram for the system MnS-H_2O-Cl^- calculated on a basis of 0.1 mole/liter for the compounds SO_4^{2-}, Cl^- and Mn^{2+} [3].

The basis for the calculations was a concentration of Mn^{2+} and Cl^- of 0.1 M. He validated the calculations by polarization of MnS electrodes to 200 mV vs. SHE in an air-free unbuffered 0.1M NaCl solution, with the result of sulfide dissolution.

Eklunds calculations were supported by Wranglén [7] who calculated a standard potential of – 0.10 V vs. SHE for reaction (1).

$$MnS = S + Mn^{2+} + 2e^- \quad (1)$$

Suter *et al.* [17] performed electrochemical investigations at single MnS inclusions using an electrochemical microcell along with a metallurgical microscope. Potentiodynamic and potentiostatic polarization at MnS inclusions in a DIN 1.4301 stainless steel were performed in 1 M Na_2SO_4. During the potentiodynamic polarization at an oval 10 µm x 5 µm MnS inclusion, the inclusion started to dissolve at a potential of 400 mV vs. SCE. The dissolution process lasted to a potential of 600 mV vs. SCE. The dissolution of the inclusion was indicated on the polarization curve as a rectangular current transient between the two potential values. No stable pitting occurred in this electrolyte. Potentiostatic measurements of MnS inclusions at 300 mV vs. SCE showed that the dissolution caused current densities of approximately 0.02 nA/µm^2. For large MnS inclusions (d > 2 µm) the dissolution lasted between a few minutes and 1-2 hours. For small MnS inclusions (d < 2 µm) the lifetime was clearly shorter. In the experiments both active and inactive inclusions were observed, i.e. some of the MnS inclusions did not dissolve.

It can be summarized that MnS inclusions are seen to dissolve in the passive region of the stainless steel, without the initiation of metal dissolution. Potential values for the dissolution of MnS inclusions have been both calculated and measured.

3.1.6. Dissolution of Inclusions as an Initial Step for Pit Initiation

As described in the previous sections dissolution of inclusions has been observed. The dissolution of inclusions is suggested to be the initial step for the initiation of pitting on stainless steels and several investigations have focused on the processes leading to pitting subsequent to dissolution of the inclusions.

Eklund [3, 6] suggested that pitting was initiated at sulfide inclusions as a result of preferential dissolution of the sulfide. The dissolution was suggested by Wranglén [7] to be a result of preferential adsorption of chloride ions onto the surface of the inclusions, further facilitating anodic dissolution. The preferential adsorption was explained to be caused by the higher electron conductivity of the inclusions compared to the surrounding oxide film of the stainless steel. As a result of the dissolution Eklund [3, 6] suggested that, in the cavity from the dissolved inclusion, pure metal is exposed to the electrolyte, which contains aggressive products from the dissolution process. He confirmed a sulfide dissolution process by showing that elemental sulfur particles had formed on the MnS surface after the polarization of MnS electrodes to 200 mV vs. SHE in an air-free unbuffered 0.1M NaCl solution. He suggested that, as the electronic conductivity of the sulfides is lower than for the rest of the metal matrix, dissolution will take place preferentially at the boundary of the inclusion, leaving behind a small crevice between the inclusion and the metal matrix.

This crevice may further, depending on the environment inside it, lead to stable pitting. The formation of a micro-crevice between MnS inclusions and the metal matrix have also been observed by others, e.g. by Webb *et al.* [25] in the investigation of a 304 stainless steel in NaCl.

Wranglén [7] presented the following reaction sequence for the electrochemical dissolution of MnS inclusions in neutral chloride solutions:

$$MnS + 4H_2O = Mn^{2+} + SO_4^{2-} + 8H^+ + 8e^- \quad (2)$$

$$2O_2 + 8H^+ + 8e^- = 4H_2O \quad (3)$$

Lott and Alkire [27] proposed another reaction sequence for the electrochemical dissolution of MnS in deaerated 0.1N NaCl, after performing anodic polarization of MnS electrodes:

$$2MnS + 3H_2O = S_2O_3^- + 2Mn^{2+} + 6H^+ + 8e^- \quad (4)$$

$$2H^+ + MnS = Mn^{2+} + S + H_2 \quad (5)$$

The two reaction sequences include a different number of electrons. After analyzing the charge passed during the dissolution of MnS inclusions in 1 M Na_2SO_4, in the investigation described in section 3.1.5, Suter *et al.* [17] assumed reaction (4) and (5) to be the most probable in their experiment. They based this assumption on their measurements indicating that an average number of 4.4 electrons per MnS were used in the dissolution reaction, which is close to the number of electrons per MnS used in the reaction mechanism suggested by Lott and Alkire [27].

Several investigations have focused on the dissolution products released from the dissolution of sulfide inclusions and their role in the initiation of pitting.

Eklund [3] suggested that the dissolution of manganese sulfides release metal ions (manganese, iron and chromium) that can undergo complex reactions and give rise to low pH. The low pH will hinder repassivation in the cavity from the dissolved inclusion. Hydrogen sulfides may also be formed. In this aggressive environment, at a certain composition, metal dissolution will occur. He showed by thermodynamic calculations that chromium released into a chloride containing solution forming hydroxy complexes will lower the pH at potentials above -400 mV vs. SHE. Wranglén [7] also indicated that a lowered pH was needed to activate the stainless steel for pitting in combination with the dissolution of inclusions.

Other investigations also suggest that chromium contributes to the formation of an aggressive environment. Williams *et al.* [4] suggested a mechanism in which chromium is released into the solution from the dissolution of inclusions. This Cr^{3+} will be released into the local environment in the porous structure of a polysulfide layer created around the inclusion, described in more detail in section 3.1.8. The combination of Cr^{3+} and presence of chloride from the bulk solution in this porous structure will, depending on both the chloride concentration and the dissolution current density, cause local acidification by forming complexes. The chemical dissolution of MnS could also release sulfide into the solution, then leading to critical

conditions by sulfide and pH with the potential of local breakdown of the steel. If the chloride content and the dissolution current density is insufficient to form complexes with Cr^{3+} in the solution, chromium oxy-hydroxides may be precipitated, causing a repassivation and thereby no further attack.

Park and Böhni [13] suggested that during metastable pitting, hydrolysis reactions occurred after dissolved metal ions were released from MnS inclusions. This suggestion was based on pH measurements of the nearby electrolyte of MnS inclusions during metastable pitting on AISI 304 stainless steel, with the use of pH microsensors incorporated into a microcapillary cell. They showed that in chloride environment metastable pits made the pH in the nearby electrolyte decrease from 5.4 to 2, while in a Na_2SO_4 electrolyte, where no pitting was initiated, the pH decreased from 5.6 to 4 when dissolution of the MnS inclusion occurred. This indicated the importance of Cl^- in the electrolyte for creating conditions promoting pitting of the stainless steel after dissolution of inclusions.

When exposing stainless steel in 0.5 M NaCl + 0.5 M H_2SO_4 + 0.08% H_2O_2 Baker and Castle [28] found a local solution composition rich in $MnCl_2$ in the cavity after dissolution of MnS inclusions. They suggested that the precipitation of a $MnCl_2$ salt film will hinder the repassivation of the exposed metal in the cavity and may induce further attack. They suggested that the probability of a pit propagating from dissolution of a MnS inclusion will be directly related to the chloride concentration in the cavity. The chloride concentration is controlled by the amount of Mn^{2+} released from the dissolution and the diffusion of Cl^- to the cavity, thus the size of the MnS inclusion is detrimental for the initiation of pitting after dissolution of the MnS inclusion.

Brossia and Kelly [29] found that aqueous sulfide was produced from the chemical dissolution of MnS inclusions in Type 304 stainless steel in neutral chloride solutions. They found that the production of aqueous sulfide was required to increase the aggressiveness of the occluded solution in a crevice, indicating that these species promoted the initiation of local corrosion.

Williams *et al.* [1] proposed that sulfur-rich compounds was formed when MnS inclusions in stainless steel dissolved. They proposed that the dissolution was catalyzed by chloride and that the current density for the dissolution reaction could be very high. They suggested that the sulfur compounds formed a crust over and around the inclusion and that the very high current density promoted a significant local concentration of chloride under the crust, as a consequence of electro-migration to support the current. The pH would also decrease under the crust as a consequence of the species (e.g. chromium ions) released during the dissolution, providing hydrolysis reactions, further creating conditions under the crust sufficiently extreme to cause depassivation and pitting of the stainless steel.

Krawiec *et al.* [11] showed that MnS inclusions in a 304L stainless steel immediately started to dissolve after immersion in 1 M NaCl. They showed that stable CrS and unstable $FeSO_4$ were formed after the dissolution. They observed pitting on grains close to the inclusions short time after immersion and suggested that these sulfur-containing species promoted depassivation of the stainless steel surface.

Lott and Alkire [27] found that dissolution of MnS in deaerated 0.1N NaCl produced thiosulfate ions, as shown in reaction (4). They found that the presence of both chloride and thiosulfate above critical amounts caused rapid depassivation of 304 stainless steel. These findings were supported by Webb and Alkire [14] who showed

that the presence of thiosulfate in a chloride solution accelerated the dissolution of MnS inclusions and caused pitting on 304 stainless steel. The hypothesis by Lott and Alkire [27] was that initiation of crevice corrosion is caused by entrapped thiosulfate ions formed from the electrochemical dissolution of MnS. Williams *et al.* [1] speculated that sulfide (S^{2-}) could be the product of dissolution at low anodic potentials, while thiosulfate could be the dissolution product at high anodic potentials, supported by measurements of the current during dissolution of MnS inclusions and SEM investigations.

Webb *et al.* [25] proposed that pitting was initiated in a micro-crevice formed by dissolution of the periphery of MnS inclusions. The pitting was initiated after a critical amount of aggressive sulfur species (thiosulfate) and chloride was reached as a result of the dissolution. The investigation comprised of a combination of mathematical modeling and experiments on single MnS inclusions in 304 stainless steels in 1 M NaCl.

Webb and Alkire [30] also detected sulfur species and thiosulfate above dissolving single sulfide inclusions, and addressed these compounds to the dissolution of inclusions. This was performed with the use of small wires of W, Ag and Pt placed within an electrochemical microcell above single sulfide inclusions. They detected sulfur when the sulfide inclusion dissolved chemically at the rest potential in 0.1 M Na_2SO_4, at pH 2. Sulfur species were not detected during polarization in neutral Na_2SO_4. This indicated that the production of sulfur species from the dissolution of inclusions only occurred under acidic conditions at low potentials. Both thiosulfate and sulfur species were detected during oxidation of sulfide inclusions in a microcell. The overall results indicated that the production of thiosulfate was due to electrochemical oxidation of the sulfide inclusion while the production of sulfur species occurred as a result of chemical dissolution under acidic conditions.

Attempts to mathematically model the pitting potential based on the local chemical environment created by products from the dissolution of sulfide inclusions (thiosulfate and hydrogen sulfide) in the presence of chloride ions have been reported by others [31].

From the above investigations it can be summarized that pitting is suggested to be initiated at sulfide inclusions as a result of preferential dissolution of the sulfide. Several reaction sequences for the dissolution of MnS inclusions are proposed. Both the release of metal ions from exposed metal beneath a dissolved inclusion and the release of products from the dissolution of inclusions, e.g. thiosulfate, are suggested to contribute to an aggressive environment in the cavity which can lead to further metal dissolution.

3.1.7. The Role of Protective Films at Inclusions

Oxide films have been observed to play an important role when it comes to sites where pitting potentially is initiated. It is indicated that MnS inclusions may be preferentially attacked due to a poor or lacking protective film.

Wranglén [7] reported that since sulfide inclusions in the surface of stainless steels are not coated with a passivating oxide film, localized attack would start at these sites, particularly in acid solutions.

Rossi *et al.* [9] found, by the use of a highly surface-sensitive Time-of-flight SIMS (secondary ion mass spectroscopy) technique, that inclusions present in a high sulfur stainless steel comprised of both MnS and chromium oxide, and that the MnS part of the inclusion was not covered by an oxyhydroxide film after mechanical polishing, like the rest of the surface of the inclusion and the metal matrix itself. This indicated that MnS inclusions represented weak points against pit initiation in chloride containing environment, because the MnS was not covered by a protective film.

The effect of a protective film on inclusions has also been investigated by others. Muto *et al.* [23] found by the use of Auger electron spectroscopy an oxide film on CrS inclusions after polarization to the transpassive region of the AISI 304 stainless steel in 0.1 M NaCl. This oxide film contained about 40 at% Cr and was thicker than the passive film formed on the metal matrix polarized to the same level, and the oxide film observed on the same inclusions before polarization. Based on these observations they suggested that the oxide film on the surface of CrS inclusions grows with increasing electrode potential, thus preventing anodic dissolution of the inclusions. Also on manganese-rich inclusions containing about 10 at% Cr an oxide film was observed before polarization. This film contained about 10 at% Cr. Based on these observations they suggested that CrS inclusions had an increased resistance to pit initiation compared to the manganese-rich inclusions, because the much lower Cr content of the oxide film formed on manganese-rich inclusions leads to lower protection against dissolution.

3.1.8. Pit Initiation Sites at Inclusions

More detailed studies concerning the actual sites at inclusions where pits are initiated and the reasons why they are initiated have been performed. Discussions have been raised based on the findings and suggestions from several investigations.

Park *et al.* [15] found that pits initiated at the interface of MnS inclusions and the metal matrix on a AISI 304 stainless steel in chloride environment. This was also observed by Muto *et al.* [24]. Baker and Castle [28] observed that corrosive attacks had initiated predominantly at the inclusion edges of MnS, but also observed some few small cavities in the middle of the inclusion. The formation of a micro-crevice was by Webb *et al.* [25] observed between MnS inclusions and the metal matrix when 304 stainless steel was polarized in chloride-containing solutions, indicating pit initiation at the inclusion-matrix boundary. Schmuki *et al.* [10] found that all pitting attacks initiated at MnS inclusions in a DIN 1.4305 stainless steel after immersion in 10% $FeCl_3$ solution, but observed different pit initiation morphologies; Inside the inclusion, around the inclusion and mixed attack. They also found that 40% of the MnS inclusions were not attacked.

Ryan *et al.* [32] proposed an explanation for the initiation of pitting at sulfide inclusions, which deviated from the explanations referred to in previous sections attributing dissolution of the inclusions as the initial step. From investigation of a 316F stainless steel by focused ion beam (FIB) and secondary ion mass spectroscopy (SIMS) methods on a nano-metre-scale, they suggested that a chromium-depleted zone is formed in the steel matrix around the sulfide inclusions during manufacturing of the steel. These assumptions were related to the work performed by Williams and Zhu [33] suggesting that a chromium-depleted zone is formed around the inclusion when the steel cools down during manufacturing. When exposed to a corrosive

environment this chromium-depleted zone then provides rapid metal dissolution, which creates a crevice adjacent to the inclusion. Hydrolysis of dissolved metal ions in contact with water creates an aggressive environment, which in turn may promote dissolution of the inclusion. Then, sulfur products from the dissolution form a crust around the former inclusion, providing an occluded environment which creates an even more aggressive environment for further metal dissolution and stable pitting. Ryan *et al.* [32] doubted on the findings by Eklund [3] and others who suggests that dissolution of the inclusion is the initial step for pitting, by posting that in dilute, neutral environments where pitting can begin, sulfides present in inclusions are themselves passive [32]. The calculations by Eklund [3] showing that MnS inclusions were unstable above -100 mV vs. SHE in chloride environment were also commented by Szklarska-Smialowska [2], mentioning that the calculations were performed for concentrations of Mn species equal to 0.1 mol/L, while for real systems the concentrations are much lower. It was reported that the true equilibrium conditions therefore could differ from the basis of Eklunds calculations.

The conclusions by Williams and Zhu [33] and Ryan *et al.* [32] have later been a topic for discussion. Meng *et al.* [34] investigated the same 316F grade steel (among others) as investigated by Ryan *et al.* [32]. They found, by the use of high-resolution scanning TEM (Transmission Electron Microscopy) and SIMS mapping, no evidence of chromium depleted zones around inclusions.

Also Schmuki *et al.* [10] concluded that a chromium-depleted zone in the metal matrix around MnS inclusions could not be the explanation for pit initiation in stainless steels. They investigated 27 MnS inclusions in a DIN 1.4305 stainless steel in a scanning Auger microscope (SAM) to find no chromium-depleted zone on the matrix side at the inclusions. They also studied 200 MnS inclusions in several samples in SEM before and after immersion in $FeCl_3$ in order to correlate pitting attack with the location in or outside the inclusion. Their results showed that for approximately 20 % of the inclusions pitting had started around the inclusion. For 25 % of the inclusions, the attack took place only inside the inclusion. 40 % of the inclusions remained unattacked, and 10 % showed mixed attack or not clearly defined behavior. Their conclusion was that a chromium-depleted zone could not be the explanation for pit initiation at inclusions, by comparing the fact that approximately 20% of the 200 inclusions showed an attack around the inclusion, possibly indicating chromium depletion here, to the fact that SAM analysis of 27 inclusions did not reveal any chromium-depleted zone. It was therefore statistically very unlikely that the SAM study would have missed such a high number of inclusions having a chromium-depleted zone around them.

A yet later work by Williams *et al.* [4] showed by measurements in SIMS microscopy an iron sulfide-enriched halo at the outer part of MnS inclusions in 316L stainless steels, probably formed during the manufacturing of the steel. They found that this boundary of the inclusions, in addition to FeS, also contained variable amounts of CrS, and that the amount of Cr was lowest in this boundary zone of the inclusion, compared to the rest of it. This demonstrated, as reported by Ryan *et al.* [32], a chromium-depleted zone around the inclusion, but inside the inclusion and not on the metal-side, showing that the work by Ryan *et al.* miss-attributed the variations in composition to the metal-side of the inclusion-metal boundary. Williams *et al.* [4] suggested that some regions of this iron sulfide-enriched halo consisted of a Mn-saturated FeS. They suggested that when FeS is in contact with MnS, FeS will preferentially dissolve in an electrolyte due to the difference in half-cell potentials,

and especially the parts of the halo consisting of Mn-saturated FeS. They surmised that the dissolution of the halo, which leads to a leach of metal cation into the solution, forms a porous metal-deficient polysulfide layer at the inclusion side, in which the porous structure would make electrolyte come in contact with bare steel. In addition, the chromium released from the dissolved inclusion will, depending on both the chromium content in the inclusion and the chloride content in the electrolyte, form either complexes or oxy-hydroxides, which in turn either contributes to local acidification and further attack or to repassivation.

Wranglén [35] also reported a deleterious effect of FeS in combination with MnS inclusions. FeS was reported to be attacked rather than MnS in steels. This is because FeS forms local corrosion cells with steel, attributed to the higher conductivity of FeS than MnS. It was reported that FeS may occur in various amounts in combination with MnS inclusions, determined by the cooling conditions. Welding could favor cooling conditions which may promote an unfavorable composition of the inclusion, i.e. a higher amount of FeS. It was also reported that MnS is on the other hand more soluble in acids than FeS.

Different explanations have been proposed regarding the actual site at inclusions where pitting is initiated. Both the outer part of inclusions and the metal matrix adjacent to the inclusion have been proposed to be the initiation site for dissolution, supported by deviating explanations. The main understanding is that pitting most often is initiated at the outer part of the MnS inclusions. FeS enriched along with MnS inclusions during cooling of the steel have been indicated to have detrimental effects on the initiation of pitting at these inclusions.

3.1.9. The Inclusion Geometry Dependency

The geometry and the orientation of inclusions have showed to play a role in the initiation of pitting and further development of pitting on stainless steels. It has been demonstrated that a critical size of inclusions is required to cause stable pitting.

Webb *et al.* [25] investigated single MnS inclusions in a 304 stainless steel by potentiodynamic sweep experiments in chloride environment. Different behavior was seen on inclusions with different geometries. During the potential sweep of shallow MnS inclusions, dissolution of the inclusions was seen, accompanied by metastable pitting events. Narrow and deep inclusions also dissolved and showed metastable pitting, but at this time the metastable pitting led to stable pitting. They found by SEM investigation that the MnS inclusions did not dissolve uniformly across the inclusion surface but preferentially at the edges. Formation of narrow micro-crevices was observed at the inclusion-metal boundary. By numerically predictions of the depassivation potential of a stainless steel surface, based on critical concentrations of thiosulfate and chloride in the micro-crevice, a critical micro-crevice geometry of 1 µm in depth was found to initiate pitting. This was in agreement with experimental findings.

Baker and Castle [28] proposed that the initiation of metallic corrosion of exposed bare metal in the cavity from a dissolved inclusion is dependent on the concentration of chloride in the cavity. The critical concentration of chloride in the cavity to attain the precipitation of a $MnCl_2$ salt film, which hinders repassivation of the exposed metal, will be determined by the amount of Mn^{2+} released from the inclusion, and thus the

size of the inclusion. Repassivation may occur if the inclusion geometry is insufficient to promote enough Mn^{2+} and chloride to precipitate a $MnCl_2$ salt film.

Ke and Alkire [36] demonstrated the effect of inclusion size on the initiation of pitting. Onset of pitting corrosion was investigated at the site of approximately 200 inclusions in a 304 stainless steel in 0.1 NaCl. They found that growth of pits to a significant size only occurred at MnS and mixed MnS/oxide inclusions which had a size above 0.7 µm. Smaller sulfide inclusions and all multielement oxides either did not initiate pits or initiated only small trenches before becoming repassivated.

Suter and Böhni [20] indicated that an inclusion diameter below 0.8 µm would be required in order to improve the pitting resistance of stainless steels substantially, when correlating the pitting potential and inclusion size in a DIN 1.4301 stainless steel in 1 M NaCl.

3.1.10. Active and Inactive Inclusions

Inclusions have been observed to be both active and inactive regarding the initiation of pitting in the same samples and environments exposed to the same electrochemical conditions.

Wranglén [7] found that sulfide inclusions showed active and inactive behavior when exposing different steel surfaces in 3% NaCl. The casting method of the steel seemed to have an effect on the number of active inclusions.

Böhni *et al.* [12] reported that MnS inclusions in stainless steels were both active and inactive during anodic polarization in chloride-free solution.

Suter *et al.* [17] observed that the inclusions sometimes were active and sometimes inactive when performing potentiostatic and potentiodynamic measurements on single MnS inclusions in 1 M Na_2SO_4. They reported that about one third of the examined MnS inclusions were inactive. Aluminum oxide particles were detected in some active inclusions, but not in inactive inclusions. This indicated that MnS inclusions containing aluminum oxide were active. Suter and Böhni [20] also found that especially mixed oxide/sulfide inclusions behaved active in NaCl compared to pure MnS inclusions, which could be inactive.

As described in section 3.1.8 Schmuki *et al.* [10] studied 200 MnS inclusions in several samples before and after immersion in $FeCl_3$ and found that 40 % of the inclusions remained unattacked, thus showed an inactive behavior.

3.2. Improvement of Corrosion Properties by Removal of Inclusions

In order to investigate the effect of inclusions on the initiation of pitting on stainless steels, methods to remove inclusions from the metal surface have been used. The removal of inclusions makes comparison of the corrosion properties of similar materials with and without inclusions possible. An improvement of the corrosion properties of austenitic stainless steel by the elimination of sulfide inclusions has

been shown in several investigations, thus verifying findings and suggestions referred to in the previous sections.

As described in section 3.1.3 Stewart and Williams [8] demonstrated that a laser treated 304 stainless steel, in which the laser treatment caused surface melting in a depth of 150 – 300 µm causing sulfur-rich inclusions to dissolve and transform to very small spherical particles, showed a markedly reduced nucleation frequency and lifetime of micro-pits compared to an untreated sample. Hence, the pitting resistance was improved by the treatment. They proposed that the pitting resistance was improved because the sulfides created by the treatment were too small to induce pitting.

Also Akgün *et al.* [37] demonstrated the beneficial effect of laser surface melting on the corrosion properties of 304L stainless steel in 3.5 wt% NaCl. After the treatment the pitting potential shifted 145 mV in the positive direction, compared to an untreated sample. They reported that the improved properties due to laser surface melting are attributed to removal and/or redistribution of sulfide inclusions. δ-ferrite in the microstructure was introduced as a result of the heat treatment. It was suggested that sulfur becomes less available for the formation of sulfide inclusions after the heat treatment, because the solubility of sulfur in δ-ferrite is higher than in austenite, resulting in entrapment of sulfur in the δ-ferrite. They also indicated that some of the manganese was evaporated during the laser treatment, and some formed Mn-Si compounds rather than MnS. Mn-Si compounds were stable in acidic solutions. Thus, both the amount of Mn and S available for the formation of MnS was reduced. This was suggested to explain the enhanced corrosion resistance. The improvement of the corrosion properties after laser surface melting was also verified by Conde *et al.* [38]. They showed an increase in the pitting potential on AISI 304 stainless steel in 0.06 M NaCl by at least 500 mV after laser surface melting.

Other methods to eliminate inclusions have also been used. Inturi and Szklarska-Smialowska [39] prepared nanocrystalline 304 stainless steel films by sputter deposition and found that the potential at which the current started to increase rapidly was approximately 850 mV higher than the conventional material when performing potential measurements in NaCl. In this investigation they attributed the improved corrosion resistance of the sputtered film to the nanocrystalline grain size and the high homogeneity of the metal surface.

Ryan *et al.* [40] studied the pitting behavior of sputter deposited pure iron-chromium films in 0.5 M HCl and found no pitting at any potential on alloys with a chromium content above 16 atom%. In a later investigation Ryan *et al.* [41] prepared 304 stainless steel films without sulfide inclusions by sputter deposition. The stainless steel films were found to be significantly more resistant to pit initiation than the conventional material after electrochemical polarization in NaCl and LiCl. They attributed the inhibition of pit initiation in the film to the absence of sulfide inclusions.

Noh *et al.* [22] compared the pitting potentials of 316 samples treated with different solutions of nitric acid from 0.65 wt% to 50 wt% for 1 hour. The pitting potentials were measured in 1 M NaCl at 70 ^{o}C. They showed that the pitting potential varied with the concentration of the nitric acid in the pre-treatment. The pitting potential increased with the concentration of the nitric acid and reached the highest level at a concentration of 20 - 25 wt%. This level was associated with an increase of the pitting potential of about 150 mV compared to an untreated sample. A further increase in

the concentration resulted in a decrease of the pitting potential. They confirmed that the acid treatment removed MnS inclusions from the surface. They also confirmed that the treatment resulted in a chromium enrichment of the passive film of the steel. However, variations in the chromium enrichment in the passive film could not explain the variations in the pitting potential between the samples treated with different nitric acid concentrations. They concluded that the removal of MnS inclusions was the principal factor responsible for the increase in pitting potential after the nitric acid passivation and that the most effective removal was obtained using nitric acid with concentrations of 20 – 25 wt%.

3.3. The Effect of Welding on the Microstructure and Corrosion Properties of Austenitic Stainless Steel

It is well known that the corrosion resistance of stainless steels is significantly decreased during welding. How welding affects the microstructure and how these changes affect the corrosion properties must be understood in order to predict and control the corrosion attack in the weld zone. MnS inclusions have been seen to be detrimental for the corrosion attack on stainless steel in general. The role of MnS inclusions in the initiation of pitting in the weld zone is of particular interest when investigating the reasons for the decreased corrosion resistance at these locations.

3.3.1. Change of the Microstructure in the Weld Zone after Welding

The changes occurring in the microstructure during welding have been the part of several investigations. Both the changes which have occurred in the weld metal, fusion line and in the heat affected zone (HAZ) have been described. Knowledge about the microstructural changes occurring in the metal during welding is important in the understanding of the changed corrosion properties in the weld zone.

The occurrence of δ-ferrite in a cellular dendritic microstructure in the weld metal have been reported in several investigations [42], [43], [44]. The chemical composition of the filler metal is prior to welding modified in order to produce small quantities of 3 – 5 % δ-ferrite in the weld metal of austenitic stainless steels. This is done because fully austenitic stainless steel welds have a high tendency towards hot cracking [42]. The δ-ferrite has beneficial effects in dissolving harmful elements influencing the susceptibility for cracking, such as sulfur, phosphorus and boron in austenite [45] . The occurrence of δ-ferrite in the weld metal has also been observed when no filler metal is used. Rodrigues and Loureiro [42] reported that the melted material consisted of a duplex microstructure of austenite and δ-ferrite after welding plates of AISI 304 and AISI 316 stainless steels using the Tungsten Inert Gas (TIG) welding process without filler metal. They found that the amount of δ-ferrite in the weld metal increased some with the increase of weld heat input and decrease in cooling rate, and was between 10 and 20 %. Some coarsening of the microstructure was also observed in the weld metal. The heat-affected zone showed no δ-ferrite and no specific coarsening.

Lu *et al.* [43] also reported the formation of δ-ferrite in the weld metal after using Gas Tungsten Arc Welding (GTAW) and Laser-Beam Welding (LBW) without filler metal

on 304 austenitic stainless steel sheets. In addition they reported micro-segregation which had occurred in the weld metal when δ-ferrite was formed during cooling, causing the formation of Cr-depleted zones. The micro-segration was reduced with faster cooling rates. They also reported that the microstructure of the base metal and the HAZ observed in an optical microscope was almost the same, except for slightly larger grains in the HAZ.

A sensitized zone was reported by de Lima-Neto *et al.* [46] in a welded AISI 304 stainless steel. Such a zone can be present in the HAZ of austenitic stainless steel, and is characterized by carbide precipitation at grain boundaries and chromium depletion in adjacent regions. The precipitation of chromium carbides will take place at grain boundaries, with the result of chromium depletion in the grains adjacent to these carbides [47]. Lima-Neto *et al.* [46] carried out welding using a shielded metal arc with two different energies: 0.7 kJ mm^{-1} and 2.2 kJ mm^{-1}. No sensitization occurred at the lowest energy input. At the highest energy input, a sensitized zone located between 3 mm and 9 mm from the weld string was detected. It was suggested that the temperature had been between 800 ^{o}C and 400 ^{o}C in this zone, which is the temperature interval in which precipitation of chromium carbide occurs.

The effects of the welding process parameters on the location and size of the sensitization zone in 304 stainless steel welds have been studied by Tsai and Eagar [48]. They made welds using gas tungsten arc welding with argon as the shielding gas and studied the sensitization zone with an optical microscope. An overview comparing the different welding parameters and the location and size of the sensitization zone in 15 welds was presented. They found that in some welds no sensitization had occurred in the transverse direction, thus no surface sensitization contributing to lower corrosion resistance had occurred. A surface free of sensitization was produced when high travel speed and low heat input was used.

Garcia *et al.* [49] prepared weldments on AISI 304 and AISI 316L stainless steel plates with the use of automatic metal inert gas (MIG) with argon as the shielding gas and an AISI 308 filler material. They studied the effect of the welding process on the microstructure of the two stainless steels. The base materials showed an austenitic structure which had some prior cold work in the surface zone and some δ-ferrite stringers in the inner region. AISI 304 had a few chromium carbides, while AISI 316L showed some isolated σ-phase particles. The content of MnS inclusions was very low. In the weld metal the two steels showed a dendritic structure, with a high content of δ-ferrite in the dendritic boundary. In the fusion line a significant decrease in the content of δ-ferrite was observed, while at the end of the fusion line, where the material had melted but not mixed with the weld metal, the quantity of δ-ferrite increased and chromium carbides were observed on austenite grain boundaries. In the HAZ recrystallization and grain growth were observed. In the farther region of the HAZ, where no recrystallization had occurred, some precipitation of chromium carbides was seen.

Silva *et al.* [50] analyzed the microstructure of the HAZ in AISI 316 stainless steel welded plates, welded with three different energy inputs. The presence of a narrow band of δ-ferrite was observed among the austenite grains. The extension of this band increased with increasing welding heat input. They suggested that partitioning of chromium and nickel between ferrite and austenite had occurred when forming δ-

ferrite. In the farther region of the HAZ the presence of spherical particles precipitated in the grain boundaries and the matrix were observed. This area of the HAZ had reached a temperature between 550 and 850 ^{o}C, which contains the temperature interval in which the precipitation of chromium carbides occur. By analysis the particles were verified to be chromium carbides of the $M_{23}C_6$ type.

Mohammadi Zahrani *et al.* [44] reported a δ-ferrite content of 8 % in the fusion zone in the weld zone of a 316L stainless steel pipe which had suffered pitting in a petrochemical plant.

3.3.2. Inclusions in the Weld Zone

The inclusions present in the weld zone have been regarded in some investigations. The knowledge about the inclusions present is an element in the understanding of the changed corrosion properties in the weld zone. The role of sulfide inclusions in the initiation of pitting in the weld zone is of particular interest, knowing their detrimental effect on the initiation of pitting in the base metal.

Wranglén [35] indicated that sulfide inclusions in the weld zone could have a significantly higher Fe/Mn ratio than sulfide inclusions in the base material. This was due to the rapid cooling of the steel, which promotes the precipitation and retainment of FeS along with the MnS inclusions. FeS has been in solid solution with MnS at high temperatures. In normal slow cooling of the steel, the Fe-rich sulfides will react with Mn in the matrix, forming practically pure MnS. By rapid cooling the sulfides rich in Fe will be retained.

In order to prevent stresses in the weld zone post-weld heat treatments may be performed, e.g. at temperatures of 700-850 ^{o}C. This may result in the formation of chromium carbides, as described in section 3.3.1, σ-phases and other types of phases (ϰ, R and η), particularly in the weld metal [51]. Intermetallic phases such as σ, ϰ (chi) and Laves may also be formed in the HAZ caused by critical temperature ranges [50].

Park *et al.* [52] reported the formation of small σ-phases along the grain boundaries in the advancing side of the stir zone of friction stirred welded 304 stainless steel. It was suggested that the σ-phase can be rapidly formed by the transformation of austenite to δ-ferrite at high temperatures and the subsequent decomposition of the ferrite under high strain and recrystallization induced by the friction stirring.

Mohammadi Zahrani *et al.* [44] found in the 316L pipe which had suffered pitting, referred to in section 3.3.1, large inclusions in the HAZ and fusion zone and confirmed by EDS that the inclusions were rich in S, Al and Si.

3.3.3. The Influence of the Atmosphere during Welding

The influence of the atmosphere during welding and how elements from the atmosphere affect the microstructure in the weld zone is of interest when investigating changes in the corrosion properties after welding.

During welding, hydrogen, nitrogen and oxygen may dissolve in the weld metal. This can lead to porosity in the weld metal, or the dissolved elements may combine with elements in the alloy to form inclusions. The elements have different effects in the weld metal; hydrogen induces cracking, nitrogen increases the yield and tensile strength but reduces the ductility, and oxygen promotes the formation of inclusions [53]. A nitrogen adsorption/desorption phenomena may lead to porosity in the weld metal, when dissolved nitrogen rapidly desorbs during solidification of the molten metal after welding [54].

Shankar *et al.* [55] demonstrated that the addition of nitrogen in the shielding gas during welding of 316L stainless steel increased hot cracking susceptibility of the weld metal. Weld metal exposed to nitrogen in the shielding gas during welding showed a tendency for coarsening and side branching of the solidification structure, which increased with higher amounts of nitrogen in the shielding gas.

Kwok *et al.* [56] reported that when using a shielding gas containing N_2 to stabilize austenite, the probability was higher of forming intermetallic precipitates and nitrides in the weld metal, which would decrease the corrosion resistance.

Enerhaug [57] referred to investigations by Vagn Hansen *et al.* [58] indicating that chromium may oxidize to Cr_2O_3 while iron may form less stable oxides such as FeO and Fe_3O_4 during welding of stainless steel when oxygen is present in the atmosphere. Although inert shielding gas is used, oxygen infiltration may still occur in various amounts. The oxygen infiltration will be sufficient to promote the formation of such high temperature oxides.

In the investigation of a super martensitic stainless steel after welding, Enerhaug [57] reported the presence of a colorful and visible oxide covering the surface of the weld zone. The color in the HAZ changed with the distance from the fusion line, and was darkest (dark blue and violet) in a distance of about 6 mm from the fusion line. The different colored bands were ascribed to constructive interference due to variations in the thickness of the iron-chromium oxide layer, and different wavelengths of the reflected light. The oxide layer was also measured instrumentally to be thinnest at about 6 mm from the fusion line.

3.3.4. The Corrosion Properties in the Weld Zone and the Effect of Microstructure and Inclusions

It is well known that the corrosion resistance is significantly reduced in the weld zone of stainless steels compared to the base metal. The attribution of changes in the microstructure and the presence of inclusions to the reduced corrosion resistance after welding have been the focus in several investigations.

Nishimoto and Ogawa [59] summarized different types of corrosion which may occur at stainless steel welds. Among these was weld metal corrosion, which they attributed to either the use of a filler metal with a lower corrosion resistance or, when

using a matching filler metal, the deterioration of the weld metal caused by micro-segregation at the grain boundaries causing precipitation of carbides or an increased amount of inclusions. Corrosion in the HAZ far from the weld metal interface in austenitic stainless steels was also defined. They explained corrosion in this zone to be induced by sensitization caused by the precipitation of chromium carbide at the grain boundaries. HAZ corrosion of stabilized types of austenitic stainless steels in the vicinity of the weld metal was also mentioned. This was explained to be caused by sensitization due the precipitation of chromium carbide, in a narrow mode of attack.

The sensitization in the HAZ leading to intergranular corrosion due to chromium depletion caused by the precipitation of carbides, as mentioned by Nishimoto and Ogawa [59], has been one of the most common observations related to corrosion in the weld zone of stainless steels [60]. As described in section 3.3.1, the precipitation of chromium carbides will take place at grain boundaries, with the result of chromium depletion in the grains adjacent to these carbides [47]. Another common observation is the preferential corrosion of the δ-ferrite in weld metals [60]. Lu *et al.* [43] reported that the weld metal in a 304 stainless steel was very sensitive to localized corrosion after the formation of δ-ferrite along with a high heat input and a slow cooling rate, causing micro-segregation and Cr-depletion.

Kwok *et al.* [56] summarized that the decreased corrosion resistance in weld metals of stainless steel could be due to local compositional variations after solidification, leading to a less stable passive film. The compositional heterogeneities could arise from micro-segregation, element partitioning in solid-state transformation from ferrite to austenite, and precipitation of intermetallic phases, causing Cr-depletion. They attributed the decreased pitting resistance in 3.5% NaCl of an austenitic stainless steel after laser welding to the presence of δ-ferrite in the weld metal.

As described in section 3.1.8 Wranglén [35] suggested that welding could favor cooling conditions which may promote an unfavorable composition of the already existing MnS inclusion, i.e. a higher amount of FeS, thereby increasing the susceptibility for pit initiation at these inclusions after welding.

Garcia *et al.* [49] evaluated the pitting corrosion susceptibility of the different zones in welded AISI 316 stainless steel. The fusion line showed the lowest resistance to pitting and a high anodic dissolution, compared to the other zones, when performing anodic polarization in a solution containing 1 M H_2SO_4 + 5 N NaCl at 30 ^{o}C. They correlated the attack in the fusion line to a high formation of δ-ferrite, promoting Cr-depleted zones which were strongly attacked. Micro-segregation, forming Cr-depleted zones was also explained as the reason for attack in the other zones of the weld.

Mohammadi Zahrani *et al.* [44] reported that the pitting observed in the HAZ and fusion zone boundary of a 316 stainless steel pipe may have been initiated by the existence of large inclusions rich in S, Al and Si, which were observed in the welded area. General corrosion of the fusion zone was also observed. It was suggested that this was caused by the galvanic effect between Cr-rich inter-dendrite δ-ferrite and Ni-rich cored austenite which were present in this zone. They also suggested that the observed general corrosion could have triggered the initiation of pitting in this area.

Cui and Lundin [45] performed pitting immersion tests on 316 austenitic stainless steel weld metals in 3% $FeCl_3$ solution. The welds were produced using shielded metal arc welding. 316H weld metals showed higher corrosion resistance that 316L weld metals. This was attributed to the lower manganese content of the 316H, which gives fewer MnS inclusions. It was also observed that the initial corrosion attack on the 316 stainless steels occurred in austenite as opposed to ferrite which also was present in the microstructure. The attack in the austenite was attributed to chromium-depletion in cell cores in the austenite due to micro-segregation and coring in the cellular dendritic microstructure formed in the weld metal.

The formation of σ-phase in the HAZ exposed to temperatures of 700^{o}C – 1000^{o}C, resulting in a Cr-depleted zone around the σ-phase was identified as a reason for the reduced pitting resistance in steels with high Cr and Mo content by Nishimoto and Ogawa [59].

Park *et al.* [52] found that the advancing side of the stir zone in a friction stir welded 304 stainless steel was corroded significantly. It was suggested that the formation of σ-phase and the depletion of Cr at the grain boundaries caused the decreased corrosion resistance in this zone.

As referred by Enerhaug [57], Vagn Hansen *et al.* [58] studied the relationship between the oxygen content in the shielding gas during welding and the corrosion resistance of CRA (Corrosion Resistant Alloy) weldments. They indicated that beneath the oxides formed during welding, described in section 3.3.3, a metal layer of typical thickness 1–1.5 grain diameters had been depleted in chromium due to the formation of chromium oxides. It was believed that the chromium depletion contributed to the reduced corrosion resistance associated with welds.

Enerhaug [57] found that the heat affected zone in a super martensitic stainless steel in a distance of about 6 mm from the fusion line was the weakest regarding the initiation of pitting. The attack was seen as distributed pits, which were clearly most frequent at this distance. This was also where the iron-chromium oxide film formed during welding was thinnest. The localized corrosion was thought to be initiated by a crevice corrosion mechanism beneath the oxide, after spalling of the oxide. Removal of the surface layer resulted in a corrosion behaviour similar to the base metal. Thus, the observed gradients in the microstructure across the HAZ seemed not to be the primary cause of the increased susceptibility to localized corrosion in the weld zone of the super martensitic stainless steel. Chromium depletion below the surface layer, as indicated by Vagn Hansen *et al*. [58], was believed to contribute to the initiation of localized corrosion in this area.

3.3.5. Other Factors Influencing the Corrosion Properties in the Weld Zone

Other factors like internal stresses and the composition of the weld metal have shown to influence the corrosion properties in the weld zone.

Chemical breakdown of the oxide films due to an increased concentration of Cl^- anions have been seen to decrease the pitting potential in the weld zone. In welds, internal stresses in local areas may be produced, causing the migration of Cl^- anions to these areas. This will further cause localized attack by the aggressive electrolyte made as a result of the increased concentration of Cl^- [60].

Pujar *et al.* [61] studied the effect of chemical composition on the electrochemical properties in the weld metal of 316 stainless steel by adding alloying elements during welding. The electrochemical properties were measured with anodic polarization in 0.5 M H_2SO_4 + 0.1 g/L NH_4SCN. It was seen that the electrochemical parameters like the pitting potential and the corrosion rate of the weld metal were strongly dependent of the alloy chemistry. The addition of Cr and Mo to the weld metal enriched the δ-ferrite content, simultaneously raising the level of micro-segregation of Cr and Mo at the δ-ferrite – austenite interface boundaries. It was suggested that the ferrite content strongly influenced the electrochemical parameters.

In the investigations referred to in the above sections, several microstructural changes occurring during welding have been described, and explanations for the decreased corrosion resistance in the weld zone compared to the base metal has been given. The formation of δ-ferrite in the weld metal has been reported, and the amount of δ-ferrite is seen to be dependent on the cooling rate. A sensitized zone characterized by carbide precipitation at grain boundaries and chromium depletion have also been detected in the HAZ. Both phenomena have been described to decrease the corrosion resistance in the weld zone, mainly due to the effects of micro-segregation and chromium depletion. The presence of an increased amount and size of inclusions has also been suggested to promote corrosion attack in the weld zone. Several types of inclusions or precipitates have been identified in the HAZ. It has been indicated that welding may influence the composition of sulfide inclusions, increasing the content of FeS in the inclusions. Elements from the atmosphere when the shielding gas is insufficient or lacking have been regarded. Elements as oxygen and nitrogen can induce porosity and promote the formation of inclusions and other precipitates in the weld zone, further contributing to a reduced corrosion resistance. The formation of chromium oxides during welding may cause a chromium depleted metal layer, which combined with a thin oxide film in a particular distance from the fusion line, would lower the corrosion resistance in this part of the HAZ. Internal stresses causing migration of Cl^- anions to the surface of the weld zone and the amount of alloying elements in the weld metal is other factors which both have been mentioned to decrease the corrosion resistance in the weld zone.

3.4. Discussion of Reviewed Literature

It is a common agreement in the literature that pitting seems to start almost exclusively at sulfide inclusions in austenitic stainless steels, and that the manganese sulfides are the most detrimental. Thus, MnS inclusions have been the main focus of the investigations regarding the initiation of pitting at inclusions. The preferential attack on MnS inclusions can still be discussed. Even though MnS inclusions have been observed to be the main initiation site, initiation has also been seen to happen at other types of inclusions. Szklarska-Smialowska [2] referred to several investigations which had found that pitting was initiated at both oxides, sulfides, silicates and precipitates of carbides and carbonitrides. The experiments had been carried out in mixed NaCl and $K_3Fe(CN)_6$ solutions. Baker and Castle [21] found that pitting had initiated at the oxide inclusion/metal matrix boundary on mixed Ti/Mn/Cr/Al oxide inclusions after exposure in 0.5 M H_2SO_4 + 0.5 M NaCl + 0.08% H_2O_2. These investigations indicate that initiation of pitting is likely to occur at other types of inclusions as well. However, most of the reported preferential attacks at MnS inclusions in other investigations referred to in the present review have been in NaCl solutions, which may not be a comparable environment to the mixed solutions of NaCl, $K_3Fe(CN)_6$, H_2SO_4 and H_2O_2 used in the experiments mentioned above.

Initiation at CrS inclusions have been observed by Muto *et al.* [23]. The initiation happened after the stainless steel was polarized up to the transpassive potential region. They also observed initiation at oxide inclusions in 8M LiCl solutions [24]. Also, at high chloride concentrations and high temperatures numerous other initiation sites than MnS inclusions in the metal matrix were observed by Park *et al.* [15] on a 304 stainless steel surface. At the same time, as described in section 3.1.4, both oxides and CrS have shown an inert behaviour in 0.1 - 1 M NaCl solutions at normal temperatures in the passive potential range of the stainless steel when MnS inclusions initiated pitting. It appears that MnS is the main initiation site in environments close to natural seawater, while in more extreme environments like solutions with increased concentrations of chloride and at high potentials and temperatures, initiation can occur more often at other types of inclusions as well.

It has been indicated that especially MnS inclusions physically associated with another type of inclusion, e.g. an oxide, are preferred sites for pit initiation, compared to pure MnS which sometimes also have shown to be inactive. The detrimental effect of mixed inclusions may be explained by galvanic effects inside the inclusion, promoting the dissolution of the least noble element, i.e. the MnS part. Galvanic effects due to the difference in half-cell potentials between the different parts of the mixed inclusion could be explained by the assumption that MnS may not be covered by an oxide film, as opposed to the rest of the inclusion. The galvanic effects may be supported by Wranglén [7]. He suggested that preferential adsorption of Cl^- onto the surface of the inclusions, further causing anodic dissolution of the MnS, happened due to the higher electron conductivity of the inclusion compared to the surrounding oxide film. Here the electron conductivity of the MnS was compared to the surrounding oxide film, but the same situation could also be adapted to the internal of mixed inclusions.

An explanation why MnS inclusions is the preferential site for pit initiation both in mixed type of inclusions and compared to other inclusions was proposed by Rossi *et al.* [9]. They observed that the MnS part of mixed types of MnS and chromium oxide

inclusions was not covered by a protective oxide film, as was the case for the chromium oxide part of the inclusions, and the metal matrix. In another study Muto *et al.* [23] suggested that CrS had an increased resistance to pit initiation compared to MnS inclusions because they were covered by a much thicker and chromium-containing oxide film than MnS. While Rossi *et al.* [9] reported no visible protective film on MnS, a protective film on MnS was reported by Muto *et al.* [23], though this was much weaker than the film covering CrS and the metal matrix. Different detection methods may explain their different observations; Rossi *et al.* [9] used a highly surface-sensitive Time-of-flight SIMS technique, while Muto *et al.* [23] used Auger electron spectroscopy to investigate the surface of the inclusions. Nevertheless, their observations indicate an explanation of why MnS inclusions are preferentially attacked.

The electrochemical behaviour of MnS inclusions have been studied and the electrochemical dissolution of MnS in the passive potential region of the stainless steel have been suggested to be the first step in the initiation of pitting. As described in section 3.1.5, Eklund [3] used thermodynamic calculations and a potential – pH diagram, as seen in Figure 1, to show that MnS could not exist at potentials higher than -100 mV vs. SHE in a pH range between 4.8 and 13.8. The calculations were based on ion concentrations of 0.1 mole/liter. The calculated potential value was also supported by calculations performed by Wranglén [7]. This calculated potential value for the dissolution of MnS as an initial step for the initiation of pitting has raised some discussions. Ryan *et al.* [32] commented on Eklunds calculations and posted that in dilute, neutral environments where pitting has been seen to initiate, sulfides as present in inclusions are themselves passive. Based on this claim they questionized Eklunds findings. A basis for this claim was however not presented. Potential levels where MnS inclusions have started to dissolve have later been measured in electrochemical experiments. Suter *et al.* [17] found using potentiodynamic polarization that a MnS inclusion dissolved in a potential range of 400 – 600 mV vs. SCE. They also found MnS inclusions dissolving at 300 mV vs. SCE with potentiostatic measurements. The potential levels of 300 mV and 400 mV vs. SCE corresponds to 541 mV and 641 mV vs. SHE, respectively [62]. Compared to the calculated value of -100 mV vs. SHE for the dissolution of MnS by Eklund [3] and Wranglén [7], these observed values are significantly higher. Also Eklund [3] performed experiments where MnS was polarized to 200 mV vs. SHE in an air-free unbuffered 0.1 M NaCl solution, resulting in dissolution of the MnS. He did not demonstrate that MnS inclusions dissolved at a potential as low as the suggested theoretical calculated value, thus the calculations are not verified with experiments. As commented by Szklarska-Smialowska [2], the concentrations of Mn or (Mn,Fe) in real systems are much lower than the concentrations used as basis for Eklunds calculations. The true equilibrium conditions could therefore differ, and give other values for the potential at which MnS becomes thermodynamically unstable. Thus, it has been verified that dissolution of MnS inclusions occur in the passive potential region of stainless steels, but there is still some uncertainty about which potential level the dissolution could start.

As described in section 3.1.6 Wranglén [7] suggested that the initial step for the initiation of pitting was dissolution of the sulfide, and that this was a result of the preferential adsorption of chloride ions onto the surface of the inclusions. As seen in several investigations the dissolution of MnS inclusions is indicated to be the initial step for the initiation of pitting in chloride containing solutions. However, dissolution of

MnS is also observed in non-chloride containing solutions, e.g. as showed by Suter *et al.* [17], without the initiation of pitting. These results show that the adsorption of chloride ions may not be the reason for the initial dissolution of MnS inclusions. The dissolution due to the instability of MnS above a certain potential, as suggested by Eklund [3], then seems to be a more likely explanation.

As proposed by Williams *et al.* [1] the dissolution of MnS may be catalyzed by an increased presence of chlorides, after the dissolution process has been started. In combination with the by Wranglén [7] suggested preferential adsorption of chloride ions onto the MnS surface, due to a higher electron conductivity compared to the surrounding oxide film, this seems likely. In section 3.1.6 it is also referred to Eklund [3], who suggested that dissolution of the sulfides would take place at the boundary of the inclusion because the electronic conductivity of the sulfides is lower than for the rest of the metal matrix. It may seem conflicting that Wranglén [7] describes the MnS to be more conductive than the surrounding oxide film, while Eklund [3] described MnS to be less conductive than the metal matrix and that both effects promote the dissolution of MnS. This is however not necessarily conflicting because the oxide film will have different electric properties than the metal matrix. The charged Cl^- ions from above the surface will choose the surface with the highest conductivity and then promote further dissolution by contributing to an aggressive environment, while the dissolution of MnS due to the electrochemical polarization of the metal would initiate as a result of the electrical contact between the inclusion and the metal matrix below the oxide.

The dissolution of inclusions to release products into the electrolyte, contributing to an increased aggressiveness of the electrolyte in combination with the presence of chlorides has been observed in several investigations. The release of certain products appears from the reviewed literature to be a crucial factor for further attack, by increasing the aggressiveness of the electrolyte and hinder repassivation of the exposed metal revealed by the dissolved inclusion. Sulfur containing species such as CrS and $FeSO_4$ has been reported, as well as aqueous sulfide, thiosulfate, elemental sulfur and metal ions like Mn^{2+}, Cr^{3+} and Fe^{2+}. The variation in the observed products could be caused by environmental factors, e.g. the pH level of the electrolyte and the temperature promoting the release of different species. Also the degree of polarization and the adjoining pH level can influence the type of products released from the dissolution of MnS inclusions, as demonstrated with the potential-pH diagram presented by Eklund [3] in Figure 1. This can be supported by discussions by Williams *et al.* [1] who speculated that sulfide (S^{2-}) could be the product of dissolution at low anodic potentials, while thiosulfate could be the dissolution product at high anodic potentials. The different observations could also be explained by the different detection methods used to identify these products. Finally, the composition of the steel and the inclusions themselves will be important.

Ryan *et al.* [32] and Williams and Zhu [33] suggested that a chromium-depleted zone in the metal matrix around sulfide inclusions, originated from the manufacturing of the steel, could cause metal dissolution and be the reason for the initiation of pitting. Their suggestion was that pit initiation started on the metal side of the inclusion-matrix boundary and not as a result of dissolution of the inclusions, which is a common understanding. This could be an argument when discussing the proposals by others, saying that initiation starts with the dissolution of inclusions. However, their suggestions were later rejected by several researchers, as described in section 3.1.6, even by Williams *et al.* [4]. They concluded that a chromium-depleted zone was

present, but inside MnS inclusions, at its periphery. Also statistics, presented by Schmuki *et al.* [10], indicates that pitting do not usually initiate at the metal side of the inclusion-matrix boundary. In addition, it appears from several investigations that MnS is much more unstable than other inclusion compounds and the metal matrix itself.

Knowing their detrimental effect on the initiation of pitting in general on stainless steel, the role of sulfide inclusions, in particular MnS inclusions, in the decreased corrosion resistance developed during welding is of interest. Whether any changes occurring in the MnS inclusions during welding influence the corrosion properties in the weld zone, or whether the reduced corrosion resistance in the weld zone only is caused by other changes in the microstructure are questions that can be raised. Wranglén [35] indicated that the composition of sulfide inclusions could be changed during welding due to an unfavorable heating cycle, promoting the precipitation of FeS along with the MnS inclusions, which would not happen at normal slow cooling of the steel. The deleterious effect of FeS in combination with MnS inclusions on the initiation of pitting has, as described in section 3.1.8, been suggested by Williams *et al.* [4] and Wranglén [35]. This indicates that sulfide/MnS inclusions may contribute to a reduced pitting resistance in the weld zone by a changed composition after the welding, leading to a more unstable inclusion, which can further dissolve and expose bare metal to the environment.

Mohammadi Zahrani *et al.* [44] reported large inclusions containing S, Al and Si in the HAZ and fusion zone of welded 316L, and attributed these inclusions to the initiation of pitting. They did not report the presence of inclusions in the base metal or whether the observed inclusions in the weld zone were larger than inclusions in the base metal. If this was the case, one could suggest that the size of inclusions could have increased compared to the base metal, as a result of the heat treatment during welding. The larger inclusions may lead to a higher susceptibility for the initiation of pitting, as described by the geometry dependency in section 3.1.9.

In general, literature regarding the influence of sulfide inclusions on the corrosion properties in the weld zone and whether the inclusions are changed during the welding process, thereby affecting the pitting resistance, is lacking.

As described in section 3.3.4, other types of precipitates have been attributed to the reduced corrosion resistance in the weld zone. These are mostly σ-phases and chromium carbides. The contribution to the reduced corrosion resistance has not been described to be caused by the precipitates themselves, but the chromium-depletion in the metal matrix adjacent to the precipitates, occurring when these were formed during cooling. Thus, an indirect contribution of these precipitates has been reported.

The other main reason reported in several investigations to reduce the corrosion resistance in the weld zone is the formation of δ-ferrite, both observed in the weld metal and the fusion zone, and also in the HAZ, as reported by Silva *et al.* [50]. Nevertheless, it has been reported by Akgün *et al.* [37] that the introduction of δ-ferrite after laser surface melting of an 304L stainless steel surface improved the pitting resistance. This was suggested to be caused by the higher solubility of sulfur in the δ-ferrite, making sulfur less available for the formation of sulfide inclusions. The observation that δ-ferrite dissolves sulfur has also been reported by Cui and Lundin [45]. The introduction of δ-ferrite was however not the complete explanation by Akgün *et al.* [37] for the improved pitting resistance, as they also reported that some

manganese was evaporated during the treatment, thereby reducing the amount of MnS inclusions. It is important to point out that this was not a welding situation. Still, the behaviour of the δ-ferrite in the weld zone may be described from this observation. It is thus indicated that the introduction of δ-ferrite may reduce the amount of MnS inclusions. In the areas containing δ-ferrite after welding, other effects than the presence of MnS inclusions must therefore explain the reduced corrosion resistance observed in this part of the weld zone. It has been reported in several investigations that when δ-ferrite is formed, chromium depleted zones are introduced. Silva *et al.* [50] suggested that partitioning of chromium and nickel would occur between the ferrite and austenite when forming δ-ferrite. Mohammadi Zahrani *et al.* [44] suggested that galvanic effects between the Cr-rich inter-dendrite δ-ferrite and Ni-rich cored austenite would occur. It seems therefore that the segregation causing chromium depleted zones is the explanation for the reduced corrosion resistance introduced by the δ-ferrite. Based on the reviewed literature in the present report, the introduction of chromium depleted zones also seems to be the main explanation for the reduced corrosion resistance in all areas of the weld zone, e.g. in the sensitized zone described in section 3.3.1. Also some other factors like internal stresses and the composition of the weld metal are in section 3.3.5 described to influence the corrosion properties in the weld zone. This shows that the corrosion properties in the weld zone are influenced in a complex manner by many contributing factors. The effect of inclusions, particularly MnS, needs to be investigated in order to clarify its contribution to the initiation of pitting in the weld zone of stainless steels.

It is indicated from the above discussions that for austenitic stainless steel base metals, dissolution of MnS, with the contribution of released products, is more probably to be the explanation for the initiation of pitting in environments close to natural seawater than other suggested mechanisms, and that it is the instability of MnS when polarized electrochemically which makes these inclusions the preferential site for pit initiation. There are however still discussions about the mechanisms causing the initiation of pitting at inclusions, whether it is the dissolution of MnS inclusions or other explanations.

A goal of the experimental work performed along with the present report is to obtain results which could be compared to or verify findings and suggestions from the reviewed literature regarding the initiation of pitting by inclusions. The observations showing that MnS is the preferential site for the initiation of pitting in austenitic stainless steel will be tried recreated. A goal is also to verify the hypothesis saying that dissolution of MnS inclusions occur prior to the initiation of pitting.

In general, literature regarding the influence of sulfide inclusions on the corrosion properties in the weld zone of stainless steels is lacking. The effect of inclusions, particularly MnS, needs to be investigated in order to clarify its contribution to the initiation of pitting in the weld zone of stainless steels. Another goal of the experimental work is thus to obtain results which can give knowledge about the effects of MnS inclusions on the corrosion properties and the initiation of pitting in the weld zone of an austenitic stainless steel.

As there have been suggested several different explanations for the reduced corrosion resistance in the weld zone, caused by microstructural changes, the corrosion behaviour and the microstructural changes in the weld zone in general and compared with the base metal will be investigated.

It has been seen that when oxygen and nitrogen is present in the atmosphere during welding, this can further reduce the corrosion resistance in the weld zone. The effect of a lacking inert shielding gas during welding on the microstructure and pit initiation by inclusions in the weld zone will also be investigated.

4. Experimental Work

The first goal of the experimental work was to obtain results which could be compared to or verify findings and suggestions from the reviewed literature regarding the initiation of pitting by inclusions. A part of this work was to try to recreate the observations showing that MnS is the preferential site for the initiation of pitting in austenitic stainless steel. The hypothesis saying that dissolution of MnS inclusions occur prior to the initiation of pitting was also tried verified.

A second goal of the experimental work was to obtain results which could give knowledge about the effects of MnS inclusions on the corrosion properties and the initiation of pitting in the weld zone of an austenitic stainless steel. Along with this, the corrosion behaviour and microstructural changes in the weld zone in general and compared with the base metal were studied. A part of the work was also to study the effect of a lacking inert shielding gas during welding.

Samples of a 316L stainless steel were first examined in SEM to study the microstructure and to identify inclusions. Then, some samples were welded, followed by SEM examination. Then all samples were polarized electrochemically with the purpose of initiating pitting. After the polarization, all samples were examined in SEM again to correlate pitting attack to inclusions and to compare microstructural changes and the corrosion behaviour in base metal and welded samples.

4.1. Methods

Cylindrical samples with a height of 10 mm and a diameter of 20 mm were cut off a 316L stainless steel rod. The samples were embedded in an epoxy cast using Epo-Fix. This was done so that the sample surface which was to be exposed to an electrolyte during the electrochemical polarization could be controlled. In order to obtain electrical contact between the sample and the potentiostat during the polarization, a screw was attached to the backside of the sample, through the epoxy cast.

Two samples for welding, with dimensions 87.5 x 11.0 x 10.5 mm were machined from the same 316L stainless steel rod.

Prior to the SEM examination the exposed surface of the cylindrical base metal samples and one side of each of the welding samples were polished. Recognisable markings were scratched onto the polished surface, so that inclusions, specific microstructures and areas of interest found in the SEM examinations could be relocated later.

A Hitachi S3400N SEM was used to examine the sample surfaces in all stages of the investigation. Energy-dispersive X-ray Spectroscopy (EDS) was used to identify

inclusions and other elements in the surface and to find the composition of the metal matrix.

In order to study the effect of MnS inclusions on the pitting potential, both in the base metal and the weld zone, some samples were prior to polarization and welding immersed in 25 wt% nitric acid for one hour. The treatment was performed in the same way as described by Noh *et al.* [22] to remove MnS inclusions from the surface. One cylindrical base metal sample and the half length of the two welding samples were immersed in the acid. The surfaces were rinsed with ethanol and distilled water after the acid treatment.

Welding was carried out using the TIG (Tungsten Inert Gas) process, with argon as the shielding gas for one of the samples. For the other sample, no shielding gas was used. This was done in order to study the effect of a lacking inert shielding gas during welding. A weld was laid on the surface at the middle of the samples, perpendicular to the length of the sample, using 316L as the filler metal. The following welding parameters were employed: current 60 A, voltage 9 V, welding time 5 s, weld length 10 mm.

A third, cylindrical sample was later welded using the TIG process with a mixture of argon and helium as the shielding gas. The filler metal was 316L. The following welding parameters were employed: current 26 A, welding time 6 s, weld length 10 mm. The voltage was unknown.

Prior to the electrochemical polarization, the two long welded samples were cut along the weld direction in two pieces, each containing one heat affected zone to be tested electrochemically. The other unpolished surfaces of the welding samples to be immersed in the electrolyte, but not to be studied, were prior to the polarization pickled with a mixture of nitric acid and hydrofluoric acid for 5 minutes.

For the electrochemical polarization an electrochemical cell, consisting of three electrodes, was set up. The 316L sample (working electrode) and a platinum wire (counter electrode) was immersed in the electrolyte and connected to a saturated calomel reference electrode (SCE) by a salt bridge. Synthetic seawater at room temperature with a pH of 7.5 was used as electrolyte. The electrolyte was deoxygenated by nitrogen gas circulating through the closed system prior to the polarization. The electrodes were connected to a Gamry Reference600 potentiostat, which was controlled by a computer.

For the electrochemical polarization, cyclic voltammetry was chosen as the test method. The initial potential was -250 mV vs. SCE. The samples were then polarized cathodically to -500 mV vs. SCE and then polarized anodically until the current started to increase rapidly, indicating that a corrosion process had been initiated. At this potential the polarization was stopped. The potential was altered with a rate of 1 mV s^{-1}. The sample surfaces were rinsed with ethanol and distilled water immediately after the polarization was ended.

5. Results

5.1. Initial Investigations

To identify the composition of the 316L stainless steel used in the experiments, EDS was used in 6 random areas in two samples to measure the composition of the metal matrix. The measurements are given in Table 1.

Table 1 Measured content of elements in the metal matrix with EDS [wt%]*

Element	Area 1	Area 2	Area 3	Area 4	Area 5	Area 6
Si	0.64	-	-	-	-	-
Cr	16.92	16.73	18.57	15.79	17.26	17.87
Fe	66.92	71.86	69.16	68.66	71.38	68.53
Ni	12.78	11.51	12.28	12.50	11.36	13.60
Mo	2.74	-	-	-	-	-
S	-	-	-	-	-	-
Mn	-	-	-	3.04	-	-

*The EDS also measured various content of carbon originating from the environment. The measured carbon content is in this table compensated for by adding it to the iron content.

The average value of the Cr and Ni content was 17.19 wt% and 12.34 wt%, respectively.

Several samples were prepared in order to compare the microstructure and the corrosion properties of the base material and the heat affected zone along with the effect of MnS inclusions removed from the surface and the effect of a lacking shielding gas during welding. The samples were called base metal samples and weld samples.

Figure 2 - Figure 5 show SEM images of the typical microstructure in different samples, and typical inclusions present in the surface. The surface of the samples used to study the base metal is oriented perpendicular to the length of the steel rod they were cut from, while the surface of the samples prepared for welding is oriented longitudinal to the length of the same rod. Table 2 and Table 3 give the measured content of elements in the inclusions shown in Figure 4 and Figure 5. The weld samples have not yet been welded.

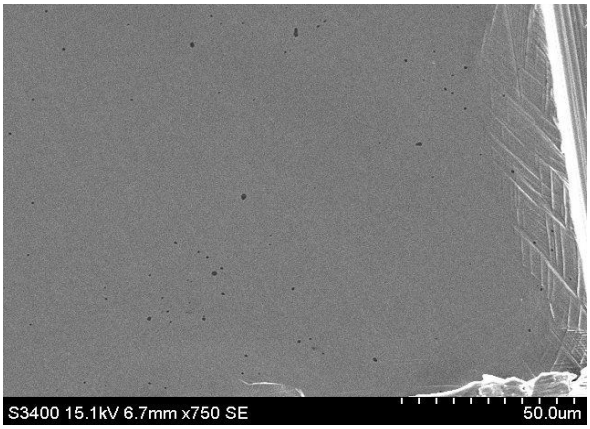

Figure 2 Typical microstructure of base metal sample.

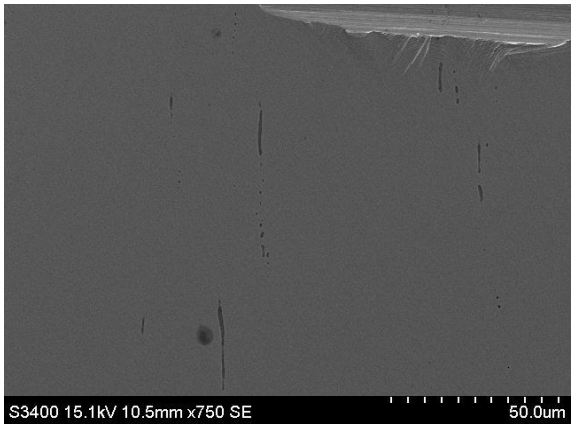

Figure 3 Typical microstructure of weld sample.

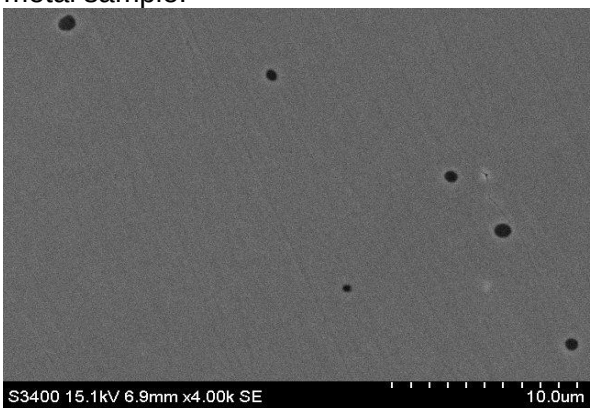

Figure 4 Typical inclusions in base metal sample.

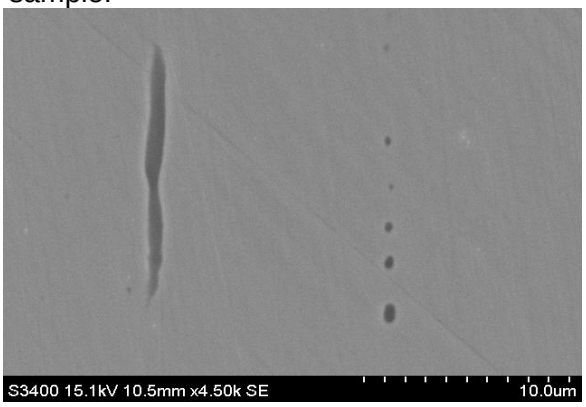

Figure 5 Typical inclusions in weld samples.

Table 2 Measured content of elements in a typical inclusion in base metal sample*.

Element	Wt%
Si	0.32
S	19.36
Cr	10.89
Mn	35.34
Fe	29.64
Ni	4.45
Total:	100.00

Table 3 Measured content of elements in a long inclusion in weld sample.

Element	Wt%
Si	-
S	19.44
Cr	7.38
Mn	42.09
Fe	25.24
Ni	5.86
Total:	100.00

* As the EDS is expected to measure down to about 5 µm below the surface, elements from below the inclusions will also be detected. This is relevant for all reported EDS measurements in this work.

In the surface oriented perpendicular to the length of the steel rod, spherical inclusions can be seen, while in the surface oriented longitudinal to the length of the same rod, both long inclusions and small inclusions oriented in the longitudinal direction of the rod can be seen. The EDS measurements show that the inclusions are rich in sulfur and manganese.

In order to later compare the corrosion properties of samples with and without MnS inclusions in the surface, the acid treatment to remove MnS inclusions from the surface as described by Noh *et al*. [22] was first performed on a base metal sample. In Figure 6 and Figure 8 an area in the sample is shown before and after the surface treatment (immersion in 25 wt% nitric acid for one hour). Figure 7 and Figure 9 show

a single MnS inclusion in the same surface. The measured content of elements in the inclusion centre before the treatment, and the inclusions centre, the inclusion edge and the metal matrix after the acid treatment is given in Table 4.

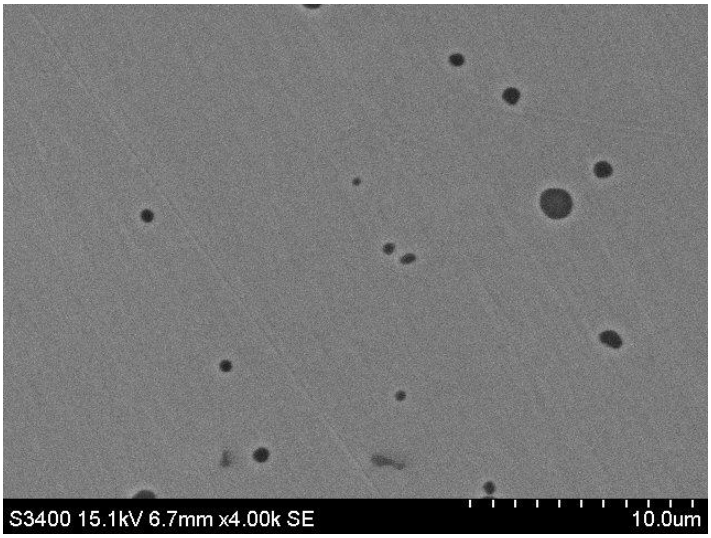

Figure 6 Inclusions in base metal sample before acid treatment.

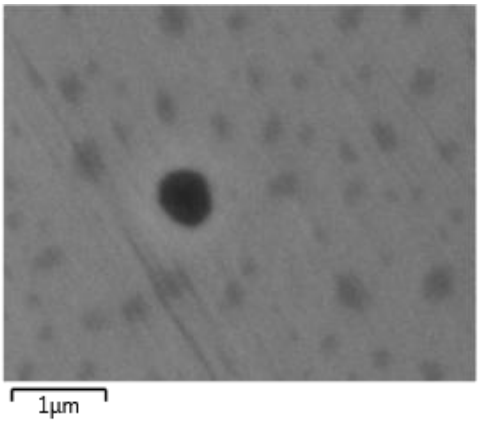

Figure 7 Single inclusion before acid treatment.

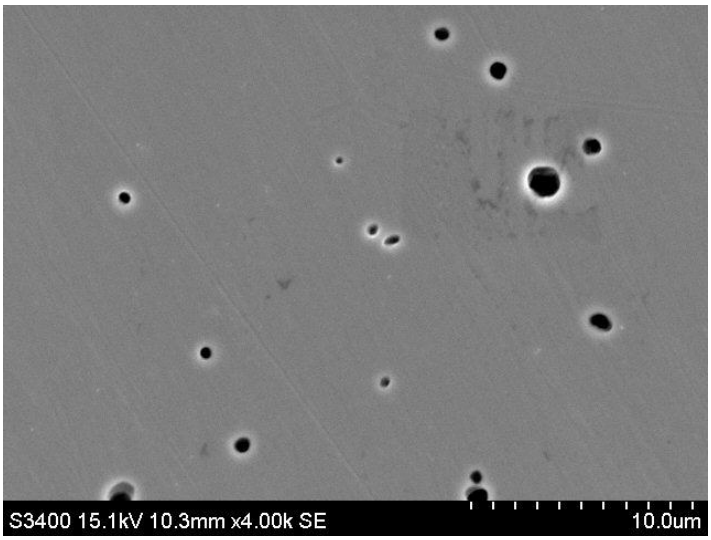

Figure 8 Inclusions in base metal sample after acid treatment.

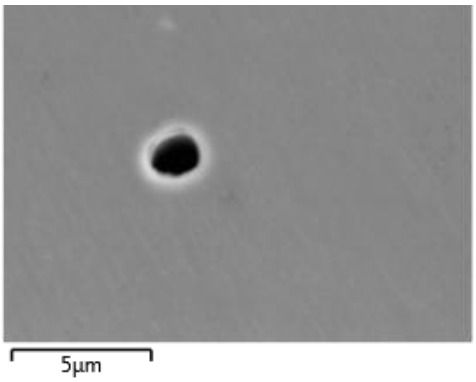

Figure 9 Single inclusion after acid treatment.

Table 4 Measured elements in inclusion and matrix in base metal sample after acid treatment.

Element	Inclusion centre before acid	Inclusion centre after acid	Inclusion edge after acid	Matrix after acid
F	-	-	0.88	2.48
Si	-	-	0.30	0.61
S	16.44	-	1.64	-
Cr	10.73	21.75	18.71	17.10
Mn	38.19	2.32	1.82	1.67
Fe	34.64	68.49	64.92	64.86
Ni	-	7.44	10.64	11.21
Mo	-	-	1.09	2.07

It can be seen in Figure 8 that the inclusions have dissolved during the acid treatment. Table 4 show that sulfur is not measured in the centre of the inclusion after the acid treatment, but in a minor amount at the edge. The measured content of chromium has increased from 10.73 wt% to 21.75 wt% in the inclusion centre, while the manganese content in the inclusion centre has decreased from 38.19 wt% to 2.32 wt%.

Two samples for welding were also treated with acid. This was done by immersing the half length of the samples in 25 wt% nitric acid for one hour. The treatment was performed in this way in order to later be able to compare the corrosion properties on both sides of the weld, where both sides thus have experienced the same welding conditions, but where MnS inclusions has been removed on one of the sides before welding. After the acid treatment, the samples were welded. Figure 10 - Figure 13 show examples of areas and inclusions in the surface of both the treated and untreated half length of the weld samples, before the immersion and then again after the welding. For the different areas, the distance from the fusion line is used to indicate the location of the areas.

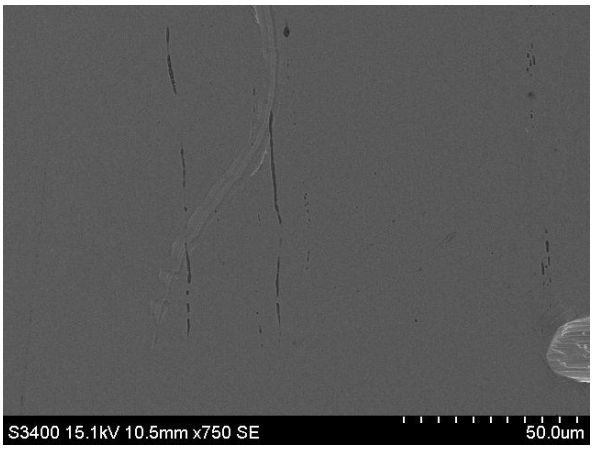

Figure 10 Area at 8 mm from the future fusion line before acid treatment and welding.

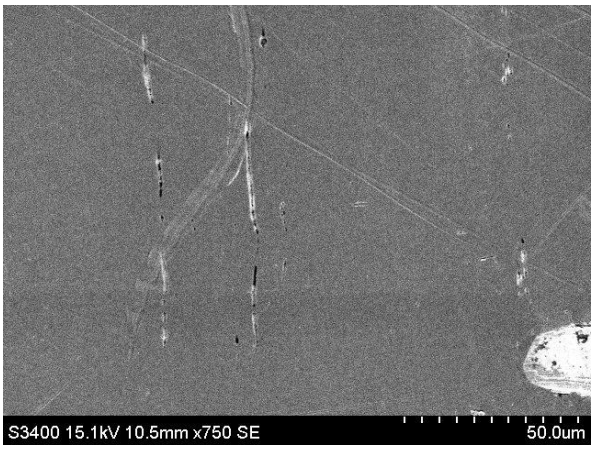

Figure 11 Area at 8 mm from the fusion line after acid treatment and welding, on the acid-treated side of the sample.

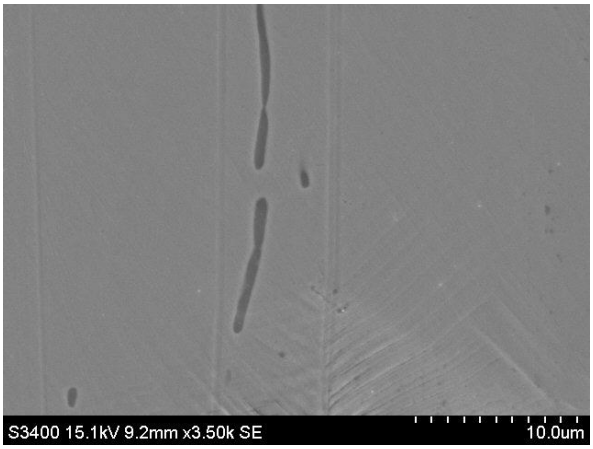

Figure 12 Inclusions located 16 mm from the future fusion line before welding.

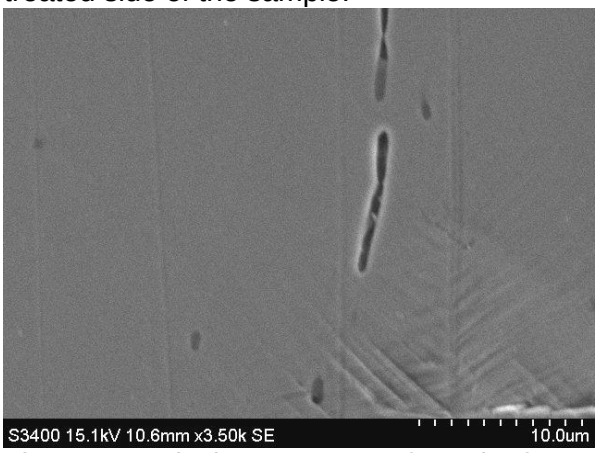

Figure 13 Inclusions at 16 mm from the fusion line after welding, on the side of the weld sample not treated with acid.

It can be seen in Figure 10 and Figure 11, which show an area 8 mm from the fusion line immersed in acid prior to the welding, that dissolution of the inclusions has occurred. Figure 12 and Figure 13 show inclusions located 16 mm from the weld metal on the other side of the weld. This part of the sample was not immersed in acid before the welding. Dissolution of some of the inclusions was observed also here. Dissolved inclusions were observed throughout the sample surface, on both sides of the weld, i.e. also at the part of the sample which was not immersed in acid prior to the welding.

In order to study the influence of welding on the MnS inclusions in the surface, and to be able to correlate this influence to the corrosion properties of the welded sample, without the possibility of having dissolved MnS inclusions before the welding, a third sample called Weld Sample 3 was prepared. No parts of this sample were treated with acid prior to the welding. Due to a limited availability of test samples, only one such sample could be prepared. The TIG process was used also for this sample, but with a current of 26 A, an unknown voltage, and with helium mixed with argon as the shielding gas. For the other samples, the current and voltage was 60 A and 9 V, respectively, and argon was used as the shielding gas. Surfaces of the sample were studied before and after welding. Figure 14 and Figure 15 show inclusions located 6 mm from the fusion line, before and after welding. The measured content of elements with EDS for the inclusions is given in Table 5 and Table 6.

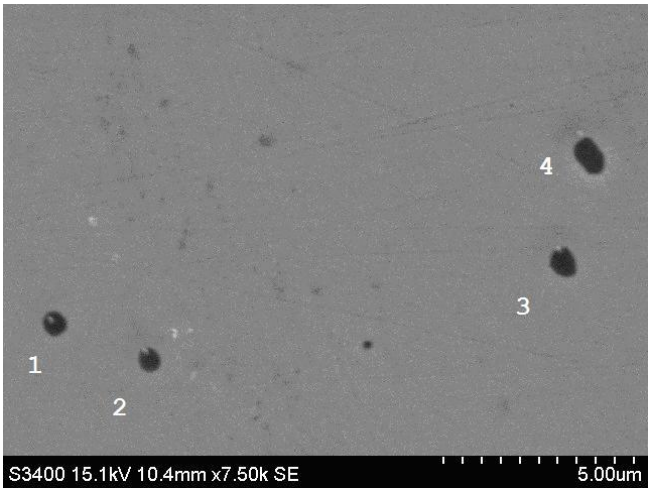

Figure 14 Inclusions located 6 mm from the fusion line in Weld Sample 3 before welding.

Table 5 Measured content of elements in inclusions before welding [wt%]*.

Element	Inclusion			
	1	2	3	4
C	6.53	5.79	5.94	4.57
Si	-	0.39	-	0.38
S	7.66	5.20	6.97	2.86
Cr	6.20	8.60	6.86	9.59
Mn	16.27	9.89	13.63	4.26
Fe	18.08	26.96	22.39	37.22
Ni	2.85	3.90	3.48	6.21
O	42.41	39.27	40.74	34.91
Total	100	100	100	100

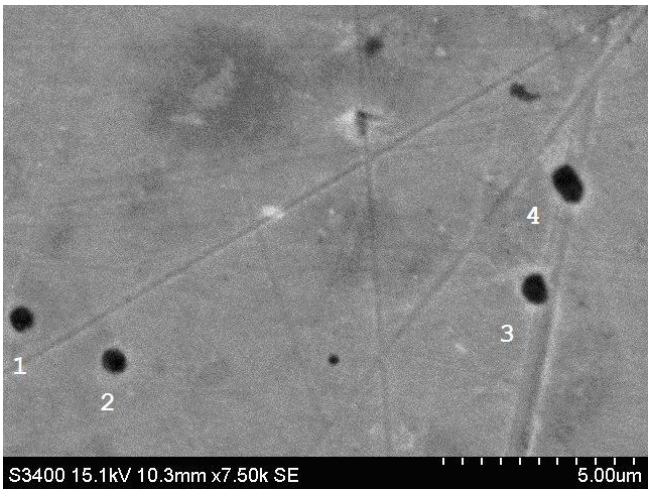

Figure 15 Inclusions located 6 mm from the fusion line in Weld Sample 3 after welding.

Table 6 Measured content of elements in inclusions after welding [wt%]*.

Element	Inclusion			
	1	2	3	4
C	4.84	5.38	4.93	4.86
Si	-	-	0.26	-
S	8.39	6.26	6.77	3.14
Cr	7.25	8.16	8.52	9.62
Mn	14.80	9.50	11.50	4.12
Fe	21.97	27.33	11.50	36.34
Ni	2.63	4.15	3.67	6.46
O	40.12	39.21	39.09	35.46
Total	100	100	100	100

*The measurements had by the EDS software been automatically normalized with a carbon and oxygen content. The differences before and after welding can still be evaluated.

The measured content of elements in the inclusions was approximately the same after welding. Among some other variations, a slightly reduction of the Mn content was seen, while S was measured in a slightly higher amount.

Figure 16 and Figure 17 show inclusions located 4 mm from the fusion line in the same sample, at the opposite side of the weld from the area where the inclusions in Figure 14 and Figure 15 were located. The sample was originally not intended to be welded. Therefore, the sample was surrounded by an epoxy cast, which immediately after the welding started to burn for a few seconds close to the area containing these inclusions.

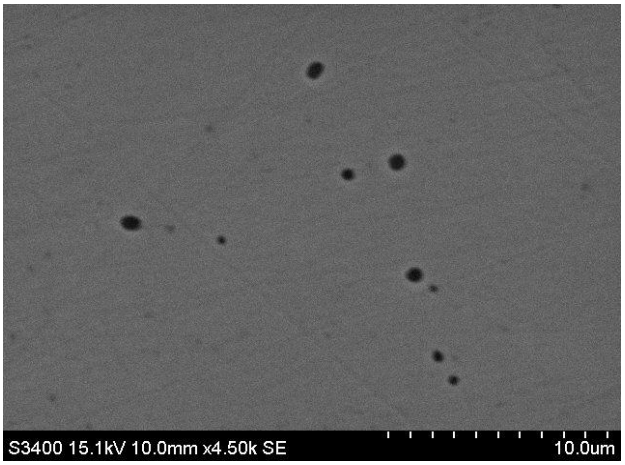

Figure 16 Inclusions located 4 mm from the fusion line in Weld Sample 3 before welding.

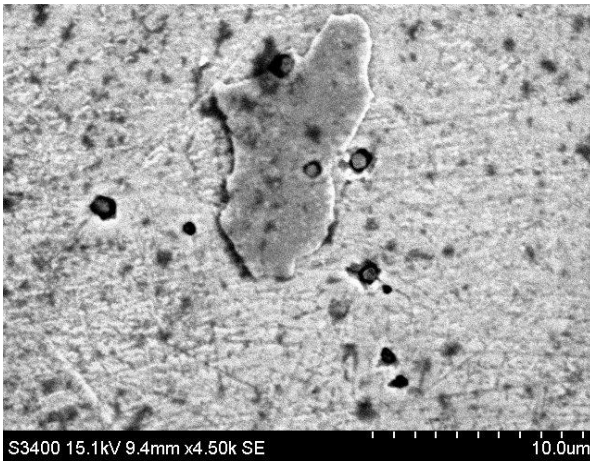

Figure 17 Inclusions located 4 mm from the fusion line in Weld Sample 3 after welding.

It can be seen in Figure 17 that the inclusions have been influenced after the welding. The inclusions can now be seen as a gray centre surrounded by a dark border. EDS measurements to document changes in these particular inclusions were not obtained. However, EDS measurements are obtained for the inclusions in Figure 18, which were located in the same area. The measurements are obtained after the sample had been electrochemically polarized. These inclusions have however the same appearance as the inclusions in Figure 17. The measured content of elements for the inclusions in Figure 18 is included in Table 7.

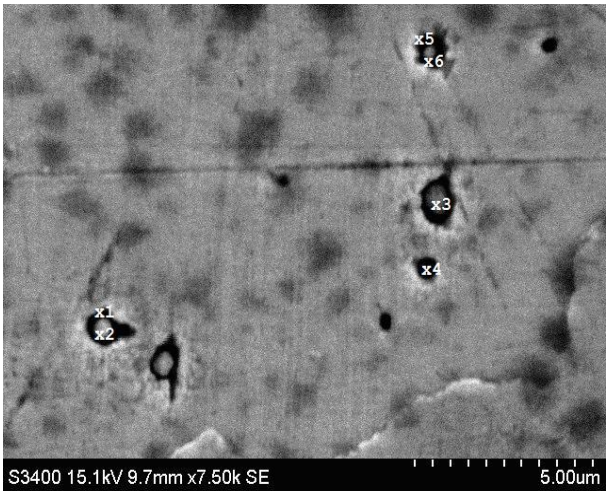

Figure 18 Inclusions located 4 mm from the fusion line in Weld Sample 3 after welding and polarization.

Table 7 Measured elements in inclusions at 4 mm from the fusion line.

Ele-ment	Site					
	1	2	3	4	5	6
O	1.9	3.1	-	2.3	2.9	-
Al	-	-	-	1.0	-	-
Si	-	1.7	1.1	1.1	1.9	1.3
S	15.9	5.3	22.6	1.0	3.7	11.7
Cr	9.8	21.8	19.5	17.6	20.4	12.9
Mn	-	-	-	2.9	-	-
Fe	25.7	53.6	38.0	60.9	57.0	36.5
Ni	46.7	14.5	19.0	13.2	14.1	37.6
Total	100	100	100	100	100	100

The measurements in Table 7 show that manganese was present in a minor amount in one of the analyzed inclusions after welding. Sulfur was measured in varying amounts.

5.2. Electrochemical Polarization

After the initial investigations and the welding of samples, the samples were ready to be electrochemically polarized in synthetic seawater. The different samples to be tested electrochemically are summarized in Table 8.

Table 8 Samples to be tested electrochemically in synthetic seawater.

Name	Description	Comment
Base Metal Sample 1	Sample representing a normal base metal.	
Base Metal Sample 2	Sample representing a normal base metal.	Similar to Base Metal Sample 1.
Base Metal Sample 3	Sample representing a base metal where MnS inclusions have been removed.	
Weld Sample 1a	Sample containing HAZ.	None-intended acid influence possibly occurred before welding.
Weld Sample 1b	Sample containing HAZ where MnS inclusions have been removed before the welding.	Consist in addition to the HAZ also most of the weld metal.
Weld Sample 2a	Sample containing HAZ, where no shielding gas have been used during the welding.	None-intended acid influence possibly occurred before welding.
Weld Sample 2b	Sample containing HAZ, where no shielding gas have been used during the welding, and where MnS inclusions have been removed before the welding.	
Weld Sample 3	Sample containing HAZ, where no treatment have been performed prior to the welding.	Consist in addition to the HAZ also the weld metal.

The polarization curves for all samples are included in Figure 19. The polarization was started at -250 mV vs. SCE, polarized cathodically to -500 mV vs. SCE and then polarized anodically until the current started to increase rapidly. The polarization was then stopped. Only the part of the polarization curve in the anodic direction above -200 mV vs. SCE is shown in the plot.

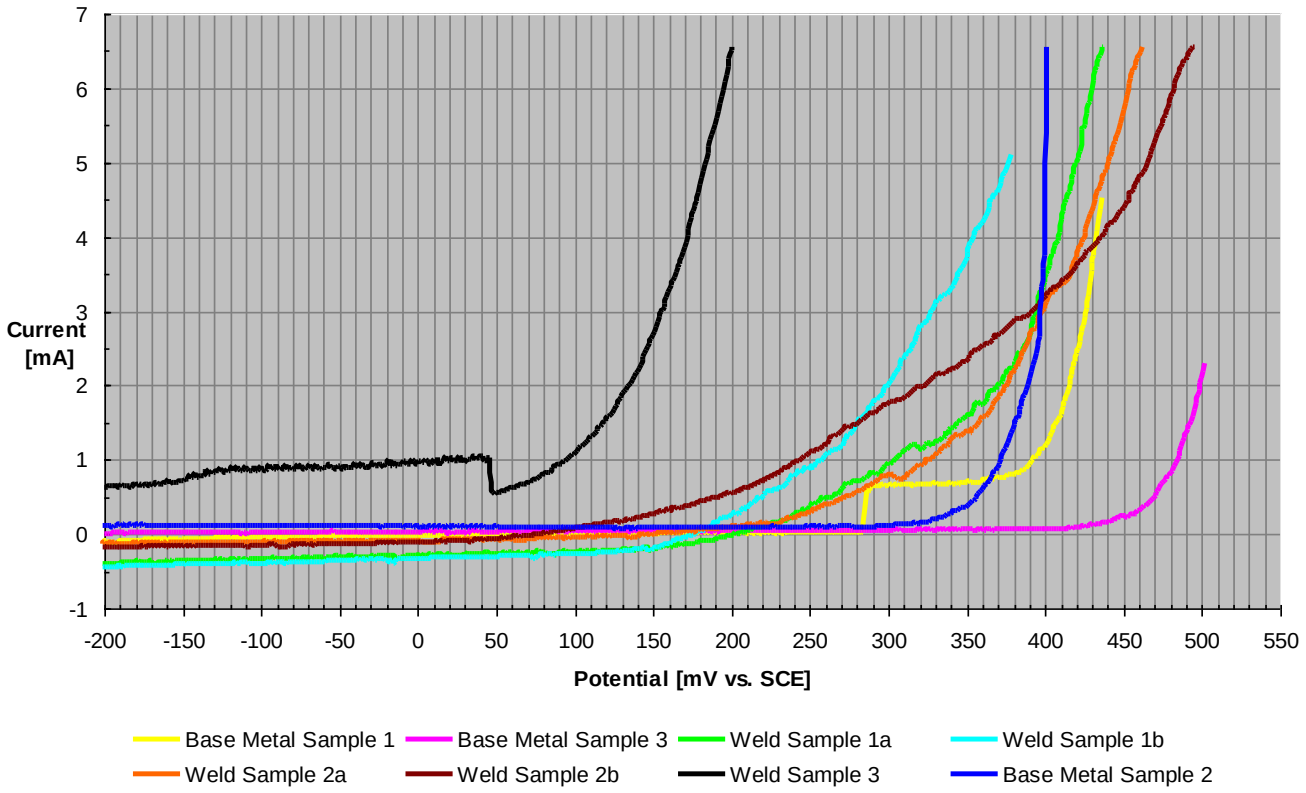

Figure 19 Polarization curves for welded and non-welded 316L samples in synthetic seawater at room temperature and pH 7.5.

To compare the electrochemical properties of the different samples, the potential where the current had reached 2 mA was used. This potential was defined as the pitting potential. At this potential a corrosion process was assumed to have been initiated and stabilized. In addition, the potential value where the current started to increase above the passive current was used to compare the samples. All potential values are measured against a SCE electrode. In the following the electrochemical properties for each sample are described.

For Base Metal Sample 1 the current in the passive potential region was about zero. At 285 mV the current jumped to 0.6 mA and stayed at this level until it started to increase rapidly at approximately 380 mV. The current reached 2 mA at 415 mV. The polarization was stopped at 437 mV. At this potential the current had increased to 4.5 mA.

For Base Metal Sample 2 the current in the passive potential region was slightly above zero. The current started to increase rapidly at approximately 340 mV. The current reached 2 mA at 390 mV. The polarization was stopped at 400 mV. At this potential the current had increased to 6.5 mA.

For Base Metal Sample 3 the current in the passive potential region was zero. The current started to increase rapidly at approximately 460 mV. The current reached 2 mA at 500 mV. The polarization was stopped at 525 mV. At this potential the current had increased to 2.4 mA.

For Weld Sample 1a the passive current was about -0.4 mA. The current started to increase gradually at about 150 mV and reached 2 mA at 370 mV. The polarization was stopped at 430 mV. At this potential the current had increased to 6.5 mA.

For Weld Sample 1b the passive current at -200 mV was about -0.5 mA. The current started to increase gradually at about 150 mV and reached 2 mA at 300 mV. The polarization was stopped at 380 mV. At this potential the current had increased to 5.1 mA.

For Weld Sample 2a the passive current was slightly below zero. The current started to increase gradually at about 200 mV and reached 2 mA at 375 mV. The polarization was stopped at 460 mV. At this potential the current had increased to 6.5 mA.

For Weld Sample 2b the passive current was also slightly below zero. The current started to increase gradually at about 50 mV and reached 2 mA at 320 mV. The polarization was stopped at 495 mV. At this potential the current had increased to 6.5 mA.

For Weld Sample 3 the passive current at -200 mV was 0.6 mA and then varied between 0.6 mA and 1 mA until it, immediately after a sudden fall, started to increase rapidly at 50 mV. The current reached 2 mA at 135 mV. The polarization was stopped at 200 mV. At this potential the current had increased to 6.5 mA.

The polarization curves for the weld samples showed a gradual increase towards higher current values, except for Weld Sample 3, which showed a more rapid current increase. Weld Sample 3 also showed the lowest pitting potential. The base metal samples showed a fast transition towards a rapid current increase. Base Metal Sample 3 showed the highest pitting potential and the highest potential level for the initial current increase.

5.3. Examination of Base Metal

An area in Base Metal Sample 1 is in Figure 20 and Figure 21 shown before and after the electrochemical polarization.

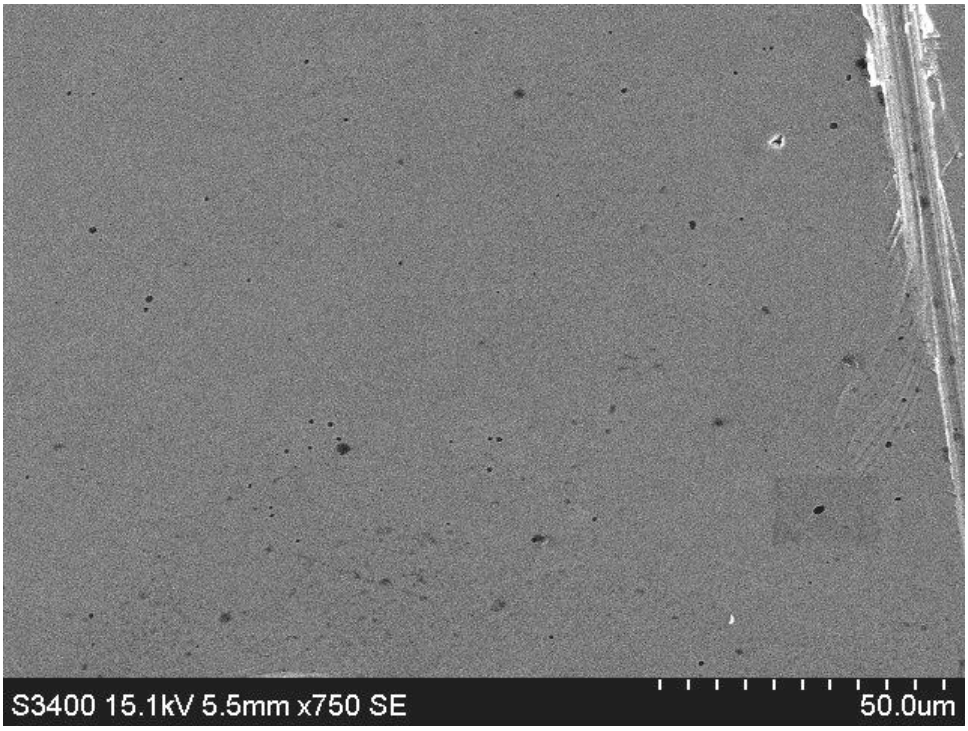

Figure 20 Area in Base Metal Sample 1 before electrochemical polarization.

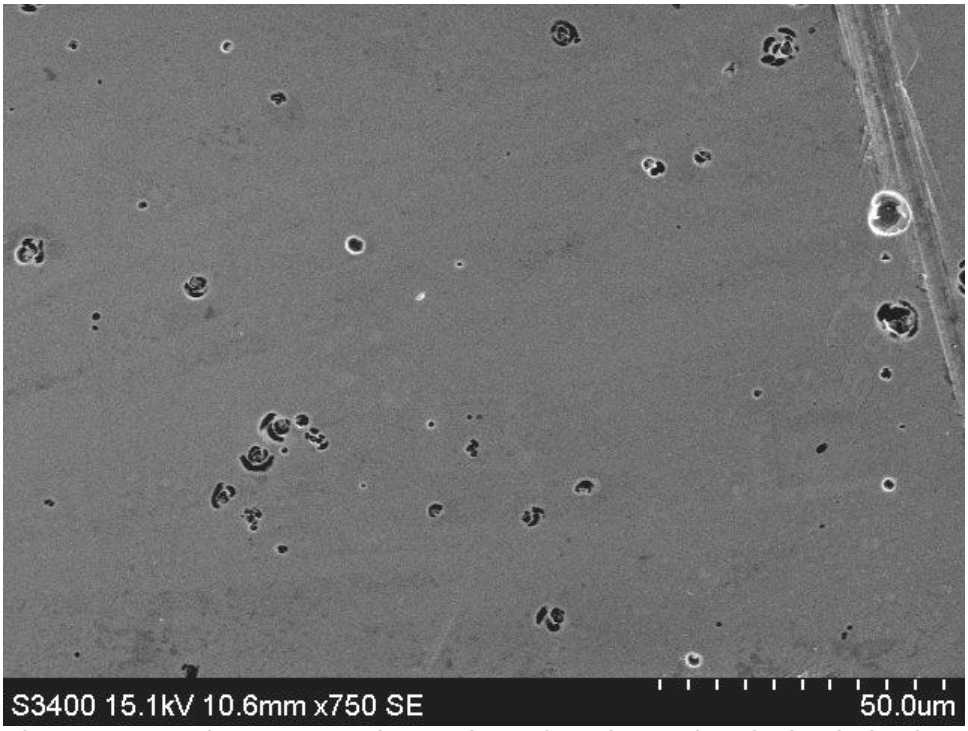

Figure 21 Area in Base Metal Sample 1 after electrochemical polarization.

About 55 inclusions were seen in the surface. After the electrochemical polarization about 38 inclusions had initiated pitting in various grades. About 30 % of the inclusions remained unattacked. Several surfaces in the same sample were examined. The average percent of inclusions which showed an inactive behavior in these surfaces was 38 %.

A more detailed view of inclusions in the surface of Base Metal Sample 1 is included in Figure 22 and Figure 23. After the electrochemical polarization it can be seen that several of the inclusions have initiated pitting. Chemical changes in inclusions are indicated by EDS measurements included in Table 9 and Table 10.

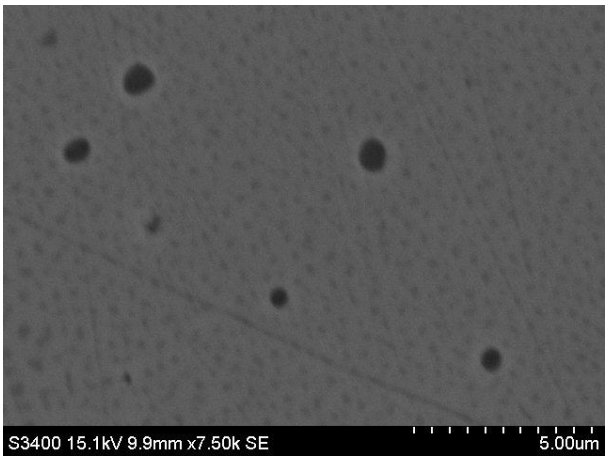

Figure 22 Inclusions in Base Metal Sample 1 before electrochemical polarization.

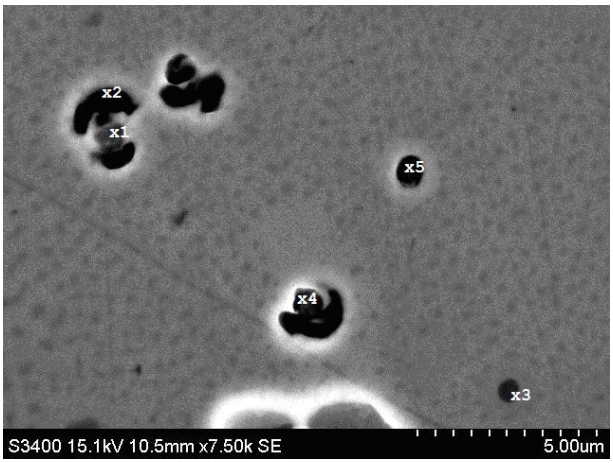

Figure 23 Inclusions in Base Metal Sample 1 after electrochemical polarization.

Table 9 Measured elements in one inclusion before electrochemical polarization [wt%].

Element	Measured content
F	1.64
Si	0.24
S	14.17
Cr	10.94
Mn	31.22
Fe	31.76
Ni	5.11
Cu	0.98
Mo	2.77
Hg	1.18
Total:	100.00

Table 10 Measured elements in attacks and inclusions after electrochemical polarization [wt%].

Element	Site				
	1	2	3	4	5
O	5.87	0.74	-	2.87	1.13
Si	2.06	-	-	1.26	0.80
S	6.05	0.44	15.39	8.33	3.98
Cr	16.23	20.67	11.47	16.61	12.68
Mn	7.88	4.73	37.88	6.68	44.17
Fe	45.52	65.36	31.23	48.72	32.37
Ni	6.43	8.05	4.03	8.47	4.88
Cu	9.95	-	-	7.05	-
Total	100	100	100	100	100

Figure 23 show that pitting has started at the MnS inclusions. Manganese and sulfur is detected in the attacks. The content of these elements are reduced compared to the measured content in the inclusion before polarization. It can be seen that one inclusion (Site 3) has not initiated pitting. The inactive behaviour of MnS inclusions can also be seen in Figure 24 and Figure 25, which show inclusions in Base Metal Sample 2 before and after electrochemical polarization. A dark quadrangular area, where the electron beam had been focused for some time was seen containing these

inclusions. A similar area can vaguely be observed in the lower right corner of Figure 20 and Figure 21. The area became darker after the electron beam had been focused on this area for some time during the examination of an inclusion. It can be seen that the inclusion located in this area did not initiate pitting. This behaviour has also been observed for several other inclusions. In order to indicate whether any changes had occurred in the inclusions in Figure 25 during the electrochemical polarization, EDS measurements before and after the polarization were obtained. The measurements are included in Table 11 and Table 12.

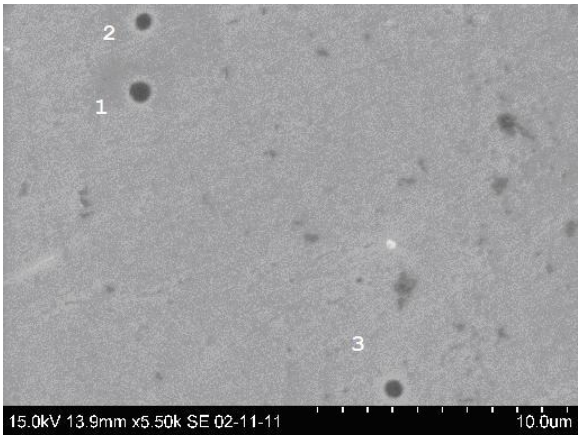

Figure 24 Inclusions in Base Metal Sample 2 before electrochemical polarization.

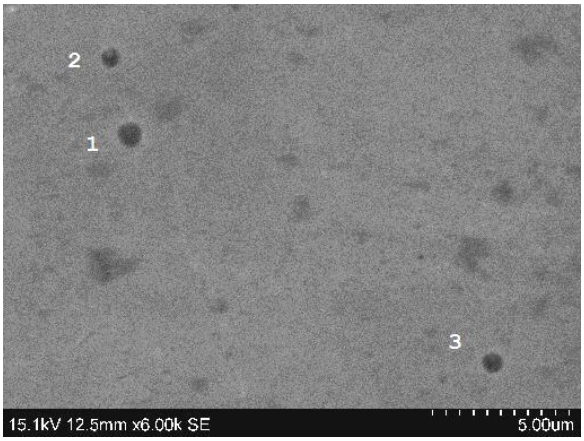

Figure 25 Inclusions in Base Metal Sample 2 after electrochemical polarization.

Table 11 Measured elements in inclusions before polarization.

Element	Inclusion		
	1	2	3
S	17.27	12.88	18.67
Cr	10.40	11.14	12.76
Mn	31.86	23.79	35.66
Fe	26.14	37.99	32.91

Table 12 Measured elements in inclusions after polarization.

Element	Inclusion		
	1	2	3
S	10.91	13.61	16.05
Cr	15.64	14.02	12.19
Mn	18.11	26.91	34.49
Fe	55.34	45.46	37.28

It can be seen that no pitting was initiated in these inclusions during the electrochemical polarization. The measured chemical composition of Inclusion 2 and 3 was approximately the same before and after the polarization. For Inclusion 1 the measured content of both S and Mn was less after the polarization, while the measured Cr and Fe contents were higher. The type of inactive behavior seen for these inclusions was also observed for other MnS inclusions in the sample. It was found that 23 inclusions examined closely before polarization did not initiate pitting.

In Base Metal Sample 3, which had been treated with acid to remove MnS inclusions, few initiated pitting attacks after the electrochemical polarization were observed. This is documented by Figure 26 and Figure 27 which show an area before and after the polarization. In this area one initiated pit can be observed. It was seen that the pit had initiated at a former inclusion. A minor amount of sulfur (1.89 wt%) was detected in the middle of the initiated pit after the polarization. Manganese was not detected.

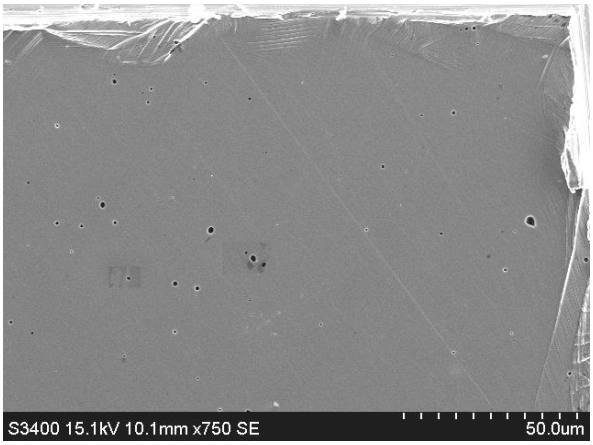

Figure 26 Area in Base Metal Sample 3 after acid treatment, before polarization.

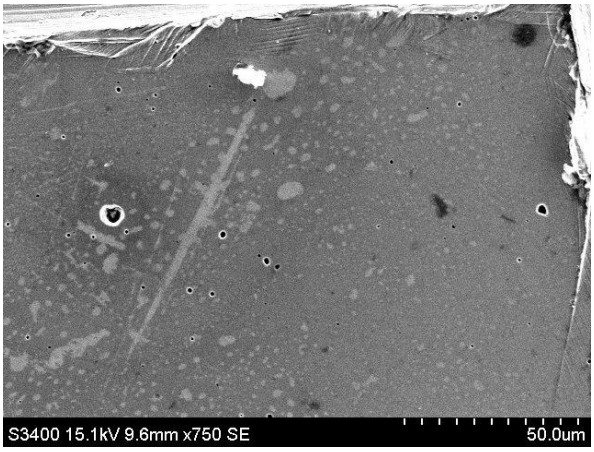

Figure 27 Area in Base Metal Sample 3 after polarization.

5.4. Examination of Welded Samples

Figure 28 show a photograph of Weld Sample 1b. The sample has been cut in the middle of the weld metal, longitudinal to the weld direction. It can be seen that a visible heat affected zone is located between the fusion line (at 0 mm) and 4 mm away from the fusion line. The color is changed throughout the surface, starting with a bright zone between 0 mm and 1 mm. This zone is followed by different colored bands between 1 mm and 4 mm. Beyond 4 mm the surface is similar to the base metal. The extent of the heat affected zone observed for Weld Sample 1a and 1b is also relevant for Weld sample 2a and 2b, which were welded using the same welding parameters.

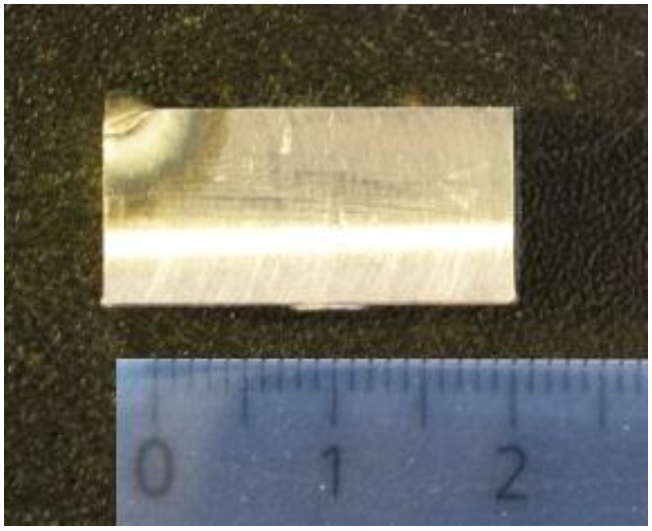

Figure 28 Photograph of Weld Sample 1b.

Figure 29 and Figure 30 show SEM images of areas in the HAZ between 0 mm and approximately 0.7 mm from the fusion line in Weld Sample 1a and Weld Sample 2b after welding. The images compare the surface of the weld samples welded with shielding gas and without shielding gas, and show the appearance of the microstructure in the HAZ.

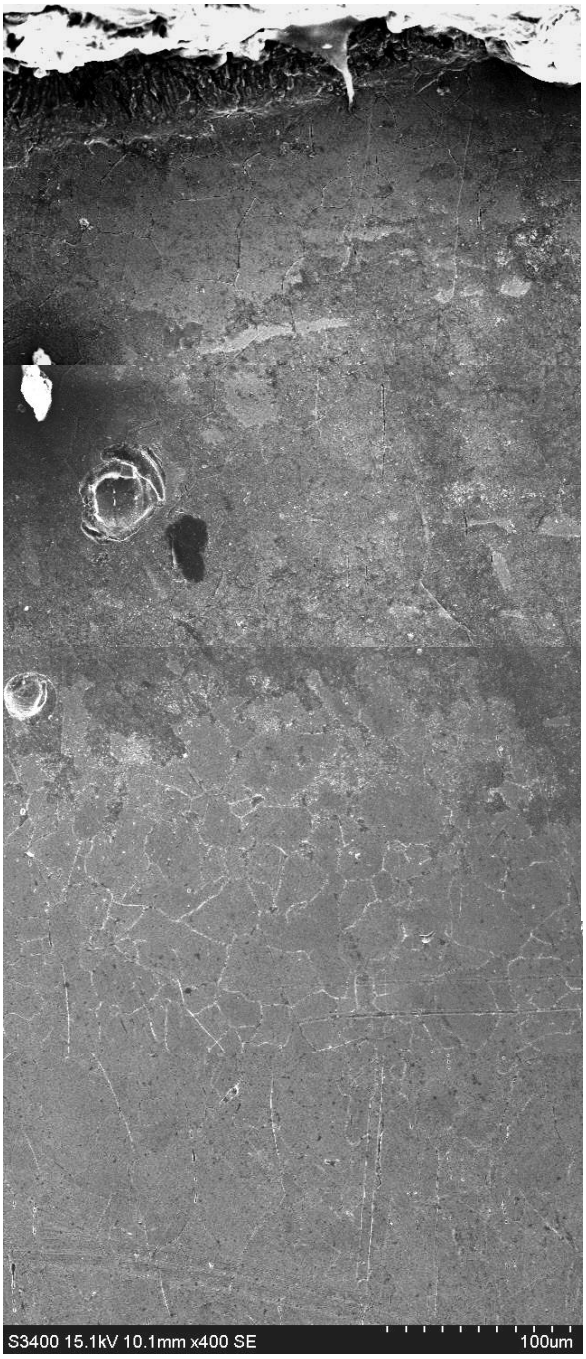

Figure 29 Area between 0 mm (top of image) and 0.7 mm from the fusion line in Weld Sample 1a.

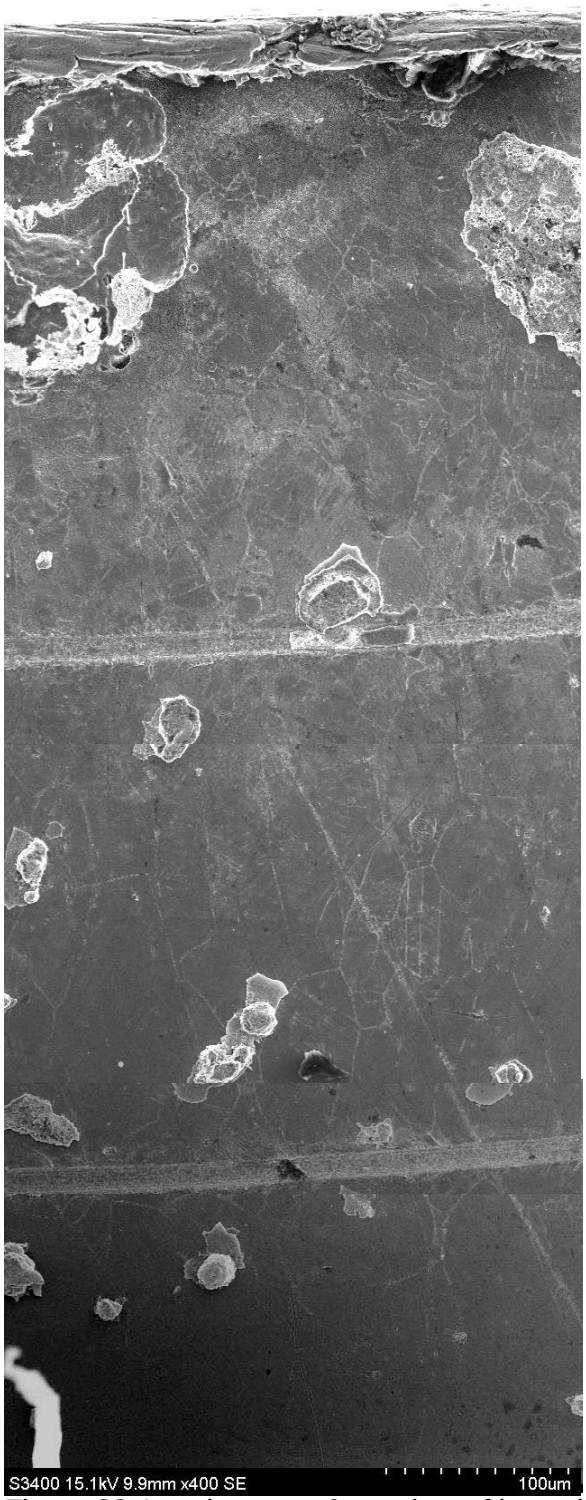

Figure 30 Area between 0 mm (top of image) and 0.7 mm from the fusion line in Weld Sample 2b.

Some large grains can be observed close to the fusion line. Further out, a darker area with slightly dendritic shapes is seen, mostly in Figure 29. Some smaller grains are then seen, followed by a coarser grain structure. Further out, from a distance of about 1 mm from the fusion line, no clear grain structure was seen. For the sample welded without shielding gas (Weld Sample 2b), tungsten particles have been spread out from burning of the tungsten electrode, and can be seen in the surface as big and

bright particles. Weld Sample 2b has been cut at the fusion line. Different corrosion attacks were observed in the samples after the electrochemical polarization. Figure 31 shows an area between the fusion line and 1.0 mm from the fusion line (top of image) in Weld Sample 1b after the polarization.

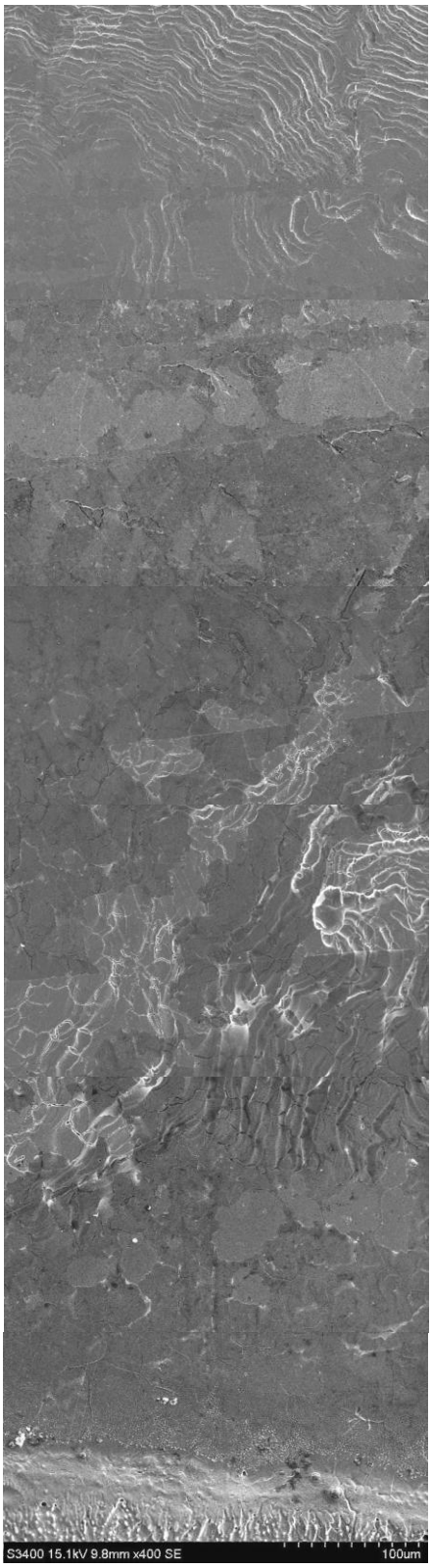

Figure 31 HAZ of Weld Sample 1b.

In the area located about 1.0 mm from the fusion line the structure shown in more detail in Figure 32 was observed.

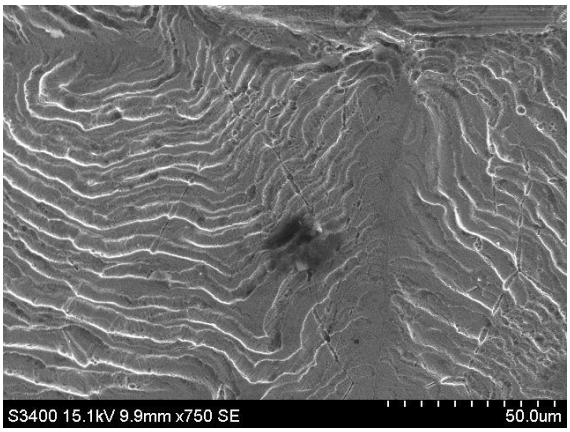

Figure 32 Area approximately 1.0 mm from the fusion line.

At approximately 0.2 – 0.6 mm from the fusion line, grain boundary corrosion was observed. A close view is included in Figure 33.

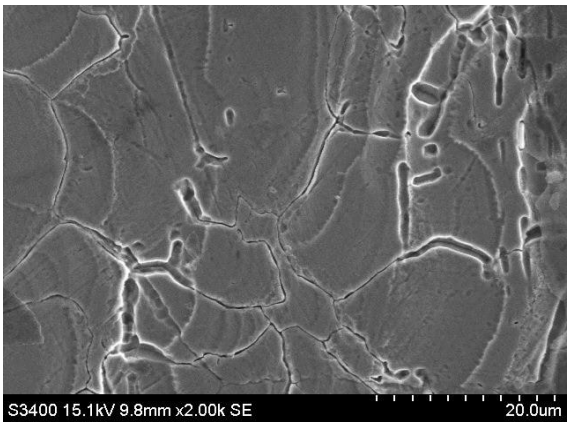

Figure 33 Grain boundary corrosion in an area located 0.5 mm from the fusion line.

Grain boundary corrosion was also observed at the other side of the weld (Weld Sample 1a), in a distance of approximately 0.75 – 1.0 mm from the fusion line.

The structure seen in Figure 32 was limited to a distance of 1.0 – 2.5 mm from the fusion line and was seen on both sides of the weld, in the approximate same distance. Figure 34 show an overview of the structure on the other side of the weld, i.e. in Weld Sample 1a, and in more detail in Figure 35 and Figure 36.

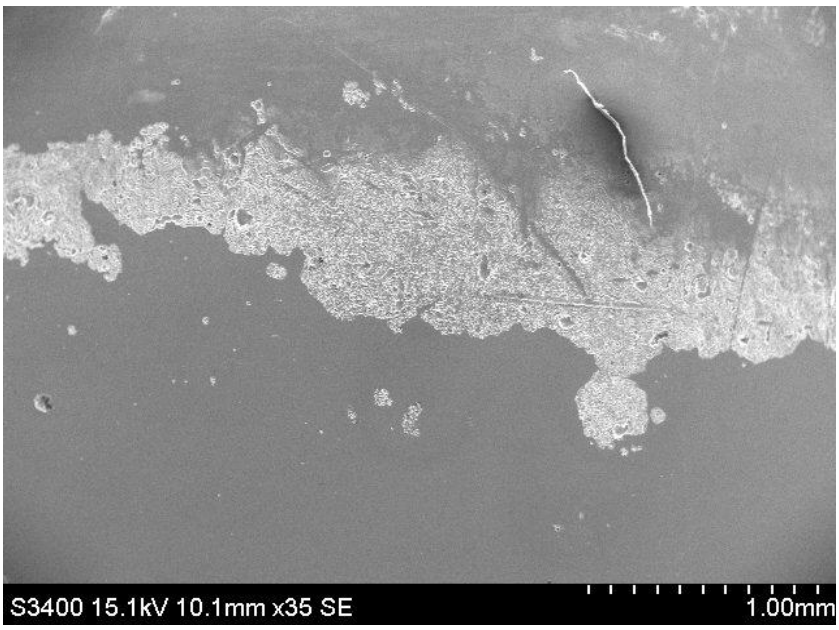

Figure 34 Area at 1.0 mm – 2.5 mm from the fusion line in Weld Sample 1a.

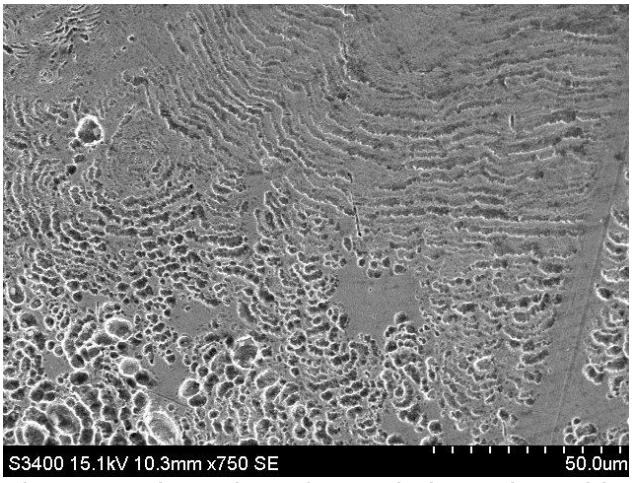

Figure 35 Close view of corroded area in Weld Sample 1a.

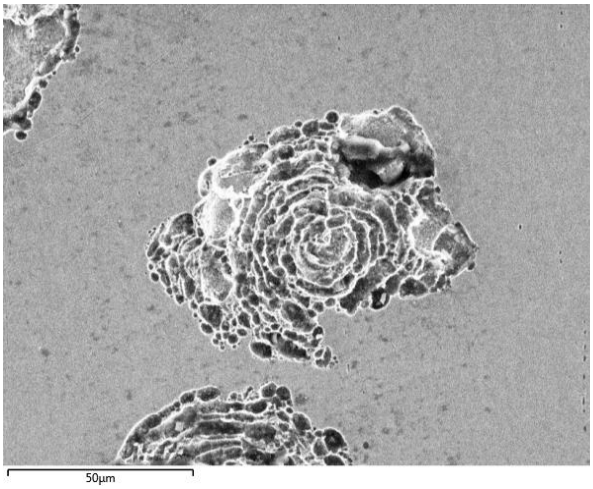

Figure 36 Another close view of corroded area in Weld Sample 1a.

A closer examination, as documented in Figure 35 and Figure 36 revealed pitting-like corrosion in clusters in the distance 1.0 – 2.5 mm from the fusion line. The attack seemed to be more severe further from the fusion line. By EDS measurements of the dark areas the content of elements were found to correspond to the content of the metal matrix given in Table 1, except for a somewhat higher amount (2 – 3 wt%) of chromium. In addition, oxygen was measured in amounts of 2 – 12 wt%. A brighter

area also showed the chemical composition similar to the metal matrix, except for a measured oxygen content of 5 wt%.

In the area described above crystal-like particles, which can be seen in Figure 37, were discovered. By EDS measurements it was detected that these particles consisted of potassium and chloride. Similar particles were also observed along with corrosion attacks in other samples.

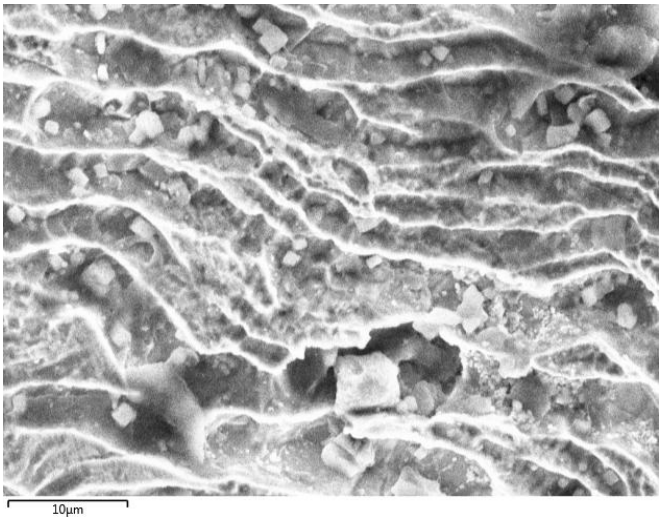

Figure 37 Corroded area in Weld Sample 1a containing crystal-like particles.

Initiated pitting attacks were observed further away from the weld and the fusion line in Weld Sample 1a. The amount of attacks seemed to increase with increasing distance from the fusion line. Figure 38 - Figure 41 show the surface at different distances from the fusion line. Some markings for the SEM examination have been done in the surface.

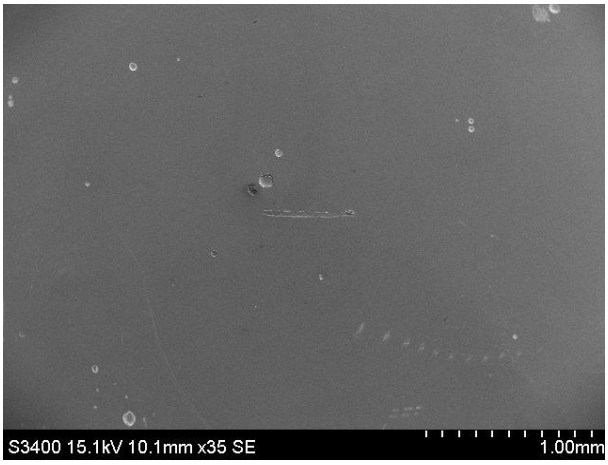

Figure 38 Area at 5 mm from the fusion line.

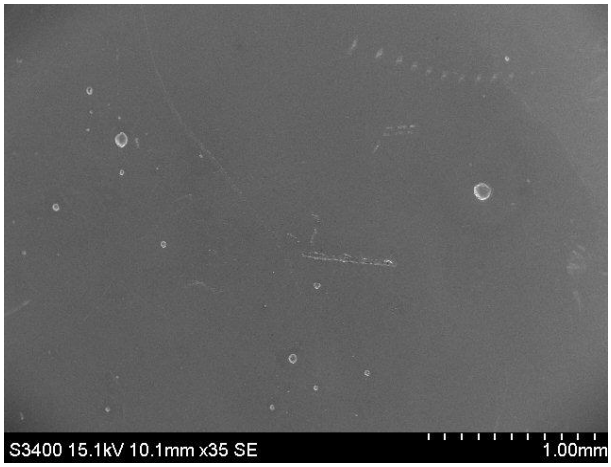

Figure 39 Area at 7 mm from the fusion line.

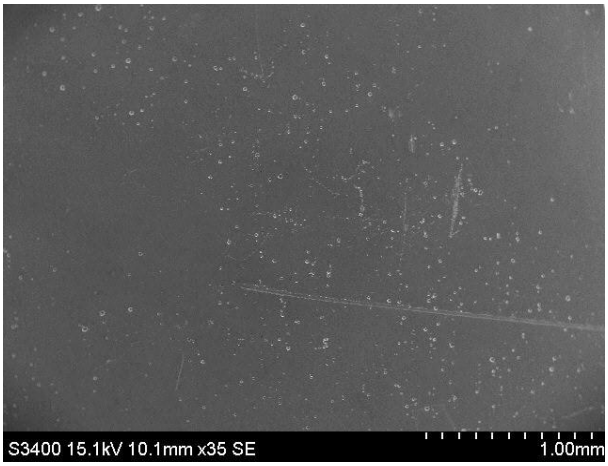

Figure 40 Area at 16 mm from the fusion line.

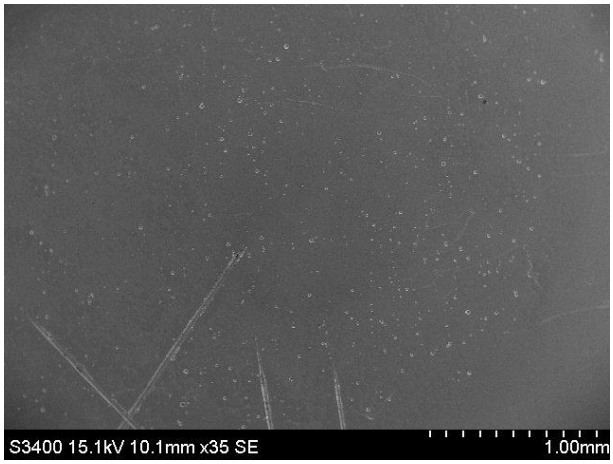

Figure 41 Area at 20 mm from the fusion line.

It is seen that the initiated pitting attacks are more frequent in the areas located 16 mm and 20 mm from the fusion line than at 5 mm and 7 mm. The pitting attacks had been initiated at inclusions. One example is included in Figure 42.

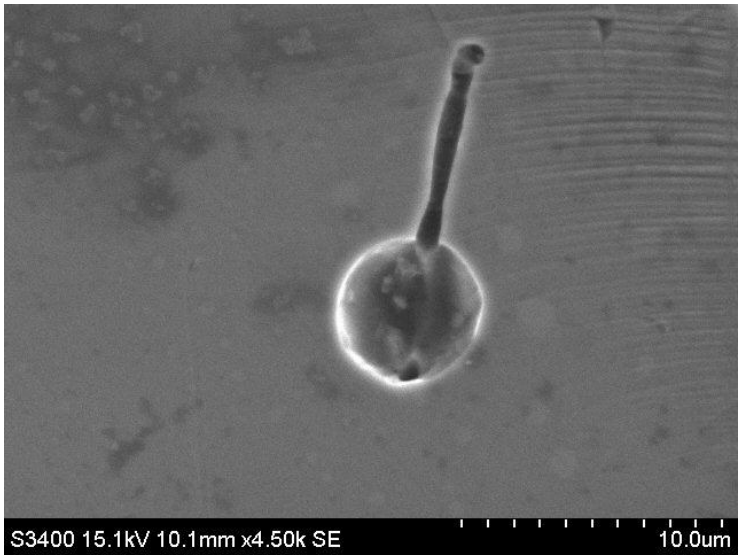

Figure 42 Initiated pit at 20 mm from the fusion line.

In Weld Sample 2b some initiated grain boundary corrosion was observed approximately 0.4 mm from the fusion line. This is shown in Figure 43 and Figure 44. The similar appearance was observed at the other side of the weld, i.e. in Weld Sample 2a, in a distance of 0.3 – 0.8 mm from the weld.

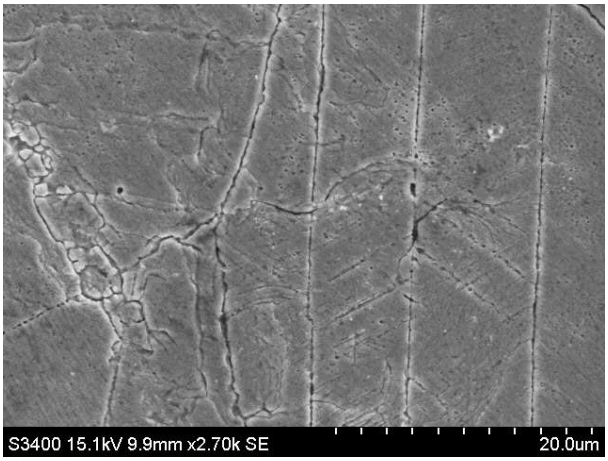

Figure 43 Grain boundaries located 0.4 mm from the fusion line.

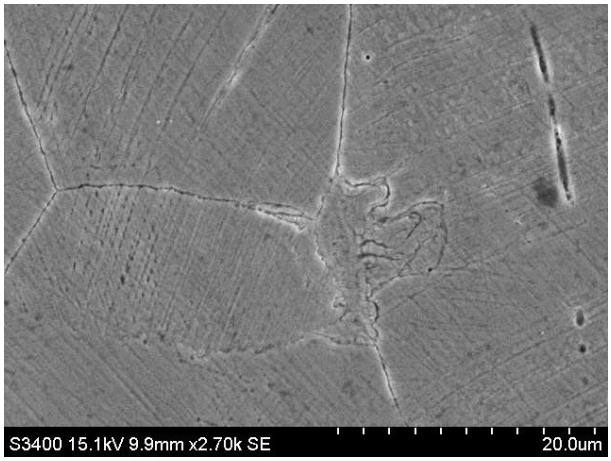

Figure 44 Grain boundaries and former inclusion at 0.4 mm from the fusion line.

At the part of the sample which had not been treated with acid before the welding (Weld Sample 2a), pit initiation at inclusions was observed in some distance from the fusion line. Figure 45 show initiated pits at a distance of 15 mm.

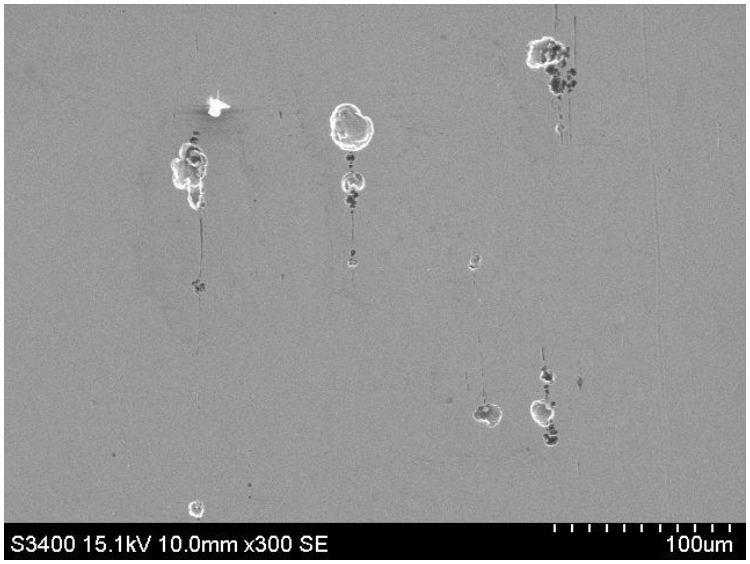

Figure 45 Initiated pits at inclusions located 15 mm from the fusion line in Weld Sample 2a.

In Weld Sample 3 the extent of the heat affected zone, visible as colored bands changing with the distance from the fusion line was approximately 3 mm. The colored bands can be seen on the cylindrical sample surface in Figure 46. In addition, a reddish brown color is covering most of the sample surface. The 10 mm long weld has been laid in the middle of the sample surface, in the vertical direction.

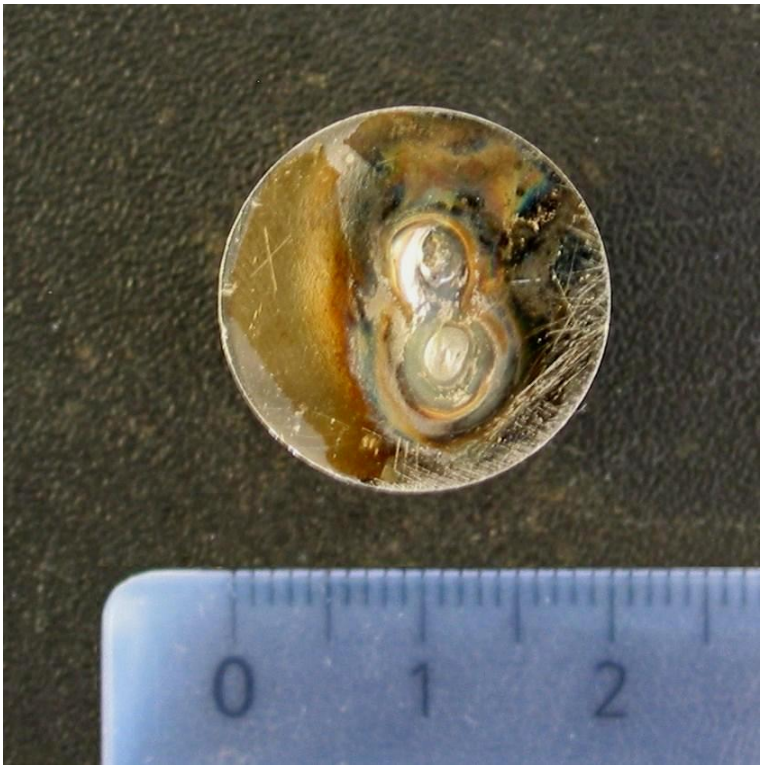

Figure 46 Photograph of the cylindrical Weld Sample 3, showing the 10 mm long weld and the heat affected surface.

In the SEM, a visible grain structure was detected out to about 1.5 mm from the fusion line. Beyond this distance, no evident change of the surface was observed. The part of the HAZ between 0 mm and 0.8 mm from the fusion line is shown after electrochemical polarization in Figure 47.

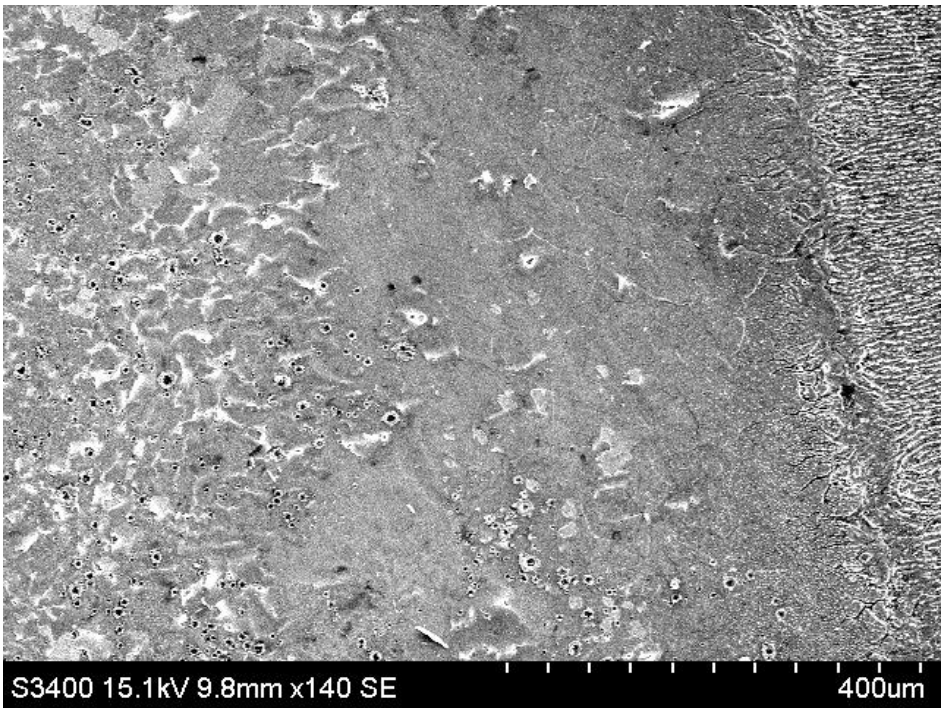

Figure 47 HAZ between 0 mm (to the right) and 0.8 mm from the fusion line in Weld Sample 3.

It was observed after the electrochemical polarization that the grain boundaries had been attacked close to the fusion line, in the coarse grain structure. Detailed views are included in Figure 48 - Figure 50.

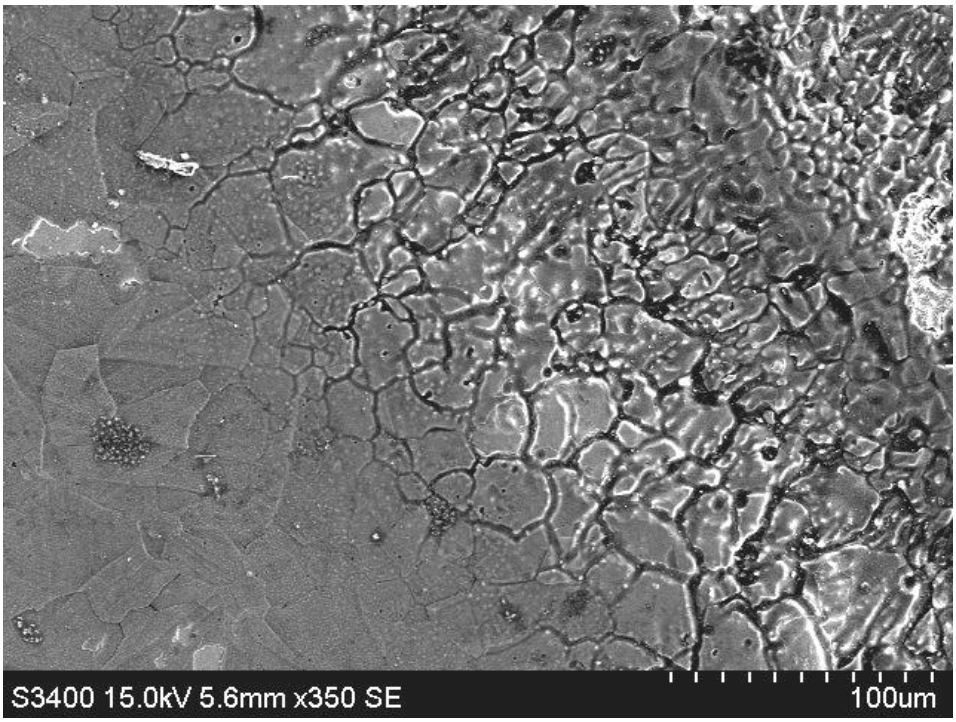

Figure 48 Grain boundary attack close to the fusion line in Weld Sample 3.

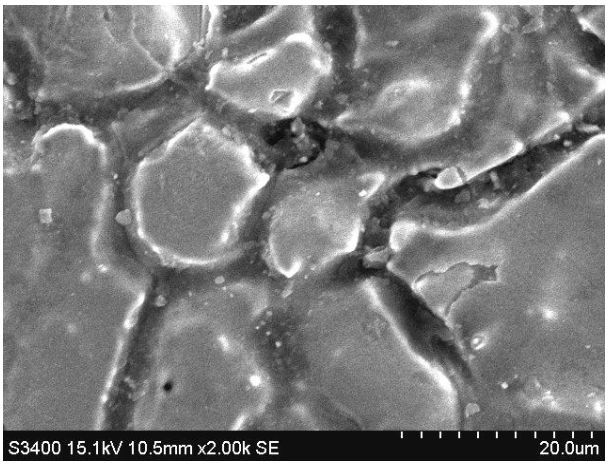

Figure 49 Close view of grain boundary attack in Weld Sample 3.

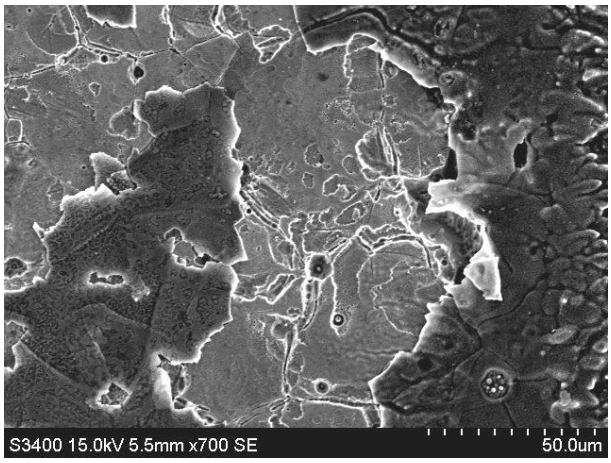

Figure 50 Corrosion at grain boundaries close to the fusion line.

Also seen in Figure 47, further away from the weld, at about 0.3 mm and beyond, inclusion-like formations are present. This is showed in detail in Figure 51. EDS measurements to identify elements present in these formations were performed. The measurements are included in Table 13. These inclusions were observed in a distance between 0.1 mm and 1 mm from the fusion line, along the weld, in the rest of the sample surface.

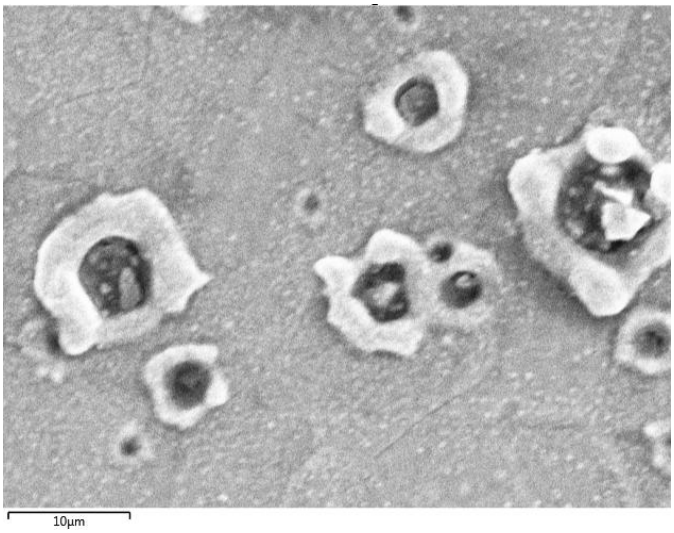

Figure 51 Inclusion-like formations in Weld Sample 3.

Table 13 Measured elements in attacked inclusion-like formations in Weld Sample 3 [wt%].

Ele-ment	Dark centre I	Dark centre II	Dark centre III	Gray centre	Bright outer part I	Bright outer part II	Bright outer part III	Metal matrix
O	25.14	11.26	15.24	46.47	11.89	13.08	13.46	15.56
Al	1.87	1.81	3.65	7.75	-	-	-	-
Si	2.57	6.44	13.70	27.15	-	0.76	1.06	0.92
S	1.64	-	-	-	1.24	0.85	-	-
Cl	1.08	-	0.81	-	-	-	-	-
Cr	10.26	11.52	11.35	-	16.94	16.00	15.87	15.22
Mn	10.20	5.96	2.35	-	3.93	5.16	3.40	2.62
Fe	47.25	63.00	44.54	7.79	56.62	57.70	55.10	57.88
K	-	-	0.66	9.74	-	-	-	-
Ni	-	-	4.22	-	9.38	6.44	11.11	7.80
Mg	-	-	-	1.09	-	-	-	-
Na	-	3.48	-	-	-	-	-	-

In the inclusions small amounts of sulfur were detected, some in the centre and some in the outer part. Si was detected in a significantly larger amount in the dark centre than in the bright outer part, and in the highest amount in the gray spots in the centre. Chromium was detected in a larger amount in the bright outer part than in the centre. This was also the case for nickel. Oxygen was also detected in various large amounts in all areas. Manganese was detected in most of the areas, and in the largest amount in a dark centre. The dark centre indicated that some attack had been initiated at these inclusions. The inclusions were observed not further out than about 1 mm from the fusion line.

At a distance of 1.6 – 2.7 mm from the fusion line in Weld Sample 3 the same type of pitting-like corrosion in clusters which was observed for Weld Sample 1a and 1b was observed. Two examples are included in Figure 52 and Figure 53.

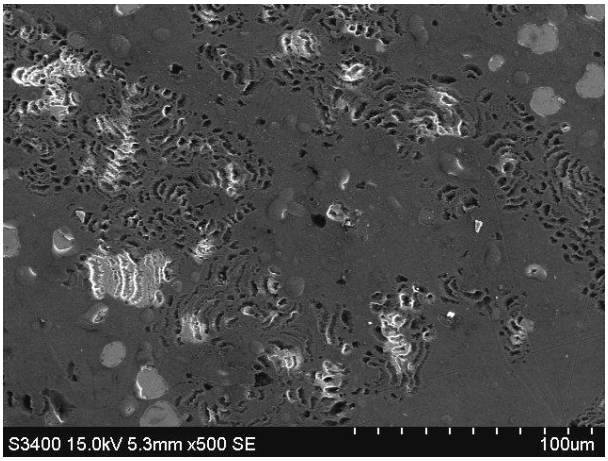

Figure 52 Pitting-like attacks at 2.0 mm from the fusion line in Weld Sample 3.

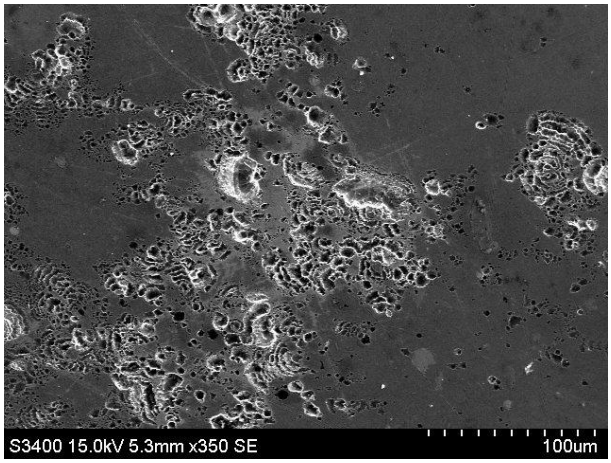

Figure 53 Pitting-like attacks at 2.6 mm from the fusion line in Weld Sample 3.

The attacks were more severe at 2.6 mm than at 2.0 mm from the fusion line.

In the non-heat affected zone in Weld Sample 3 pitting was also seen to initiate at inclusions. Figure 54 show pitting which have been initiated in an area outside the HAZ.

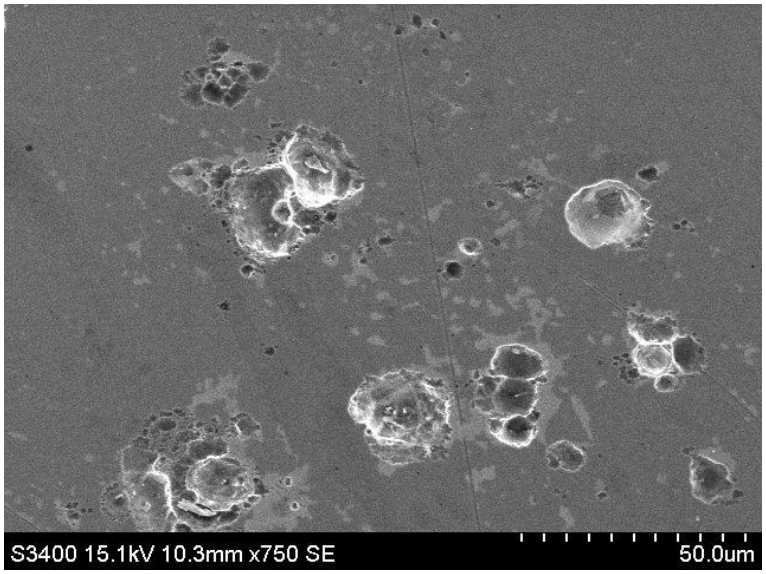

Figure 54 Initiated pitting outside of HAZ in Weld Sample 3.

6. Discussion of Results

6.1. Results from the Initial Examination of Samples

In order to identify the composition of the 316L stainless steel studied in this work, EDS was used to measure the composition of the metal matrix in 6 random areas in two samples. The result of the analysis presented in Table 1 showed expected amounts of Cr and Ni. Sulfur was not detected by the EDS in the metal matrix. It can be assumed that the content of sulfur in the steel was too low to be detected by the EDS. A realistic content of sulfur could be in the order of 0.017 wt%, which was the content of an austenitic stainless steel studied by Suter *et al.* [17]. They reported similar electrochemical properties as Base Metal Sample 1 and 2 in the current experiments, when comparing the pitting potential of stainless steels with different sulfur contents.

The EDS is expected to measure signals down to about 5 µm below the surface when a voltage of 15 kV is applied. Due to this, the measured content of elements in inclusions reported in this work should be regarded as indications, as elements from below the inclusions, i.e. the metal matrix, will be measured as well. The measured composition of the inclusions will thus differ from the actual composition.

As can be seen in Figure 2 - Figure 5 a lot of visible inclusions are present in the stainless steel. The EDS measurements included in Table 2 and Table 3 indicate that the inclusions are manganese sulfides, as the main elements detected, beside iron, were manganese and sulfur. The majority of inclusions discovered in the sample surfaces had the same appearance as the inclusions seen in Figure 2 - Figure 5, and several EDS measurements confirmed the similar content of manganese and sulfur in these inclusions. These are thus assumed to be MnS inclusions as well.

The nitric acid treatment performed in order to remove inclusions from the sample surface was verified with SEM examination and EDS measurements. It is evident from Figure 6 - Figure 9 that dissolution of the inclusions has occurred. The EDS measurements included in Table 4 indicates that both the manganese content and the sulfur content in the centre of an inclusion have been strongly decreased. Sulfur was not measured at all in the inclusion centre after the acid treatment, only in a minor amount near the inclusion edge. The measured chromium content detected in the inclusion centre (and from below the inclusion) had increased from 10.73 wt% to 21.75 wt% after the acid treatment. Compared to typical inclusion contents, which are described by Table 2 and Table 3, a chromium content of 10.73 wt% is a normal measurement. However, the chromium content of 21.75 wt% after the acid treatment is also larger than the content measured in the metal matrix. In addition to more signals from the metal matrix after the acid treatment this higher amount of chromium may also have been caused by the same effect as reported by Noh *et al.* [22]. They reported a chromium enrichment of the passive film of the steel after acid treatment. It could also originate from chromium released from the inclusion itself, which can be dissolved in various amounts in the MnS inclusion, as reported by Eklund [3]. The comparison of the inclusions before and after the acid treatment showed that the treatment resulted in dissolution of the inclusions. Changes in the content of the metal matrix were not detected.

A similar nitric acid treatment was performed for the samples prepared for welding, by immersing the half length of the samples in acid for one hour. As can be seen in Figure 11 and Figure 13, inclusions seem to have dissolved on both sides of the samples, i.e. also at the part which were not immersed in acid. It can be discussed whether the inclusions dissolved as a result of the welding process. This seems unlikely because the inclusions which appeared dissolved or partly dissolved also were seen in a far distance from the fusion line, e.g. at 16 mm. By comparison, the visible heat affected zone seen in Figure 28 extended to about 4 mm from the fusion line. It is also unlikely by considering the melting point of pure MnS, which have been determined to 1655 ± 5 ^{o}C [26]. This temperature has not occurred at this location. It is believed that some influence of acid, maybe caused by acid vapour, on the part of the sample not intended for immersion has occurred, and that this part was not protected enough from possible acid influence. This may have lead to some dissolution of MnS inclusions also here. As can be seen in Figure 13, the inclusions may not seem as dissolved as the inclusions seen in Figure 11. This indicates that the acid had a stronger effect in the surface seen in Figure 11, located on the part which was immersed in the acid. This is in accordance with the intended treatment. A better control of the acid treatment may have prevented the dissolution of MnS inclusions on the part not intended for inclusion removal. The consequence is that comparison of a heat affected zone containing MnS inclusions and a similar heat affected zone where MnS inclusions have been removed was impossible.

Due to the above effect, a third sample was welded, without any acid treatment before the welding. Due to a limited availability of test samples, a similar sample to Weld Sample 3 could not be prepared. Inclusions were examined before and after the welding, e.g. at 6 mm from the fusion line (Figure 14 and Figure 15). No clear dissolution of inclusions as seen in the first weld samples was seen here, though a brighter edge after the welding may indicate that some minor dissolution has occurred. This lack of clear dissolution here indicates that it was not the welding that caused the dissolution of the MnS inclusions in the first samples. Manganese was measured in a slightly reduced amount after the welding, while sulfur was detected in a slightly larger amount. A minor removal of Mn may have occurred. It is also possible that this is variations in the EDS measurements, and not actual changes in the inclusions. The normalization with C and O by the EDS software may also have influenced the measurement results.

It was observed that inclusions had been changed in Weld Sample 3, in a location 4 mm from the fusion line at the other side of the weld. This is seen in Figure 17. Before the welding the inclusions seen in Figure 16 had the same appearance as other observed MnS inclusions, and were thus assumed to be MnS inclusions as well. After the welding the inclusions could be seen as a gray centre surrounded by a dark border. EDS measurements were obtained for some similar inclusions at the same location (Figure 18). This was done after the sample had been electrochemically polarized, but the inclusions did not seem to have been influenced or to have initiated any corrosion. Thus, these inclusions were assumed to be representative for the first inclusions. It is believed that the inclusions had been changed by the heat treatment, and it appears that some segregation has occurred. The EDS measurements indicated that manganese was present in a minor amount in one of the analyzed inclusions only, while sulfur was present in varying amounts. The

inclusions may have been partly dissolved during the heat treatment and precipitated with a changed composition in a segregated manner during the cooling. The epoxy cast which was surrounding the sample (originally not intended for welding) started to burn for a few seconds immediately after the welding, close to the area containing these inclusions. This may also have contributed to the change of the inclusions seen in this area.

6.2. Results from the Electrochemical Polarization

When discussing the electrochemical properties of the different samples the pitting potential, defined as the potential where the current had reached 2 mA, is used. This definition is used for a better readability of the discussions, even though initiated pitting not necessarily was the cause for the current increase in all samples. Other corrosion mechanisms in the welded samples are probably the cause of the measured initial current increase in the electrochemical polarization.

Comparing the polarization curves for the base metal samples, Base Metal Sample 3 showed the highest potential for where the current started to increase above the passive current and the highest pitting potential, i.e. 500 mV vs. SCE. This was expected, as Base Metal Sample 3 had been treated with nitric acid to remove MnS inclusions in the surface. The pitting potential was 120 mV higher than Base Metal Sample 2 and 80 mV higher than Base Metal sample 1. Neither of these samples had been treated with acid. This observation supports the suggestion that pitting starts with the dissolution of MnS inclusions, followed by the release of compounds contributing to an aggressive environment. The measurements also support the findings by Noh *et al.* [22], who reported that the pitting potential increased with 150 mV for a 316 stainless steel treated in the same way.

It could be assumed that if a pit only had been initiated in general as a result of the cavity formed from the dissolved inclusion in an untreated sample, this would have lead to a similar pitting potential as for the samples where inclusions already had been dissolved. It is thus indicated that the release of compounds during the dissolution of MnS inclusions have an important role in the pit initiation process. Another reason why pitting was not initiated in the already dissolved inclusions could be because the cavities from the previous inclusions now had been passivated by an oxide film due to atmospheric exposure. However, this cannot be confirmed from the work reported here.

Base Metal Sample 2 had a pitting potential 40 mV lower than Base Metal Sample 1. The samples and the electrolyte were similar, but the samples were not tested in the same electrochemical cell. This could explain why the measured potential levels differed. The difference may also be within expected variation.

Metastable pitting, sometimes followed by stable pitting, as well as dissolution of MnS inclusions without any further attack, has been observed in several investigations referred to in the literature review in this report. This has been observed as an increased current in a limited potential region or as current peaks, often in the last part of the passive potential region. Among others, such observations have been reported by Böhni *et al.* [12] and Webb *et al.* [25]. During the electrochemical

polarization of base metal samples containing inclusions in the present work, no such current peaks were observed before the current started to increase rapidly towards stable pitting. A reason why temporary current increases due to metastable pitting or dissolution of inclusions were not observed could be due to the size of the inclusions. If electrochemical dissolution of inclusions prior to the initiation of pitting occurred, this may not have had an effect on the polarization curve, due to too small currents. Also, if the scan rate during the polarization had been slower than 1 mVs^{-1}, short lasting current peaks may have been detected.

All the welded samples showed lower pitting potentials than the base metal samples. This was expected as it is a general knowledge that welding leads to a reduced corrosion resistance. Weld Sample 1a and 2a showed the highest pitting potential (375 mV vs. SCE) compared to the other welded samples. These two samples were not immersed in acid before the welding (but may have been influenced by acid, as discussed earlier). The fact that these samples showed the best corrosion resistance of the welded samples, indicate that MnS inclusions were not responsible for the first initiation of corrosion. Weld Sample 2a was welded without the use of an inert shielding gas. The pitting potentials measured for these two samples were approximately similar. This indicates that the lacking shielding gas did not have any effect on the pitting potential in this sample.

Weld Sample 2b, where an inert shielding gas was lacking during welding and where MnS inclusions had been removed from the surface before welding, showed a pitting potential about 55 mV lower than Weld Sample 1a and 2a. This indicates that another type of corrosion than pitting initiated by inclusions was responsible for the increased current. The observed corrosion attacks in the weld samples, discussed further in section 6.5, support this indication. Weld Sample 1b, where only MnS inclusions had been removed from the surface, showed an even lower pitting potential (300 mV vs. SCE). The current started however to increase above the passive current at a lower potential for Weld Sample 2b than 1b, but the potential curve for Weld Sample 1b was steeper, indicating more localized corrosion.

The potential curves for the weld samples did not increase towards higher currents as rapidly as the potential curves for the base metal samples. This also indicates, as discussed above, that the initial corrosion on the weld samples was not due to the initiation of pitting, but some other process. The jumps in the measured current seen in two potential curves, was due to internal measurement errors in the potentiostat. This is indicated by the fact that for one of the potential curves, the current remained passive also after the jump, while for the other curve, the current jumped downwards.

Weld Sample 3, in which the test surface was not near any acid before the welding, thereby consisting of MnS inclusions in the same amount as the base metal, showed a significantly lower pitting potential and potential for the initial current increase than the other weld samples. The pitting potential was 165 mV lower than for Weld Sample 1b. The current also increased less gradually, i.e. the potential curve was steeper towards higher currents compared to the other weld samples. This may indicate that localized corrosion was more dominant in this sample. The lower corrosion resistance could also indicate that the presence of MnS inclusions in the surface had been influenced by the welding, leading to an easier initiation of pitting. Another factor which may have influenced the corrosion properties for this sample

was the welding parameters which differed from the other samples. The welding current for Weld Sample 3 was about half the value compared to the other weld samples. As the applied voltage for this sample (which could have been higher) was unknown, a comparison based on the welding parameters is not possible. The extent of the heat affected zone for Weld Sample 3 was however seen to be approximately the same as for Weld Sample 1a and 1b, deviating with less than 1 mm. This indicates that the heat input could have been approximately the same, and that this was not responsible for the much lower corrosion resistance. It can also be speculated whether the geometry of the sample had an effect. This could not be verified.

A part of the side walls of all weld samples were also immersed in the electrolyte. It is a possibility that corrosion could have been initiated at these sides, or at the edges. The surfaces not to be studied were however pickled, and the edges were grinded to avoid sharp initiation sites, before the polarization. The main attack is therefore believed to have occurred on the desired surfaces.

6.3. Observed Corrosion in Base Metal

In Figure 20 and Figure 21 it is seen that pitting have been initiated at inclusions present in the surface of Base Metal Sample 1. The pitting was seen to initiate at inclusions similar to the typical inclusions presented in Table 4. These inclusions were confirmed by EDS measurements to be manganese sulfides. All other examined surfaces in the same sample had a similar appearance. It can thus be verified that the main initiation site for pitting seems to be MnS inclusions in the surface. The observation is in accordance with the findings by Eklund [3], Wranglén [7] and others. The initiated pitting at MnS inclusions is seen in more detail in Figure 22 and Figure 23. The EDS measurement of an inclusion before the electrochemical polarization shows that the main constituents are sulfur and manganese, besides iron and chromium. The iron and chromium were most likely detected mainly from the metal matrix below the inclusion, but may also have been present in the inclusions themselves, as reported by Eklund [3].

It was seen that the manganese content in the inclusion area after a pit has been initiated, was greatly reduced. This was also the case for sulfur. This is an indication of that manganese and sulfur have been removed from the inclusion, possibly by a dissolution process before the pit initiation. It was seen from the EDS measurements that in the inclusions examined before polarization, manganese was detected in a significantly larger amount than sulfur. In the attacks after the polarization, manganese was detected in a much lower amount compared to its original amount than was the case for sulfur. This may indicate that the MnS inclusion has been partly dissolved during the polarization, leaving behind only sulfur species and then initiated pitting. This is in accordance with the hypothesis described in section 3.1.6. One could assume that the measured sulfur could originate from the release of thiosulfate ($Na_2S_2O_3$), which has been observed by Lott and Alkire [27] and Webb *et al.* [25]. They proposed that the thiosulfate accelerated MnS dissolution and caused pitting after reaching a critical amount. The detected sulfur could also be elemental sulfur particles, as observed by Eklund [3] after the dissolution of MnS inclusions in an air-free unbuffered 0.1 M NaCl solution. A minor amount of sulfur crust, as suggested by

Williams *et al.* [1] to be formed over and around the inclusion after dissolution may also have been detected.

The possibility of the MnS inclusions being cathodic to the metal matrix, and thereby to initiate pitting in the metal matrix next to the inclusions should be discussed. This can be disproved by the observations of dissolved inclusions combined with the initiation of pitting as seen in the current results. If the inclusions were cathodic one could assume that the inclusions themselves would have been unaffected, at least until stable pitting has developed. Several investigators have performed more detailed studies regarding the actual site at inclusions where pitting have initiated. As described in section 3.1.8, pitting has in several cases been observed to initiate on the inclusions side at the interface of the inclusion and the metal matrix. This was not possible to see from the results in the current work, and could not be verified. If such initiation at the border of the inclusions have occurred, it would have been difficult to see in the SEM, due to a limited resolution. Also, the pitting attacks observed after the polarization had grown to a state where it was difficult to see where at the inclusion the attack had started.

In Figure 20 about 55 inclusions is seen in the surface. As seen in Figure 21, about 38 of the inclusions have initiated pitting in various grades, i.e. about 70 %. Thus, about 30 % of the inclusions remained unattacked. The inactive behavior of inclusions is also seen in Figure 23, where some of the inclusions have not initiated pitting. The average percent of inclusions which showed an inactive behavior when several surfaces in the sample were examined, was 38 %. This is in accordance with the findings by Suter *et al.* [17] and Schmuki *et al.* [10], who found that one third and 40% of the inclusions were inactive, respectively, when performing corrosion tests on stainless steel.

It is vaguely seen in Figure 20 and Figure 21 that a dark quadrangular area has formed where the electron beam had previously been focused, during the examination of inclusions. This was also observed in other similar surfaces. It was observed that inclusions located in these areas did not initiate pitting, as opposed to nearby inclusions. One could surmise that the electron beam may have influenced the examined inclusions before the sample was electrochemically polarized, such that the inclusions did not initiate pitting as easily as the other inclusions in the surface, which was not examined closely. This effect is not necessarily the case for all examined inclusions prior to polarization. As an example, several of the inclusions seen in Figure 22 did initiate pitting, despite a close examination. The period of the electron beam being in focus on the inclusions may contribute to this effect.

For some of the inclusions which have not initiated pitting, like inclusion 1 in Base Metal Sample 3 seen in Figure 24 - Figure 25, a reduction of both the sulfur and manganese content was detected after polarization. This could indicate that the inclusions have started to dissolve during the electrochemical polarization. The dissolution may have been a minor dissolution, as it was not evident from the SEM examinations. The dissolution of inclusions prior to the initiation of pitting is in accordance with the reviewed literature, e.g. the suggestions by Eklund [3], Wranglén [7] and Lott and Alkire [27]. No pitting was however initiated. These particular inclusions were also seen to be surrounded by a similar dark quadrangular area from the electron beam as described above, which could be an explanation why pitting

was not initiated. The suggested inactive behavior as a result of the focus of the electron beam could be supported by the fact that 23 inclusions examined closely before polarization did not initiate pitting, while at the same time more than 60 % of the inclusions in general in this stainless steel initiated pitting. Statistically, about 14 of those 23 inclusions should have initiated pitting.

In Base Metal Sample 2, which had been treated with nitric acid before the electrochemical polarization, very few already dissolved inclusions initiated pitting, as shown in Figure 27. It can be assumed that the inclusion actually seen to initiate pitting in Figure 27 could have been only partly dissolved. The fewer initiated pitting attacks supports the observation of the improved corrosion resistance by the polarization curve for this sample, compared to the untreated samples.

It can be expected that even more of the inclusions in the sample surfaces would have initiated pits if the potential had been increased, or, as reported by Park *et al.* [15], if the temperature or the chloride concentration of the electrolyte had been increased. They demonstrated that pitting was obtained more easily when these parameters were increased. The size of the investigated inclusions which have been observed not to initiate pitting, seen both in Figure 23 and Figure 25, were not bigger than 1 µm. Critical sizes of 0.7 µm, 0.8 µm and 1 µm to initiate pitting have been reported, as described in section 3.1.9. Thus, the size of the inclusions could also explain why pitting was not initiated.

6.4. Effects of Welding

In Figure 28 the photograph of Weld Sample 1b show a visible heat affected zone out to approximately 4 mm from the fusion line. A variation of colors is seen throughout the surface, starting with an almost white part between 0 mm and 1 mm, followed by different colored bands between 1 mm and 4 mm. The microstructure is believed not to have been affected beyond 4 mm from the fusion line, as the surface here was similar to the rest of the base metal. In the SEM, however, no clear change of the microstructure was seen beyond about 1 mm from the fusion line. Even though it was not discovered in the SEM examination, this does not mean that the microstructure was unaffected beyond 1 mm. Weld Sample 1a, i.e. at the other side of the weld, had the same location and appearance for the heat affected zone. The different colored bands seen in Figure 28 are believed to have been caused by differences in the thickness of the oxide film, as was reported by Enerhaug [57]. The thickness was believed to vary throughout the heat affected zone, due to the varying temperatures peaks obtained during welding, causing varying levels of oxidation.

The extent of the visible heat affected zone, and the similar colored bands in the same distance from the fusion line were seen also in Weld Sample 2a and 2b, which were welded without inert shielding gas. Also the extent of the zone where microstructural changes was discovered in the SEM was approximately the same for the samples welded with and without inert shielding gas. This can be seen by Figure 29 and Figure 30. It was however difficult to compare the exact differences in the extent of the microstructural changes in the HAZ, as the different zones were more evident in Weld Sample 1a than in Weld Sample 2b.

In a distance of about 100 µm from the fusion line, some dendritic structure was seen in Weld Sample 1a. This could be a zone containing δ-ferrite, as reported in several investigations. Further out, small grains followed by bigger grains, indicating grain growth, were seen. This is in accordance with reported observations in the literature. The surfaces of Weld Sample 1a and 1b were cleaner than the surfaces of Weld Sample 2a and 2b. This is because tungsten particles from the burning tungsten electrode during the welding without shielding gas had been spread out. These surfaces may also have been more oxidized due to the lacking inert gas, possibly explaining why it was difficult to compare the surfaces exactly in the SEM, even though this was not visible by studying the sample surfaces.

6.5. Observed Corrosion in Welded Samples

Different corrosion attacks were seen at different distances from the fusion line in the HAZ after electrochemical polarization. This is seen in Figure 31. Starting closest to the fusion line, grain boundary corrosion was discovered in a distance between 0.2 mm and 0.6 mm. It is believed that the temperature in this zone has been between 400^{o}C and 800^{o}C, such that chromium has been depleted near the grain boundaries due to the precipitation of chromium carbides, described as the sensitized zone in section 3.3.1. The presence of chromium carbide was however not evident from the SEM examination, but it could be the dark spots seen in the attacks in Figure 33. Also, at the other side of the weld in the same sample, some grain boundary corrosion was seen in a distance of 0.7 – 1.0 mm from the fusion line. This was not far from the same distance seen at the other side, and gives more evidence that it was grain boundary corrosion caused by a temperature interval in a particular distance from the fusion line. The presence of this grain boundary corrosion was most likely the reason why corrosion was seen to initiate at a lower potential than the non-welded samples, and with a more gradually current increase, suggesting that the initiation was not caused by pitting. Also in Weld Sample 2a and 2b, some attack at grain boundaries was observed in a distance between 0.3 and 0.8 mm from the fusion line, seen in Figure 43 and Figure 44. Numerous small dark spots were seen, which could be chromium carbides. This was however not confirmed. It is by these observations thus indicated that sensitization, as reported in several investigations, characterized by carbide precipitation and chromium depletion at grain boundaries, has occurred.

In a distance of about 0.8 – 2.5 mm from the fusion line on both sides of the weld (Weld Sample 1a and 1b), some sort of attack, which can be seen in the overview in Figure 31 and Figure 34 and more closely in Figure 32, was found. A closer examination, seen in Figure 35 and Figure 36, revealed pitting-like corrosion in clusters in this area. By the fact that the corrosion attack was limited to a distance, which was approximately the same at both sides of the weld, it can be assumed that the temperature reached in this zone during welding was determining for the presence and location of the corrosion attack. From the photograph of the weld sample in Figure 28, it can be seen that the distance of 0.8 – 2.5 mm corresponds to the distance from the fusion line between where the color is changed from light to dark, to the darkest colored band. As described in section 3.3.4, Enerhaug [57] showed that the distance from the fusion line where the color was darkest (dark blue and violet), i.e. where the oxide film was thinnest, corresponded to the weakest zone

regarding the initiation of pitting in a super-martensitic stainless steel. Pitting attacks, seen as distributed pits, were clearly most frequent at this distance. It could be assumed that there is a correlation between Enerhaugs results and the observed attacks in the present investigation, though the stainless steel was different and the appearance of the attacks differed. By EDS measurements the content of elements was estimated in the corroded area seen in Figure 35 and Figure 36. The content of elements was found to correspond to the content of the metal matrix, except for a somewhat higher amount of chromium (2 – 3 wt%) in the dark areas. A content of oxygen, in amounts of 2 – 12 wt% was also detected. This may be measured from chromium oxides which have been formed as a result of the welding. The formation of chromium oxide was suggested by Vagn Hansen *et al.* [58], who indicated the oxidation of chromium to Cr_2O_3, also when shielding gas was used, due to oxygen infiltration. Inert shielding gas was used during the welding of Weld Sample 1a and 1b in the current work, but it cannot be guaranteed that the atmosphere was totally oxygen free. The formation of chromium oxides is therefore assumed to be possible. The formation of chromium oxide, with the result of chromium depletion in a metal layer below the oxides may have happened. This in combination with the observed thinnest oxide film in a particular colored area in a distance from the fusion line, as reported by Enerhaug [57], may explain the corrosion attack. Closer to the fusion line, a thicker oxide film may exist after the welding, causing this area to be more resistant to such corrosion, while further out no oxidation to the same extent, and no formation of chromium oxides have occurred, due to lower temperatures reached during welding.

The observed particles consisting of potassium and chloride in the area described above, seen in Figure 37, are believed to be remnants from the synthetic seawater used as the electrolyte in the electrochemical polarization.

A similar corrosion attack as described above was also observed in Weld Sample 3, in a distance of 1.6 – 2.7 mm from the fusion line. This is seen in Figure 52 and Figure 53. The attack seemed to be worsened at the furthest part of this zone, which also was the case for Weld Sample 1a and 1b. The furthest part seemed to correspond to the darkest colored band observed in the HAZ seen in Figure 46, indicating a correlation with the thickness of the oxide film.

The pitting cluster attack described above was not observed in Weld Sample 2a and 2b, which were welded without inert shielding gas. One reason could be the presence of large amounts of tungsten particles from the burning tungsten electrode which covered much of the surface close to the weld. Another reason may be that a thicker oxide film was formed throughout the heat affected zone, because more oxygen was present in the welding atmosphere for these samples. This may indicate that the atmosphere is a contributing factor. This may further have improved the resistance towards the type of pitting cluster attack seen in Weld Sample 1a/b and Weld Sample 3. However, the colored bands indicating the variations in oxide film thickness, described earlier, were not observed to differ significantly between the samples welded with and without shielding gas. The thickness of the oxide film was not measured in this work, thus more exact variations in oxidation between the different samples after welding could not be decided.

In Weld Sample 3, a particularly strong attack of grain boundaries was observed in the coarse grain structure close to the fusion line, compared to the other samples. This is documented in Figure 48 - Figure 50. One explanation for this may be a possibly different temperature reached in this part of the HAZ during welding, compared to the other samples, leading to more carbide precipitation or oxidation and thus chromium depletion at the grain boundaries in this zone. It was however not confirmed that chromium carbides or chromium oxide had been precipitated in this zone. These more strongly appearing attacks at the grain boundaries can be correlated to the markedly lower corrosion resistance described by the polarization curve for this sample.

Also observed in Weld Sample 3 after the electrochemical polarization, was some inclusions assumed to have been created as a result of the welding. This can be seen in Figure 47 and in more detail in Figure 51. The inclusions were observed in a distance between 0.1 mm and 1 mm from the fusion line, which indicates a relation to the welding process and the temperature reached in this zone. The appearance of the inclusions suggests that some attack may have been initiated in the centre of the inclusions when the sample was electrochemically polarized. This is suggested by the dark centre of the inclusions. EDS measurement, included in Table 13, showed that manganese was measured in the centre, and also in minor amounts in the bright border of the formations. Sulfur was detected in small amounts, yet larger than the expected sulfur content in the metal matrix in both the centre and the bright outer part. Silicon was measured in relatively high amounts, and highest in the small gray area in the centre. A significant amount of aluminium was also detected here. Content of aluminium oxide in sulfide inclusions have been reported by several researchers, as described in section 3.1.4. In all parts of these inclusions, and in the metal matrix in the same area, oxygen in relatively high amounts was detected. The results of the EDS measurements indicate that the inclusions could be mixed manganese and silicon oxides, possibly containing some aluminium oxide. These types of inclusions have not been observed in the base metal, or in the other welded samples in this investigation. By the measured content of manganese and sulfur, it can be suggested that these inclusions are former MnS inclusions, possibly containing silicon. The content of silicon oxide in MnS inclusions have been reported by Webb *et al.* [25]. It can be suggested that manganese sulfides, possibly containing silicon oxide, have been transformed to segregated manganese-silicon oxides during the heat treatment by the welding, and that the temperature level, time and the amount of oxygen infiltration in this distance from the fusion line was favourable to form these types of inclusions. Akgün *et al.* [37] reported that some Mn rather formed Mn-Si compounds than MnS when a 304L stainless steel surface was melted with laser surface melting. This support the suggestion that such compounds can be formed.

It could also be suggested that FeS has been formed during cooling after the welding, as described by Wranglén [35]. The small amounts of detected sulfur, and the large amounts of Si and O indicate however that FeS was not a major constituent of the inclusions in Figure 51 formed after welding. It is more possible that the inclusions seen in Figure 17 are FeS. The EDS measurements indicated that the major elements in these inclusions were iron and sulfur. These inclusions showed however no attack, possibly because of an unfavourable composition, or because a

thicker oxide film had been created in this area, due to heat affection caused by the epoxy cast which started to burn close to this area after welding.

The inclusions in Figure 51 could be the same type as reported by Mohammadi Zahrani *et al.* [44]. They reported that large inclusions, rich in S, Al and Si were present in the HAZ and fusion zone of a 316L stainless steel.

The varying composition inside the inclusions described above may have favoured the initiation of some attack, due to internal galvanic effects. This may be related to the particular active behaviour of mixed inclusions to initiate pitting, reported by Suter *et al.* [17] and Suter and Böhni [20]. The active behaviour of MnS inclusions containing SiO and also MnS inclusions containing aluminium oxide have been reported, as described in section 3.1.4. It could be suggested that attack at these inclusions may have contributed to the much lower measured pitting potential compared to the other samples in this investigation. Following this, it could be suggested that MnS inclusions are at least partly responsible for the lowered corrosion resistance in the weld zone, and an explanation could be that the inclusions have been transformed to mixed oxide inclusions which, due to internal compositional variations, are more prone to initiate pitting than the non-affected inclusions in the base metal. An evident attack was however not seen in these inclusions, indicating that the other corrosion attacks seen in this sample (grain boundary corrosion and pitting clusters) dominated. Further investigations should be performed to clarify the behaviour of such inclusions, and their susceptibility towards the initiation of corrosion.

The lack of evident attack at inclusions in the HAZ of Weld Sample 3 and the various grades of both grain boundary corrosion and pitting cluster attack in the HAZ observed for the other welded samples indicate that these attacks were more important for the failure of the stainless steel investigated in this work than pitting initiated at MnS inclusions changed by the welding process.

Outside the heat affected zone in Weld Sample 3, pitting was also seen to initiate, most likely at inclusions. This was expected, because the sample surface contained MnS inclusions in the same manner as the base metal, where pitting had been seen to initiate at about 60 % of the inclusions. In the surface seen in Figure 46, a reddish brown color is seen covering most of the surface also far from the weld. This is believed to originate from oxidation of the surface, possibly occurred when the epoxy cast originally surrounding this sample started to burn after the welding, or by the welding itself. The initiation of pitting at inclusions indicates that the inclusions have not been influenced by this oxidation. Typical initiated pitting attacks, documented in Figure 54, appeared more severe than in the other weld samples. This can explain the steeper polarization curve for Weld Sample 3, than seen for the other weld samples, indicating more localized corrosion.

Despite the non-intended dissolution of inclusions in some of the weld samples before welding, pitting were seen to have initiated at inclusions after electrochemical polarization here as well, but in a less amount than the non-treated base metal samples 1 and 2. Pit initiation at inclusions was only detected at the side of the weld which was not immersed in acid before welding, i.e. in Weld Sample 1a and 2a, which was expected. Pit initiation at inclusions was not seen in the heat-affected

zone of these weld samples. This could be explained by the initiation of other corrosion attacks which dominated in this zone. It may also be explained by non-intended acid influence which is believed to have occurred closer to the weld in these samples, i.e. in the HAZ.

In Weld Sample 1a pit initiation was more frequent further away from the fusion line. As can be seen in Figure 38 - Figure 41, small initiated pitting attacks is far more numerous in the area located 16 mm from the fusion line, than at 5 mm and 7 mm. It seems also that the area at 20 mm have less attacks than at 16 mm. Even though it cannot be excluded, it is not believed that the areas at 5 mm and 7 mm have been influenced by heat during the welding, enough to change the corrosion properties of the surface. This is assumed by looking at the sample surface in Figure 28, where no visible change of the surface had occurred beyond 4 mm from the fusion line, or by the SEM examination which showed no visible change in these distances from the fusion line. An explanation for the increased number of initiated pitting further from the fusion line can be the less influence by acid before the welding, leading to less dissolution. Another explanation for the reduced initiation of pitting closer to the fusion line could be that an oxide film had been formed during the welding, which became thicker closer to the fusion line, and thereby covering the MnS inclusions such that the inclusions became more resistant to dissolution. The introduction of an oxide film with varying thickness in the weld zone even if shielding gas is used was reported by Enerhaug [57]. As described in section 3.1.7, it has been indicated that the MnS inclusions in the surface of stainless steels are weak points due to a poor or lacking oxide film. The introduction of an oxide film due to welding may therefore explain an increased resistance of otherwise unaffected inclusions to initiate pitting. The presence of an oxide film could not be verified by the SEM examination. More specialized instruments have to be used to obtain this information.

The observation that there may be less frequent pitting attacks even further from the fusion line, i.e. at 20 mm compared to 16 mm, could be explained by a varying number of inclusions to initiate pitting present in those two areas. The SEM image of a typical attack included in Figure 42 show that it was initiated at a typical MnS inclusion. Figure 45 also show that pitting has started at inclusions in Weld Sample 2a, which was not treated with acid before the welding. The initiated pitting attacks at inclusions and thus localized corrosion in this samples could explain the somewhat steeper polarization curve compared to weld samples were inclusions had been removed.

7. Conclusions

A literature review of the investigations focusing on the initiation of pitting by sulfide inclusions in austenitic stainless steel in general has been provided.

A literature review of investigations focusing on the effects of welding on the microstructure, inclusions and the corrosion properties in the weld zone of austenitic stainless steels has also been provided.

The main knowledge from the literature review was:

- It has been shown that MnS inclusions are the main initiation site for pitting on austenitic stainless steels in chloride environment.
- At the inclusion, pitting has been observed to initiate at the boundary between the inclusion and the metal matrix, but also inside the inclusion.
- Dissolution of MnS inclusions, with the release of dissolution products, is the most common suggested explanation to the initial step for pit initiation. Other hypotheses for the initiation process are also suggested. MnS inclusions can also be inactive.
- Chloride content is required to initiate pitting of the metal surrounding inclusions, but dissolution of MnS inclusions does also occur in non-chloride environments, without further attack of the metal.
- MnS is seen to be more unstable than other types of inclusions, and to have a poor or lacking protective film.
- The geometry and size of inclusions, and also the association with other compounds has been shown to influence the occurrence of pit initiation.
- The effects of micro-segregation and chromium depletion due to carbide precipitation in a sensitized zone in the HAZ or by the formation of δ-ferrite in the HAZ or the weld metal are the main explanations for the decreased corrosion resistance due to microstructural changes in the weld zone.
- The presence of an increased amount and size of inclusions has also been suggested to promote corrosion attack in the weld zone.
- It has been indicated that welding may influence the composition of sulfide inclusions.
- Oxygen infiltration during welding may cause the formation of oxides, and when chromium is involved, cause chromium depletion in a metal layer, further contributing to a reduced corrosion resistance.

The following can be concluded from the experimental work:

It has been verified that the main initiation site for pitting in the base metal of a 316L austenitic stainless steel was MnS inclusions in the surface.

It was indicated that dissolution of the MnS inclusions started the pit initiation process, with the contribution of released compounds from the inclusions.

A treatment with 25 wt% nitric acid to remove MnS inclusions improved the pitting resistance significantly.

The average percent of inclusions which showed an inactive behavior when several surfaces were examined was 38 %, verifying similar observations reported in earlier investigations.

Microstructural changes that occurred as a result of welding have been studied. Different grain sizes in the HAZ at different distances from the fusion line were observed.

Welding caused the initiation of corrosion at lower potentials, during electrochemical polarization in synthetic seawater. The corrosion mechanism was probably grain boundary corrosion caused by precipitation of chromium carbides in the grain boundaries.

The heat affected zones in samples welded with and without inert shielding gas were compared. The surface where no shielding gas was present may have been more oxidized, while the surface where shielding gas was used showed a more evident HAZ, due to a cleaner surface. A lacking inert shielding gas during welding did not have any effect on the potential for the initiation of corrosion when comparing two samples welded with and without shielding gas.

It was indicated that compositional changes had occurred for MnS inclusions in a certain distance from the fusion line. These changes my have caused the inclusions to be more prone to initiate pitting. Further investigation should be performed to clarify the behaviour of such inclusions, and their susceptibility towards the initiation of corrosion.

Grain boundary corrosion in various grades had occurred in the HAZ in certain distances from the fusion line.

Pitting-like corrosion in clusters, possibly induced by chromium depletion after forming chromium oxides, had occurred in the HAZ in a further distance from the fusion line, which was indicated to correspond to where an oxide film formed during welding was thinnest.

The grain boundary corrosion and the pitting cluster attack are from the experimental results believed to be more important for the failure of the welded stainless steel investigated in this work, than pitting initiated at MnS inclusions changed by the welding process.

References

[1] Williams, D.E., T.F. Mohiuddin, and Y.Y. Zhu, *Elucidation of a trigger mechanism for pitting corrosion of stainless steels using submicron resolution scanning electrochemical and photoelectrochemical microscopy,* Journal of the Electrochemical Society, 145, 1998, p. 2664.

[2] Szklarska-Smialowska, Z., *Pitting corrosion of metals,* National Association of Corrosion Engineers, Houston TX, 1986.

[3] Eklund, G.S., *Initiation of pitting at sulfide inclusions in stainless steel,* Journal of the Electrochemical Society, 121, 1974, p. 467.

[4] Williams, D.E., *et al*., *Composition changes around sulphide inclusions in stainless steels, and implications for the initiation of pitting corrosion,* Corros. Sci., 2010.

[5] Pardo, A., *et al*., *Pitting corrosion behaviour of austenitic stainless steels-combining effects of Mn and Mo additions,* Corros. Sci., 50(6), 2008, p. 1796-1806.

[6] EKLUND, G., *Relation between Pitting and Non-Metallic Inclusions,* Jernkontorets Ann, 155 (9), 1971, p. 637-642.

[7] Wranglen, G., *Pitting and sulphide inclusions in steel,* Corrosion Science, 14 (5), 1974, p. 331-349.

[8] Stewart, J. and D. Williams, *The initiation of pitting corrosion on austenitic stainless steel: on the role and importance of sulphide inclusions,* Corros. Sci., 33 (3), 1992, p. 457-463, 465-474.

[9] Rossi, A., *et al*., *XPS, AES and ToF-SIMS investigation of surface films and the role of inclusions on pitting corrosion in austenitic stainless steels,* Surface and interface analysis, 29 (7), 2000, p. 460-467.

[10] Schmuki, P., *et al*., *The composition of the boundary region of MnS inclusions in stainless steel and its relevance in triggering pitting corrosion,* Corros. Sci., 47 (5), 2005, p. 1239-1250.

[11] Krawiec, H., *et al*., *Influence of the chemical dissolution of MnS inclusions on the electrochemical behavior of stainless steels,* Journal of the Electrochemical Society, 152, 2005, p. B213.

[12] Böhni, H., T. Suter, and A. Schreyer, *Micro- and nanotechniques to study localized corrosion,* Electrochimica Acta, 40 (10), 1995, p. 1361-1368.

[13] Park, J.O. and H. Böhni, *Local pH measurements during pitting corrosion at MnS inclusions on stainless steel,* Electrochemical and Solid-State Letters, 3, 2000, p. 416.

[14] Webb, E.G. and R.C. Alkire, *Pit initiation at single sulfide inclusions in stainless steel I*. Electrochemical microcell measurements, J. Electrochem. Soc., 149 (Copyright (C) 2011 American Chemical Society (ACS). All Rights Reserved.), 2002, p. B272-B279.

[15] Park, J., S. Matsch, and H. Böhni, *Effects of temperature and chloride concentration on pit initiation and early pit growth of stainless steel,* Journal of the Electrochemical Society, 149, 2002, p. B34.

[16] Degerbeck, J. and E. Wold, *Some aspects of the influence of manganese in austenitic stainless steels,* Materials and Corrosion, 25 (3), 1974, p. 172-174.

[17] Suter, T., T. Peter, and H. Böhni. *Microelectrochemical investigations of MnS inclusions*, Trans Tech Publ, 1995.

[18] Lim, Y.S., *et al*., *The influences of microstructure and nitrogen alloying on pitting corrosion of type 316L and 20 wt.% Mn-substituted type 316L stainless steels,* Corros. Sci., 43 (1), 2001, p. 53-68.

[19] Ilevbare, G. and G. Burstein, *The role of alloyed molybdenum in the inhibition of pitting corrosion in stainless steels,* Corros. Sci., 43 (3), 2001, p. 485-513.

[20] Suter, T. and H. Böhni, *A new microelectrochemical method to study pit initiation on stainless steels,* Electrochimica Acta, 42 (20-22), 1997, p. 3275-3280.

[21] Baker, M. and J. Castle, *The initiation of pitting corrosion of stainless steels at oxide inclusions,* Corrosion Science, 33 (8), 1992, p. 1295-1303, 1305-1312.

[22] Noh, J., *et al*., *Effects of nitric acid passivation on the pitting resistance of 316 stainless steel,* Corrosion Science, 42 (12), 2000, p. 2069-2084.

[23] Muto, I., S. Kurokawa, and N. Hara. *Microelectrochemistry on CrS and MnS Inclusions and Its Relation with Pitting Potentials of Stainless Steels*, ECS, 2009.

[24] Muto, I., D. Ito, and N. Hara, *Microelectrochemical Investigation on Pit Initiation at Sulfide and Oxide Inclusions in Type 304 Stainless Steel,* Journal of the Electrochemical Society, 156, 2009, p. C55.

[25] Webb, E., T. Suter, and R. Alkire, *Microelectrochemical measurements of the dissolution of single MnS inclusions, and the prediction of the critical conditions for pit initiation on stainless steel,* Journal of the Electrochemical Society, 148, 2001, p. B186.

[26] Staffansson, L.I., *On the Mn-MnS phase diagram,* Metallurgical and Materials Transactions B, 7 (1), 1976, p. 131-134.

[27] Alkire, R.C. and S.E. Lott, *The Role of Inclusions on Initiation of Crevice Corrosion of Stainless Steel,* Journal of the Electrochemical Society, 136, 1989, p. 3256.

[28] Baker, M. and J. Castle, *The initiation of pitting corrosion at MnS inclusions,* Corrosion Science, 34 (4), 1993, p. 667-682.

[29] Brossia, C.S. and R.G. Kelly, *Occluded solution chemistry control and the role of alloy sulfur on the initiation of crevice corrosion in type 304ss,* Corros. Sci., 40 (11), 1998, p. 1851-1871.

[30] Webb, E.G. and R.C. Alkire, *Pit initiation at single sulfide inclusions in stainless steel II. Detection of local pH, sulfide, and thiosulfate,* J. Electrochem. Soc., 149 (Copyright (C) 2011 American Chemical Society (ACS). All Rights Reserved.), 2002, p. B280-B285.

[31] Webb, E.G. and R.C. Alkire, *Pit Initiation at Single Sulfide Inclusions in Stainless Steel,* Journal of the Electrochemical Society, 149, 2002, p. B286.

[32] Ryan, M.P., *et al*., *Why stainless steel corrodes,* Nature, 415 (6873), 2002, p. 770-774.

[33] Williams, D.E. and Y.Y. Zhu, *Explanation for initiation of pitting corrosion of stainless steels at sulfide inclusions,* Journal of the Electrochemical Society, 147, 2000, p. 1763.

[34] Meng, Q., *et al*., *Metallurgy (communication arising): Stainless-steel corrosion and MnS inclusions,* Nature, 424 (6947), 2003, p. 389-390.

[35] Wranglen, G., *Review article on the influence of sulphide inclusions on the corrodibility of Fe and steel,* Corrosion Science, 9 (8), 1969, p. 585-602.

[36] Ke, R. and R. Alkire, *Initiation of corrosion pits at inclusions on 304 stainless steel,* Journal of the Electrochemical Society, 142, 1995, p. 4056.

[37] Akgun, O.V., M. Urgen, and A.F. Cakir, *The effect of heat treatment on corrosion behavior of laser surface melted 304L stainless steel,* Materials Science and Engineering A, 203 (1-2), 1995, p. 324-331.

[38] Conde, A., *et al*., *Corrosion behaviour of steels after laser surface melting,* Mater. Des., 21 (5), 2000, p. 441-445.

[39] Inturi, R. and Z. Szklarska-Smialowska, *Localized corrosion of nanocrystalline 304 type stainless steel films,* Corrosion, 48 (05), 1992.

[40] Ryan, M., *et al*., *The Pitting Behavior of Iron − Chromium Thin Film Alloys in Hydrochloric Acid,* Journal of the Electrochemical Society, 145, 1998, p. 1566.

[41] Ryan, M., *et al*., *Corrosion pits in thin films of stainless steel,* Journal of the Electrochemical Society, 146, 1999, p. 91.

[42] Rodrigues, A. and A. Loureiro. *Effect of Cooling Rate on the Microstructure and Hardness of Austenitic Stainless Steel Welds*, Trans Tech Publ, 2004.

[43] Lu, B., *et al*., *Pitting and stress corrosion cracking behavior in welded austenitic stainless steel,* Electrochimica acta, 50 (6), 2005, p. 1391-1403.

[44] Mohammadi Zahrani, E., A. Saatchi, and A. Alfantazi, *Pitting of 316L stainless steel in flare piping of a petrochemical plant,* Engineering Failure Analysis, 17 (4), 2010, p. 810-817.

[45] Cui, Y. and C.D. Lundin, *Austenite-preferential corrosion attack in 316 austenitic stainless steel weld metals,* Mater. Des., 28 (1), 2007, p. 324-328.

[46] de Lima-Neto, P., *et al*., *Determination of the sensitized zone extension in welded AISI 304 stainless steel using non-destructive electrochemical techniques,* Corrosion Science, 50 (4), 2008, p. 1149-1155.

[47] Santillan, S., *et al*., *Corrosion of the heat-affected zone of stainless steel weldments,* Anti-Corrosion Methods and Materials, 57 (4), 2010, p. 180-184.

[48] Tsai, N. and T. Eagar, *The size of the sensitization zone in 304 stainless steel welds,* Journal of materials for energy systems, 6 (1), 1984, p. 33-37.

[49] Garcia, C., *et al*., *Pitting corrosion of welded joints of austenitic stainless steels studied by using an electrochemical minicell,* Corrosion Science, 50 (4), 2008, p. 1184-1194.

[50] Silva, C.C., J.P. Farias, and H.B. de Sant'Ana, *Evaluation of AISI 316L stainless steel welded plates in heavy petroleum environment,* Mater. Des., 30 (5), 2009, p. 1581-1587.

[51] Smith, J. and R. Farrar, *Influence of microstructure and composition on mechanical properties of some AISI 300 series weld metals,* International materials reviews, 38 (1), 1993, p. 25-51.

[52] Park, S.H.C., *et al*., *Corrosion resistance of friction stir welded 304 stainless steel,* Scripta materialia, 51 (2), 2004, p. 101-105.

[53] DebRoy, T. and S. David, *Physical processes in fusion welding,* Reviews of Modern Physics, 67 (1), 1995, p. 85.

[54] Kokawa, H., *Nitrogen Absorption and Desorption by Steels during Arc and Laser Welding,* Journal of the Japan Welding Society, 72 (5), 2003, p. 112-121.

[55] Shankar, V., *et al*., *Effect of nitrogen addition on microstructure and fusion zone cracking in type 316L stainless steel weld metals,* Materials Science and Engineering: A, 343 (1), 2003, p. 170-181.

[56] Kwok, C., *et al*., *Pitting and galvanic corrosion behavior of laser-welded stainless steels,* Journal of materials processing technology, 176 (1-3), 2006, p. 168-178.

[57] Enerhaug, J., *A study of localized corrosion in super martensitic stainless steel weldments*, Doctoral Thesis, The Norwegian University of Science and Technology (NTNU), Department of Machine Design and Materials Technology, 2002.

[58] J. Vagn Hansen, E.M., P. Aastrup, P.F. Larsen, *Beskyttelsesgasdækning og korrosionsbestandighed efter sveising af rustfrie stålrør*, Report 87.66, Korrosjonssentralen ATV, Denmark, 1987.

[59] Nishimoto, K. and K. Ogawa, *Corrosion properties in weldments of stainless steels (1). Metallurgical factors affecting corrosion properties,* Welding international, 13 (11), 1999, p. 845-854.

[60] White, W.E., *Observations of the influence of microstructure on corrosion of welded conventional and stainless steels,* Materials characterization, 28 (3), 1992, p. 349-358.

[61] Pujar, M., *et al*., *Evaluation of microstructure and electrochemical corrosion behavior of austenitic 316 stainless steel weld metals with varying chemical compositions,* Journal of materials engineering and performance, 14 (3), 2005, p. 327-342.

[62] Karoliussen, H., *Notat-10 Referanseelektroder - Potensiometrisk titrering, LO082 Fysikalsk kjemi*, Høgskolen i Sør-Trøndelag, AFT, Program for Kjemi og Materialteknikk, 2007.